1990

Aspects of thin-walled structural behaviour

Mohsen Salaheldin
University of Wollongong

ASPECTS OF THIN-WALLED STRUCTURAL BEHAVIOUR

A thesis submitted in fulfilment of the requirements

for the award of the degree of

Doctor of Philosophy

from

THE UNIVERSITY OF WOLLONGONG

by

MOHSEN SALAHELDIN, CPEng., B.E.(Civil),

M.E.(Hons), MIEAust.

DEPARTMENT OF CIVIL AND

MINING ENGINEERING

1990

Acknowledgements

The author wishes to express sincere appreciation to his supervisor, Professor Lewis Schmidt, for his pertinent advice and constant encouragement.

Thanks is also due to Mr. Norm Gal, Mr. Richard Webb and Mr. Tony Mowbray for their assistance during the experimental work.

The author expresses gratitude to Mr. Zaim Basiran, Mr. Jasmadi Johari and Mr. Noridan Turiman for their valuable assistance in typing the script and preparing the drawings.

Acknowledgement is made to the Department of Civil and Mining Engineering for providing facilities for the work.

Abstract

It is believed that thin-walled structures have an important role to play in the development of new concepts of structural systems. It is, therefore, important to understand the behaviour of these structures and to express this understanding in a form of changes and development of design rules.

Aspect ratio is one of the main parameters which influences the behaviour of thin-walled structures. The study herein recognises the influence of aspect ratio on different types of thin-walled structural behaviour.

It is shown that a simply supported box girder experiences transverse membrane stresses along the centre-line of the flanges. These stresses are sensitive to the flange aspect ratio. An idea due to Heyman is presented which assumes a box-section to be the assembly of two channels built-up toe-to-toe. A concentrated load, which acts on the web/flange junction, introduces a twisting effect. In order to keep the box in the no-twist-position a lateral force is needed. Based on this idea and a parametric finite element study, two simple empirical equations are introduced. The equations predict the magnitude and the distribution of transverse membrane stresses along the centre-line of the flange. These stresses, in some cases, have a value which is several times the value of the associated longitudinal stresses.

The same argument is used to evaluate the transverse membrane stresses in I-beams which are regarded as being assembled by placing two channels back-to-back. Simple equations are again presented to predict these stresses.

The study is extended to investigate the influence of the aspect ratio on the bending lag phenomenon in the compressive flanges of box girders. When elastic buckling of the flange is assumed negative bending lag is detected.

The study also covers the influence of the aspect ratio on the behaviour of profiled sheets when subjected to concentrated loads causing flexure. The results show that local plastic failure occurs initially in shorter spans rather than longer spans when the profile height is shallow. These anomalous results are evaluated and recommendations are given in view of the evaluations.

It has been the aim to provide a physical understanding of the structural behaviour in addition to the evaluation of stresses and deformation in the various cases studied.

TABLE OF CONTENT

Chapter 1

Introduction

1.1 Introduction

The efficiency of thin-walled structures has long been recognised. The ancient Egyptians, more than 5,000 years ago, developed a sailing craft made of planks fastened around a wooden framework. Also, the ancient Vikings developed a craft structural system of planks which were tied on the inside to ribs (Troitsky, 1976). The structural theory behind these types of constructions is not, in principle, far from the theory used in the design methods of modern aircraft where thin metal sheets are stiffened by longitudinal stringers and transverse frames.

Nature has provided mankind with various examples which demonstrate economic and elegant structural design of thin-walled structures. Fig. 1.1 displays one of these examples, which is a leaf reinforced by ribs and diaphragms. The leaf can resist in-plane tension and shear forces, while the diaphragms and ribs help to resist compressive and out-of-plane forces. The

resemblance between this structural arrangement and a stiffened plate is apparent.

Another example of a superior and efficient design is displayed in Fig. 1.2, which is a marine animal shell. The form of the material (corrugation) helps to strengthen the structure against lateral forces and bending stresses. A man-made copy of this structure is the ubiquitous profiled sheet, where the strength of the sheeting is based on the shape or form.

The efficiency and effectiveness of thin-walled structures are demonstrated in the increasing industrial use of these types of structures. A continuous effort to increase the understanding of thin-walled structural behaviour is essential for the development and innovation in this promising area of structural design.

The present research work encompasses more than one aspect of thin-walled structural behaviour, but the central theme is the influence of the "aspect ratio" on each of these aspects. The aspect ratio herein is defined as the ratio of width to length of a thin-walled structural element.

In the past the effect of the aspect ratio on different types of behaviour of thin-walled structures has been investigated. Some of the results are presented in the following paragraphs.

Bulson (1984) discussed the effect of the change in the aspect ratio on the buckling coefficient 'k' of stiffened plates. He concluded that long plates (low aspect ratio), simply supported on one longitudinal edge, buckle into only a single longitudinal half wave. This buckling mode exists whether the other edge is free, or whether it is supported by a lip. He also added that as

the aspect ratio decreases, the value of k for a lipped plate falls below that for a plate with a free edge.

An approximate analytical solution of Marguerre's equations for rectangular plates was presented by Murray (1984). The study showed the effect of the aspect ratio on the critical elastic load, P_{ce}. Three cases of end support have been considered (Fig. 1.3).

The result of the analysis for Case (a) is:

$$P_{ce} = - \frac{\pi^2 \left(\frac{b}{\ell} + \frac{\ell}{b}\right)^2}{12 \left(1 - \mu\right)^2 \left(1 + \mu \left(\frac{\ell}{b}\right)^2\right)} \left(\frac{t}{b}\right)^2$$

For Cases (b) and (c)

$$P_{ce} = - \frac{\pi^2 \left(\frac{b}{\ell} + \frac{\ell}{b}\right)^2}{12 \left(1 - \mu^2\right)} \left(\frac{t}{b}\right)^2$$

Where ℓ is the plate length, μ is Poisson's ratio, b is the plate width, and t is the plate thickness.

The shear lag effect is another area where the influence of the aspect ratio is dominant. Abdel-Sayed (1969) examined the deck-plate bridge effective-width problem (due to the influence of shear lag). He considered sine-wave loading to be acting on the main girder. As a result of the analysis, formulae and tables were presented by which the effective width could be calculated. The analysis confirmed the view that the shear lag effect is dependent on the aspect ratio.

Moffat and Dowling (1975) studied the shear lag effect in steel box girder bridges using a finite element analysis technique. They concluded that the effect of shear lag, in the box girder flange, is dependent significantly on the aspect ratio. The shear lag effect influences both deflections and stresses.

Lamas and Dowling (1979) investigated the effect of shear lag on the inelastic buckling behaviour of thin-walled structures. They stated that: "provided the effects of residual stresses are neglected, the maximum efficiency of a flange of a simply supported beam, even if very stocky, can never be attained for aspect ratios (the ratio of the width of the flange to the span length) greater than a certain limit ". In the case of unstiffened flanges this limit is 0.577.

The British Standard (1982) adopted the concept of a stress effective breadth and a deflection effective breadth to quantify the influence of shear lag on the behaviour of box girder flanges; the actual breadth (width) of the flange is replaced by a reduced width. This reduced width can be used in conjunction with the elementary theory of bending to predict the actual flange stresses and deflections. Tables are presented (British Standard 5400, 1982) to calculate the effective width; a review of these tables shows the aspect ratio to be the principal influence on the shear lag effect.

Recently an analytical solution method for the problem of shear lag was presented by Koo and Cheung (1989). A comparative comment investigating some of the numerical results presented in this paper can be found in Appendix 3.

The first part of this thesis (Chapters 2-5) is concerned principally with the influence of the aspect ratio on transverse stresses in thin-walled beams. A view is expressed that an I-beam and a box girder can be thought of as two

channels placed together back to back in the case of an I-beam, and toe to toe in the case of a box girder. This hypothesis is examined, for the case of box girder, using finite element studies. A further investigation results in a simple empirical procedure to predict the magnitude and the distribution of the transverse stresses in a box girder flange. The transverse stresses are seen to be of significance in some circumstances.

The same argument concerning the behaviour of an I-beam is also examined and proved to agree with the finite element results. Simple rules to calculate the transverse stresses in the flange of an I-beam are also presented.

The second part of this thesis (Chapter 6) is focussed on the influence of the aspect ratio on the bending lag effect of the box girder flange. The effect of the elastic buckling due to this phenomenon is also presented.

Chapter 7 is devoted to the investigation of profiled sheet behaviour under a concentrated load. The aspect ratio is shown to have a significant effect on the deflection behaviour of these types of structural elements. The study helps to explain an intriguing phenomenon arising where simply supported profiled sheets were tested under concentrated load. During the test it was observed that initial local buckling occurred at earlier load in sheets with smaller rather than larger spans.

Chapter 8 is an attempt to present the practical implications of the work which has been undertaken.

The last chapter of this thesis is the conclusions where a brief review of the main results is presented.

Overall, the aim has been to present not only the information regarding the influence of the aspect ratio on stresses and deflections of these types of structures, but also an understanding of the physical meaning associated with different patterns of behaviour. The physical understanding of different aspects of thin-walled structural behaviour is necessary if good engineering design practice is to be achieved.

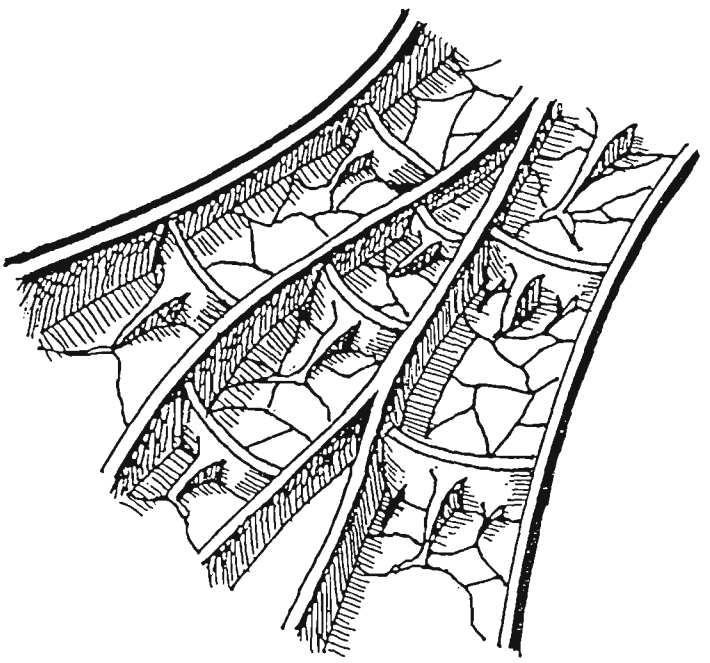

Fig. 1.1 Leaf having ribs and diaphragms (Troitsky, 1976)

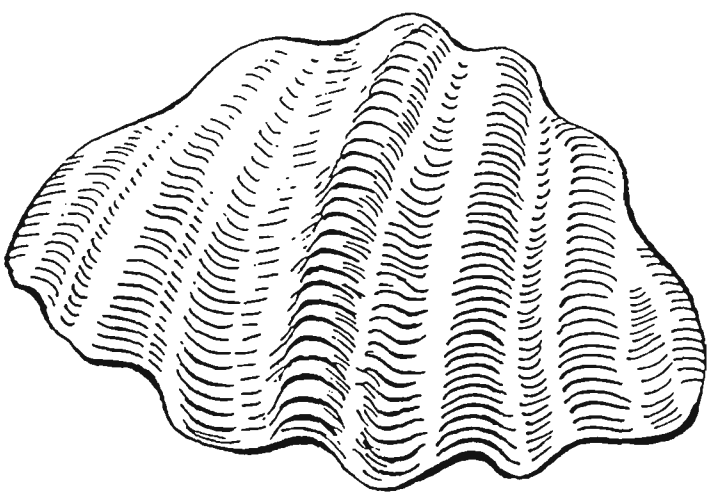

Fig. 1.2 Marine animal shell (Troitsky, 1976)

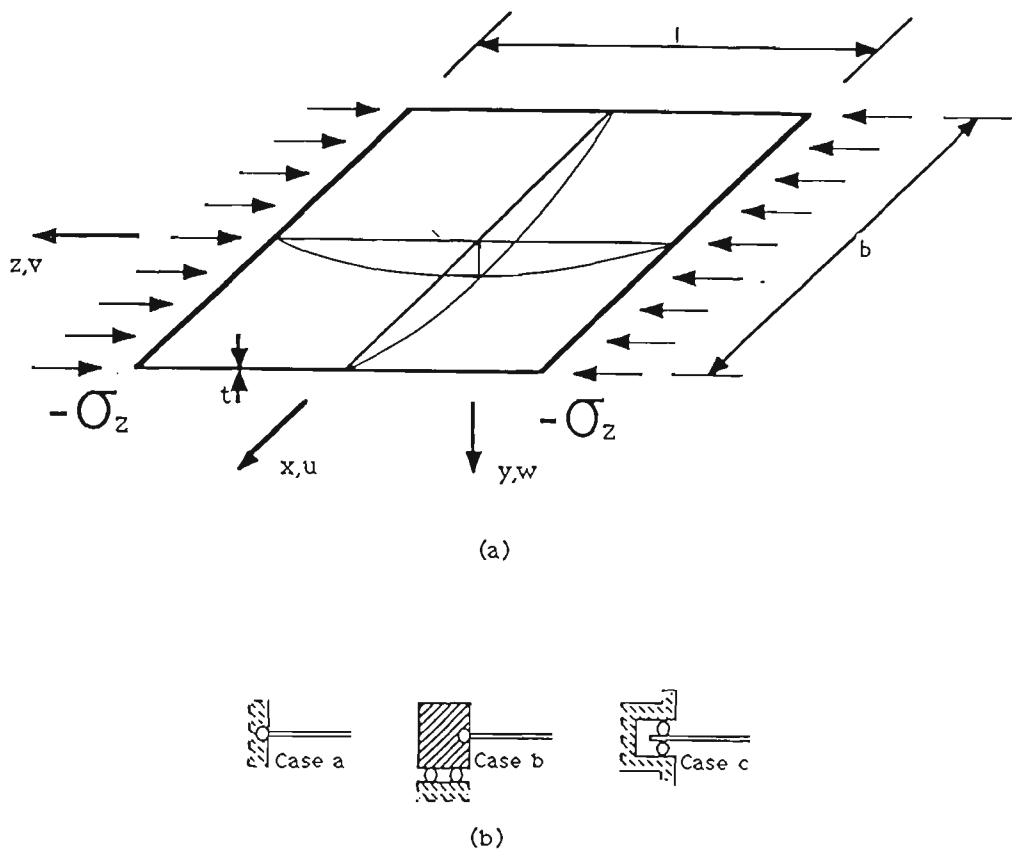

Fig. 1.3 (a) Simply supported rectangular plate with initial deflection and in-plane stresses; (b) boundary condition along x ± b/2 (Murray, 1984)

Chapter 2

The Deformation Behaviour of a Box Girder

2.1 Introduction

Box girders represent an efficient form of construction as they provide an effective distribution of the material and are particularly stable against torsional deformation. However, in some cases, this deformation can give rise to substantial additional stresses. It is therefore essential to improve the physical understanding of such behaviour in order to achieve good design practice.

2.2 Deformation Under Eccentric Loading

Analytical studies have shown that a box girder subjected to torsional loads undergoes deformation of the cross-section (Abdel-Samad, et al., 1968). This deformation results in significant longitudinal stresses , due to the warping effect ,and high transverse distortional stresses due to the lateral deformation.

When investigating the general case of box girder under eccentric loading (Fig.2.1) it can be seen that the loading has two components; bending and torsional.

If the torsional component is applied as shears on the plate elements that are in proportion to the St. Venant shear flows (Fig.2.1-e), the section is twisted without deformation of the cross section. It follows that the resulting longitudinal warping stresses are small, and no transverse flexural distortion stresses are induced. However, in a practical application, the torsional load is applied as shown in Fig.2.1-d. As a result of this loading condition there are forces acting on the plate elements which tend to deform the cross section (Fig.2.1-f). Thus, the movement of the plate elements of the cross section causes distortion in the transverse direction which is associated with warping stresses in the longitudinal direction (Wright, et al., 1968).

An attempt to explore and clarify the deformation behaviour of box girders under some representative conditions was made by Chapman, et al. In this investigation, the following techniques have been used.

(a) The theory of torsion of undeformed section (Timoshenko and Goodier, 1951).
(b) The beam on elastic foundation analogy for deforming section (Wright, et al., 1968).
(c) The finite element method, using the extensional - flexural rectangular and quadrilateral elements.

In the finite element analysis, a simply supported single cell box girder bridge was considered. The cross section had a depth of 1.8 m, width of 1.8 m, and a

length of 44 m. An eccentric point load was applied at midspan. The box had diaphragms only at the supports.

The eccentric load was separated into three components; bending, torsional and distortional. Each of these components was assumed to cause only the phenomenon suggested by its title, and was treated independently.

In order to asses the significance of the different types of stresses associated with the deformations, these stresses are given as a percentage of the bending stresses under the same load, calculated on the basis of the simple theory of bending (σ_B).

Under the torsional component there is no tendency of the cross section to distort, provided the shearing displacement of the sides are compatible with a rigid body rotation, and hence torsional warping stresses do not occur. A square box with sides of equal thickness satisfies this criterion. For a rectangular section, if the distortion is prevented, warping stresses due to the torsional component will develop. The finite element solution (Chapman, et al., 1971) shows that some distortion does take place under the torsional component causing distortional stresses equal to 3% of σ_B.

Under the flexural component, distortional stresses equal to 4% of σ_B occur. Transverse in-plane stresses equal to 2% of σ_B at mid-span also arise due to the tendency of the two halves of each flange to curve in their own plane in opposite directions (Chapman, et al., 1971).

It is to be noted that the small amount of transverse in-plane stresses shown by the analysis, under the flexural component, corresponds to a low value of

aspect ratio (0.04). It is also to be noted that in this study the dimensions of the end diaphragms were not given.

The distortional component of loading causes longitudinal warping stresses and transverse distortional bending stresses. These stresses are relatively high when distortion is not prevented.

Chapman concluded, in his study, that for a straight, right, single cell box the procedure of considering only the distortional component of the loading for the evaluation of distortional stresses, as used in the beam on elastic foundation method, whilst not exact, is adequate for practical purposes. The comprehensive work by Chapman, et al. and its findings had an influence on the British Code (1982) where a simplified procedure is presented to calculate transverse and longitudinal stresses due to restraint of warping.

2.3 Deformation Under Symmetrical Loading

So far, the analytical investigation has been focused on the deformation behaviour of a box girder under eccentric loading. In the following paragraphs, attention will be given to the deformation behaviour of a box section under a symmetrical concentrated load.

Heyman (1982) drew the attention to the similarity of the shear stress distribution in an open channel section and that of a closed box section (Figs.2.2-b and 2.3-a) when a shear force P is acting in a direction parallel to the centre-line of the web.

In the case of the channel, the shear stresses in the flange built up linearly from zero at the tip to its largest value at the web/flange junction, then a

quadratic function of the web height represents the increase in the shear stress which reaches its maximum value at the neutral axis. Thus, a parabolic distribution of shear stress in the web is evident.

The same pattern of shear stress distribution can be applied to a closed box section (Fig.2.3-a). Heyman deduced that the box section may be thought of as two channels placed toe to toe. The shear stress distribution for the whole section, as sketched in Fig.2.3-a, lends support to this argument.

In the channel section, the integration of the shear stresses in the flange of the channel results in the total horizontal force on the flange:

$$\int_0^{b/2} \tau \, t \, dx = \frac{1}{16} P \, \frac{d \, b^2 \, t}{I} \qquad (2.1)$$

Where τ is the shear stress, t is the thickness of the channel, b/2 is the width of the flange, d is the depth of the web, P is the shear force, and I is the second moment of area of the cross section.

The integration of the shear stresses over the depth of the web results in the total vertical force which has a value of P. This result satisfies the requirement by the consideration of vertical equilibrium. The three forces in the cross section, on the two flanges and on the web, which results from the application of the vertical shear force P, are shown in Fig. 2.2-c. In order to satisfy the static equilibrium requirement, the shear force P must be applied at a point which is distance s from the web of the channel (Fig. 2.2-d) if no torsional rotation is to occur. This point is the shear centre of the channel. The value of s is given by:

$$F_s = \frac{1}{16} F \frac{db^2 t}{I} \times d \qquad (2.2)$$

or

$$s = \frac{3\ b^2}{4d + 24b} \qquad (2.3)$$

Fig.2.3-b shows a box section which is fabricated by welding two channels together. In Fig.2.4-a, the two channels are cut apart and each is loaded by a single force P acting through its shear centre. The force 2P in Fig.2.3-b is statically equivalent to the two forces P in Fig.2.4-a. The temptation is to conclude that no force would be developed in the weld, as the two channels in Fig.2.4-a will deflect equally without twisting. However, there must be some mechanism for splitting the central load 2P into the separate loads in Fig.2.4-a. Each channel must be acted upon by the forces of Fig.2.4-b which are the same as those of Fig.2.2-c. Now, Fig.2.4-b is statically equivalent to Fig.2.4-c. Forces of a magnitude of Pb/2d act on the flanges; compressive on the top and tensile at the bottom. These forces are more or less point loads. Heyman concluded that a thin-walled box girder loaded as shown in Fig.2.3-b will be subjected to a high transverse compressive load at the centre of the top flange, and therefore, the top flange must be designed to resist local buckling. In practice, a diaphragm or other stiffening element must be inserted at a loading point or at a support, not only for bearing, but also to prevent buckling of the thin flange of the box.

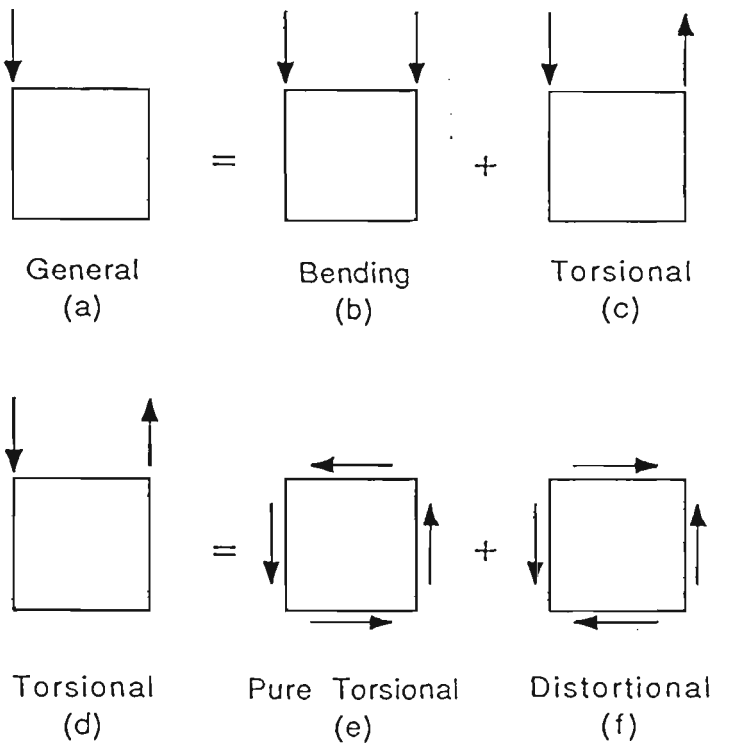

Fig. 2.1 Component of box girder loading (Wright, et.al., 1968)

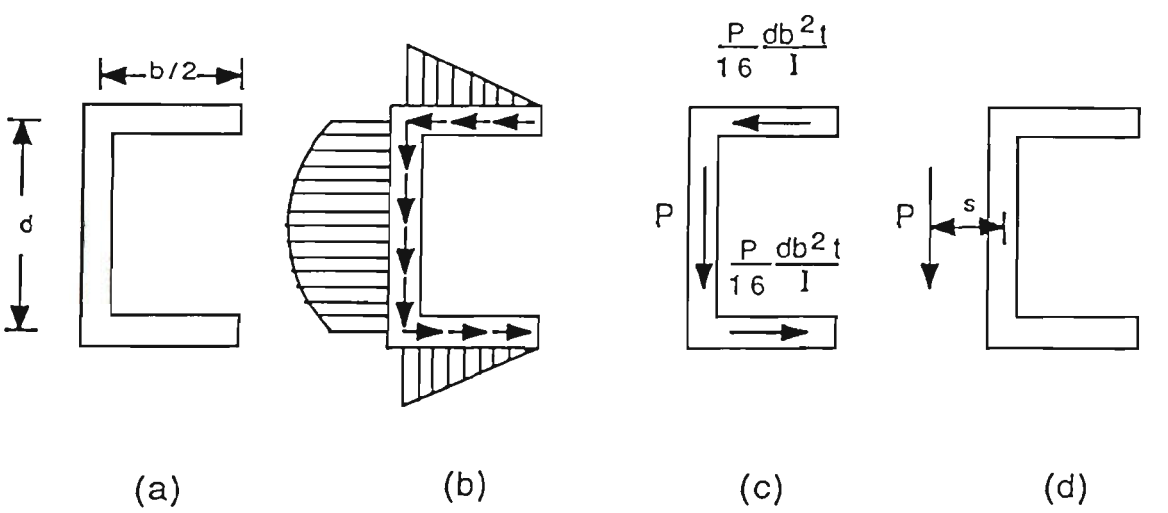

Fig. 2.2 (a) A channel section; (b) shear stress distribution in a channel section; (c) shear stress flow in a channel section; (d) shear force applied at the shear centre of a channel section (Heyman, 1982)

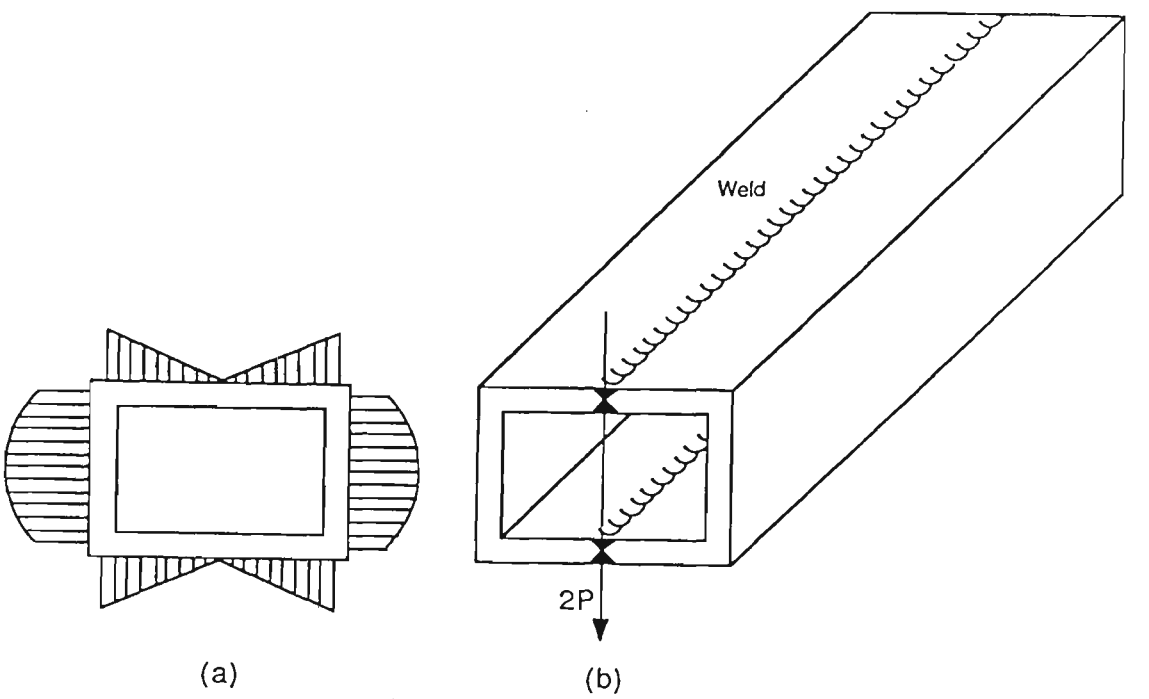

Fig. 2.3 (a) shear stress distribution in a box section; (b) box section formed by welding two channels (Heyman, 1982)

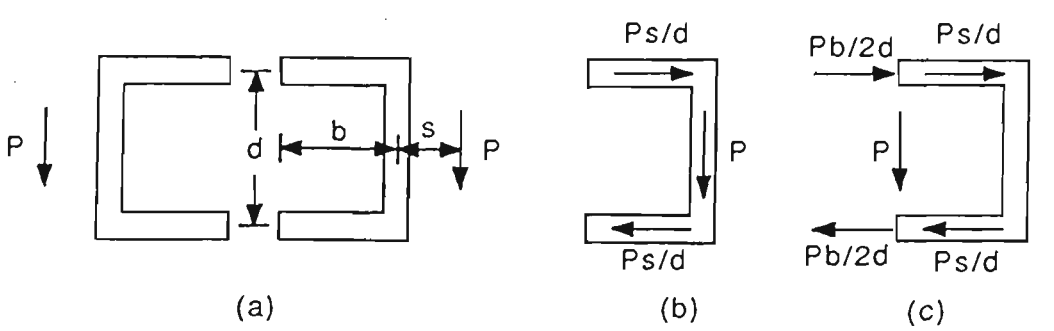

Fig. 2.4 Cross section of box composed of two channels: see text

Chapter 3

Transverse Stresses in Box Girders

3.1 Introduction

As mentioned in the previous section, Heyman (1982) proposed that a straight box girder under a concentrated central loading is subjected, as a result of its loading conditions, to a lateral point membrane force near the centre of the box in both the upper and lower flanges. This force is compressive in the compressive flange and may have a high enough value to cause concern with buckling.

The above argument, however, is based on a two dimensional simple structural mechanics analysis. Knowing the complexity of box girder behaviour, the need to investigate this argument and its practical implications becomes apparent.

A numerical investigation into the transverse stresses in the flanges of a simply supported box girder, under a symmetrical static concentrated load acting at the mid-span (Fig.3.1), is conducted using the finite element technique (Schmidt and Salaheldin, 1990). The objective of this study is to

investigate the possibility of the existence of large membrane transverse stresses in a box girder flange.

Consider the box girder to be subdivided into two channels as shown in Fig.3.2-a. The load P/2 (one quarter of the total load shown in Fig.3.1) causes a shear flow that results in the forces shown in Fig.3.2-b for each channel. Because the force P/2 is located a distance e away from the shear centre, a torque of value Pe/2 will cause the channel to twist. However, in the case of the box the tips of the channel flanges are located on the centre line, consequently in order to restore the channel to the no-twist condition concentrated lateral flange forces of value Pe/2d are needed, as shown in Fig.3.2-c. These forces can be approximated as point forces which induces transverse membrane stresses in the flanges (Heyman, 1982).

In order to verify the above allocation of cause to consequence certain lines of inquiry in connection with the behaviour of open and closed thin-walled girders are pursued.

Firstly, a wide flange I-beam, Fig.3.3-a, is considered for analysis with an applied central load acting through the shear centre of the section. Secondly, further examination of two other cross sections, (a channel and an open box girder Figs.3.3-b, c) enable a conclusion to be reached regarding the behaviour of the simple box cross section (Fig.3.3-d).

3.2 Modelling Technique

The finite element analysis employs a four-noded quadrilateral shell element. A full description of the element features is presented by MacNeal (1978). In all models considered for analysis no restrictions are imposed on the six

degrees of freedom (three translations and three rotations) of the nodes along the web/flange junction line, and thus a full interaction between the elements of the structure is allowed. An end diaphragm of infinite in-plane stiffness and zero out-of-plane stiffness is assumed at the simple supports.

In the two cases of box girders, namely, the simple closed box, and the open box, a double symmetry is assumed, and hence one quarter of the box girder is modelled. For the I-beam and the channel section, half the beam is modelled.

A concentrated load is applied at the mid-span on each web/flange junction. All the beams are assumed to be simply supported at the ends. The analysis is conducted on the assumption of linear elastic behaviour. Young's modulus E is assumed to be 200 GPa, and Poission's ratio μ is assumed to be 0.3 for the material.

As the central region of the girder is a highly stressed area, a biased mesh, allowing a fine discretisation near the mid span, is employed with the elements at the support 300% larger than the elements at the middle.

3.3 Numerical Results

(i) I-Beam Girder

The geometrical configurations are given as non-dimensional ratios from Fig.3.3-a,

$$d/b = 0.25,\ b/t_f = 40,\ \ b/\ell = 0.5,\ \text{and}\ t_f = t_w$$

where t_f is the flange thickness, t_w is the web thickness, and ℓ is the span of the centrally loaded simply supported beam.

The girder is simply supported with a diaphragm preventing in-plane deformation of the cross section at each end. The point load is applied at the mid-span on the web/flange junction, and as such it is acting through the shear centre of the I-beam.

The distribution of membrane transverse stresses across the compressive flange of the girder, at mid-span, is shown in Fig.3.4 the stresses are normalised with respect to the stress at the centre of the element near the flange centre (σ_{Tmax}). The stresses are tensile.

Fig.3.5 displays a three dimensional plot of the deflected shape. Magnification factors of 20, 200 and 400 are used for the vertical, longitudinal and lateral (transverse) deformation respectively. The figure shows the lateral expansion of the compressive flange and the contraction in the tensile flange of the I-beam. The lateral deflection has to be magnified using a rather large factor (400) in order to obtain a comprehensive picture of the deflection. A detailed study of this behaviour will be presented at a later stage.

The point is made that no twisting takes place under the assumed loading condition. Consequently the web remains vertical. It is worth noting that Ω (the ratio of the maximum membrane transverse stress to the corresponding longitudinal stress) equals –14.5 per cent.

(ii) Channel and Open Box Girder

The boundary conditions for both models, the channel section of Fig.3.3-b and the open box girder Fig.3.3-c, are similar to those of the I-beam girder including the assumption of an end support diaphragm with an infinite in-plane rigidity.

The cross sections have the values d/b = 0.5, b/t_f = 20, b/ℓ = 0.25 for the channel, while d/b = 0.25, b/t_f = 40, and b/ℓ = 0.5 for the box girder. In each case $t_f = t_w$.

The interpretation of the symmetrical condition leads to the consideration of half and one quarter of the complete model for the channel and the open box girder respectively. The objective of the exercise at this stage is to examine the similarity in the behaviour of the two models.

For the channel section, the shear centre lies on its horizontal axis of symmetry and outside its vertical web. Hence the central point load, acting on the web/flange junction, does not pass through the shear centre, and consequently twisting deformation occurs.

The study of the deflected shape of the channel section, as shown by the finite element analysis, shows excessive twisting deformation Fig.3.6. The deflection magnification factors in the vertical, longitudinal and lateral directions are 5, 10 and 20 respectively.

When assuming a cut in the lower flange of the box girder the closed section becomes an open one as in Fig.3.2-c, and the centre line of the lower flange gains the freedom to move laterally and rotate.

Fig.3.7 shows the deflected shape of one quarter of the open box girder. In order to facilitate the comparison between the channel and the open box girder the same magnification factors are used. The twisting action of the open box girder is clearly demonstrated through the tendency of each half of the lower flange to move away from the centre line.

The similarity between the behaviour of the lower flange of the channel (Fig.3.6) and the lower flange of the open box girder (Fig.3.7) is apparent.

The bending effect imposed on the upper flange of the open box girder, in the transverse direction, is resisted mainly by the plate flexural stiffness inducing transverse plate bending stresses. The deformation is also associated with a high value of membrane transverse stresses.

Fig.3.8 shows the distribution of membrane transverse stresses across the mid-span of the upper flange of the open box girder. A reference value $\Omega=\sigma_{TC}/\sigma_{NC}$ where σ_{TC} is the maximum membrane transverse stress across the mid span cross section of the compressive flange (upper flange) and σ_{NC} is the corresponding value of the membrane longitudinal stress, is introduced in order to assess the significance of the transverse stresses. An extremely high value of Ω of 2.26 is found for the geometry chosen.

The realization of the twisting action of the open box girder points the way to the logical possibility of dividing a closed box section into two channel sections in order to examine the transverse stresses.

(iii) Box Girder

A non-dimensional form of the box girder geometrical configuration, Fig.3.3-d, is given as follows.

$$d/b = 0.25, \quad b/t_f = 40, \quad b/\ell = 0.5, \text{ and } t_f = t_w.$$

Both the boundary and the loading conditions are similar to those of the open box girder.

A comparison between Fig.3.8 and Fig.3.9 shows the distinct similarity between the distribution of membrane transverse stresses across the mid-span for the open and closed box sections (upper flanges).

For the closed box, the distribution of the membrane transverse stresses, along the upper flange, has its peak value at the centre (Fig.3.10). A rapid decay is noticed when moving away from the centre. This finding indicates that the twisting effect, which creates the compressive transverse stresses, has a localized influence near the centre.

Fig.3.11 displays one quarter of the deflection shape of the closed box girder. The magnification factors used in the vertical, longitudinal and lateral directions are 100, 0.0 and 500 respectively. Ω has a relatively high value of 0.47.

3.4 Discussion

The aim has been to study the variation of the membrane transverse stresses in the flange of a simply supported girder under a concentrated load acting on the web/flange junction.

Different cross sections have been considered for the analysis. Completely symmetrical conditions (geometry, boundary conditions and loading) have been assumed for the case of a box girder.

A review, as outlined below, of the value of this parameter Ω, for different cases, helps to develop a greater understanding of the lateral deformation and the associated transverse stresses. In the case of the I-beam considered, Ω is

equal to –14.5 per cent and the upper flange undergoes lateral expansion with tensile transverse stresses.

When considering the channel section and the open box girder, large lateral deformation, reflecting the twisting effects, is encountered. The similarity between the behaviour of the lower flange of the open box girder and the lower flange of the channel section furnishes a good base for an understanding of the behaviour of the closed box girder. It is through this comparison that the idea of dividing a closed box girder into two identical channels, in order to examine the membrane transverse stresses, becomes feasible.

On examination of the membrane transverse stresses induced in the upper flange of both open and closed box girders, it is found that they have almost the same distribution across the girders.

Although the analysis shows very little difference between σ_T (open section) and σ_T (closed section) in the upper flange, at the same load level, Ω for the open and the closed section is far different and is equal to 2.26 and 0.47 respectively. An explanation of this finding lies in the influence of the torsional deformation, in the case of an open section, which increases the shear lag effect, and hence reduces the value of the longitudinal membrane stresses near the centre. It can be deduced that the high value of Ω, in the case of an open box girder, is attributed to the correspondingly small value of σ_{NC} at the centre-line resulting from the increasing influence of shear lag.

The presence of the transverse membrane stresses at the mid section of the box, as shown by the finite element analyses, indicates that the simple

mechanics of materials approach suggested by Heyman (1982) can furnish a useful yardstick for estimating their magnitude.

It is to be noted that an earlier study (Chapman, et al. 1971) showed the magnitude of transverse stresses in a simply supported box girder to be insignificant when compared with the longitudinal bending stresses. In the present study (Schmidt and Salaheldin, 1990) a relatively high value of σ_{NC} is encountered (0.47). The difference between the two results reflects the influence of the aspect ratio (b/ℓ) on the significance of transverse stresses. While the present analysis assumes the aspect ratio of the box girder flange to be 0.5, the earlier analysis (Chapman, et al., 1971) assumed an aspect ratio of 0.04.

It becomes feasible, due to the previous findings, to propose that the cross section of the box girder can be divided into two identical channels. A simple calculation of the lateral force acting on the flange of the channel, as a result of the vertical load being offset laterally with respect to the channel shear centre, can be used to assess the importance of the membrane transverse stresses in the flange of the associated box girder.

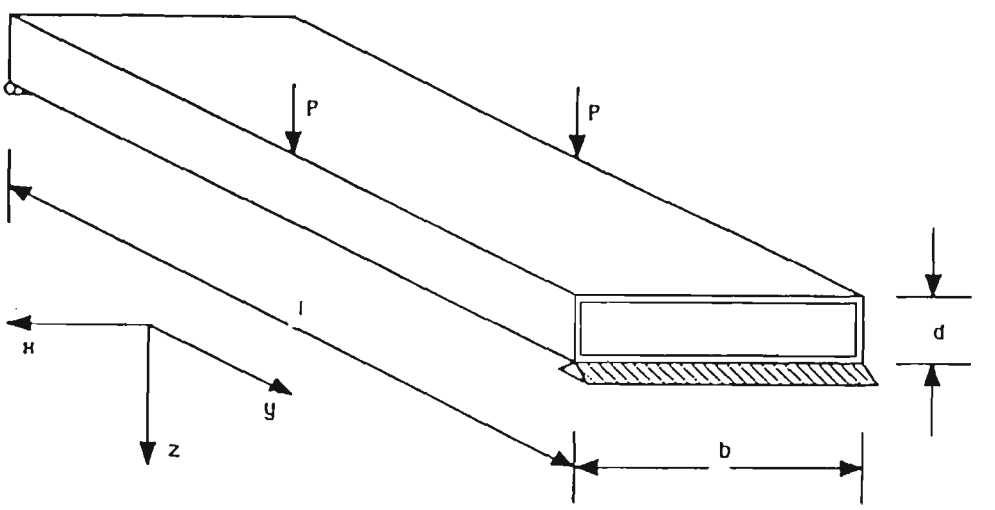

Fig.3.1 Box girder - loading and boundary conditions

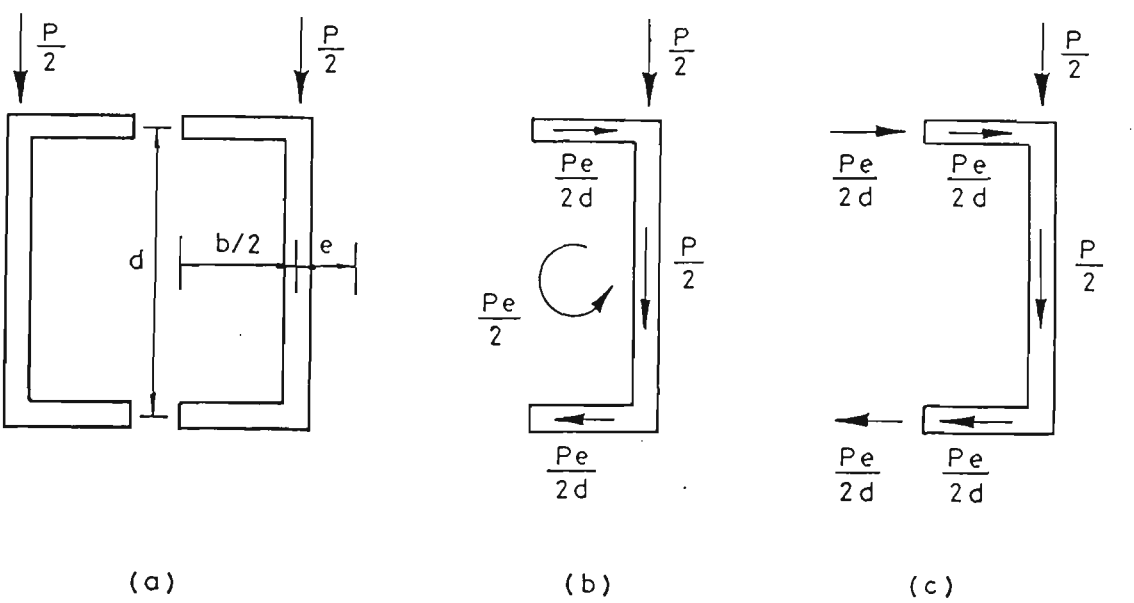

Fig. 3.2 Cross section of box composed of two channels

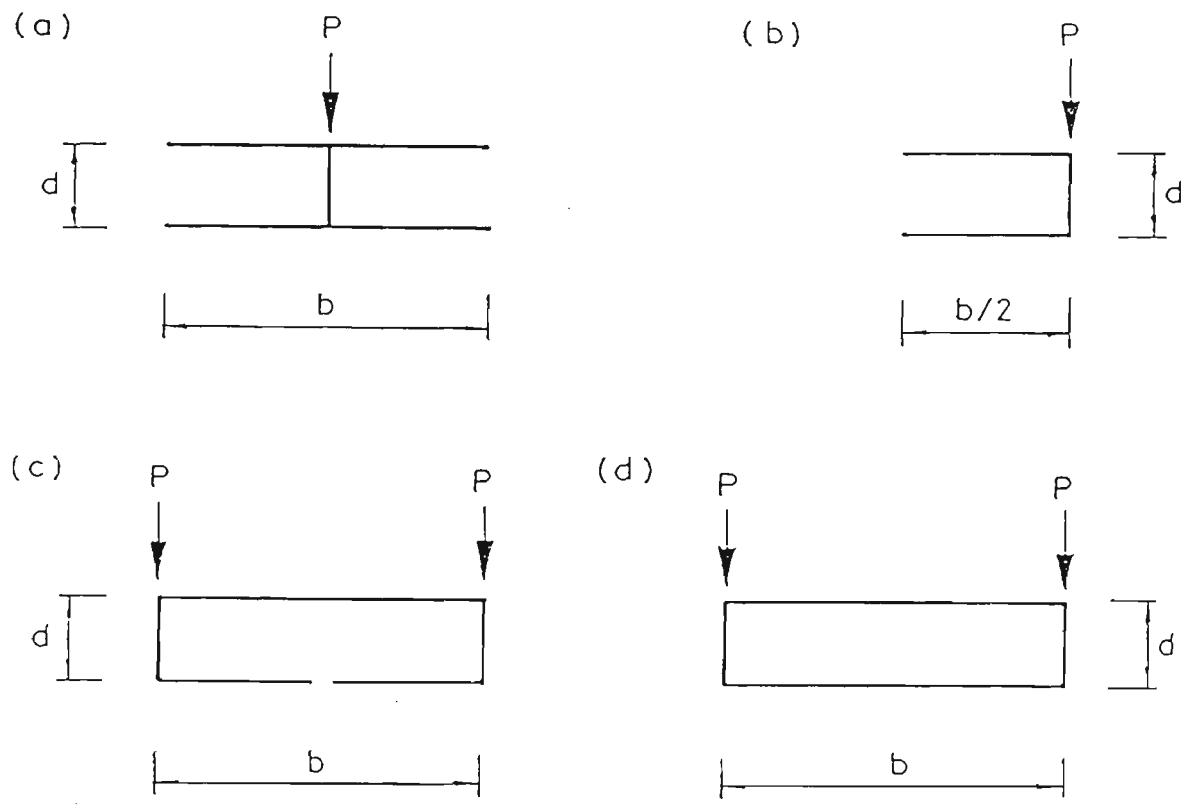

Fig. 3.3 Cross-sections investigated; (a) wide flange I-beam; (b) channel; (c) open box girder; (d) simple box girder

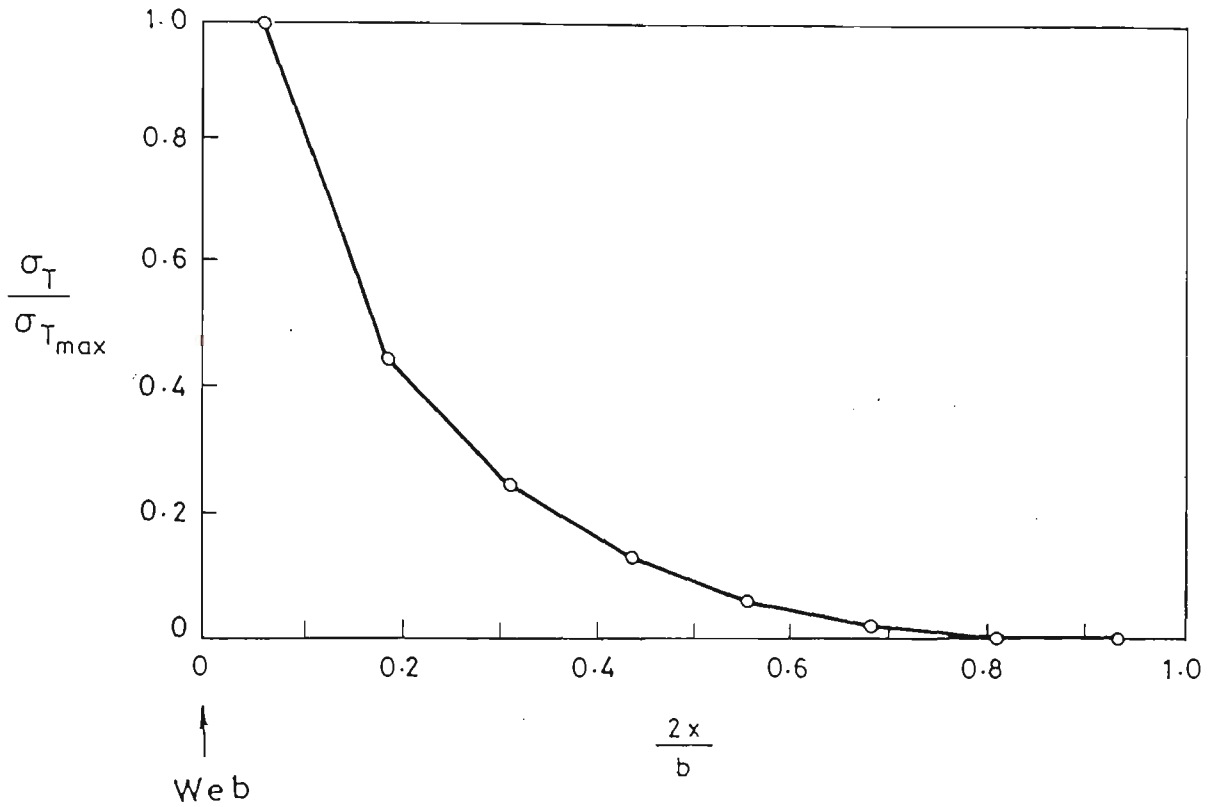

Fig. 3.4 Transverse membrane stress distribution across the upper half flange of an I-beam (mid-span)

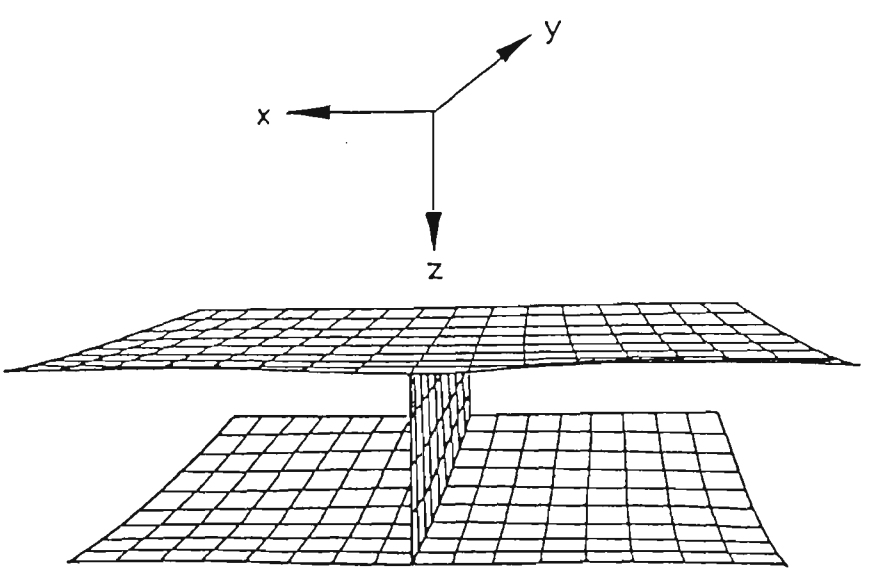

Fig. 3.5 Three-dimensional deflected shape of an I-beam; magnification factors: x 400, y 200 and z 20

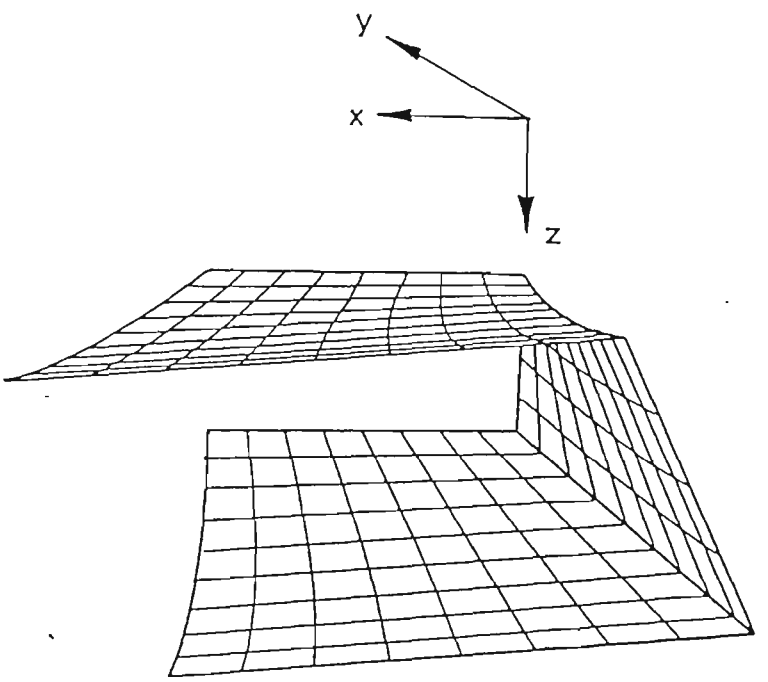

Fig. 3.6 Three-dimensional deflected shape of a channel section; magnification factors: x 20, y 10 and z 5

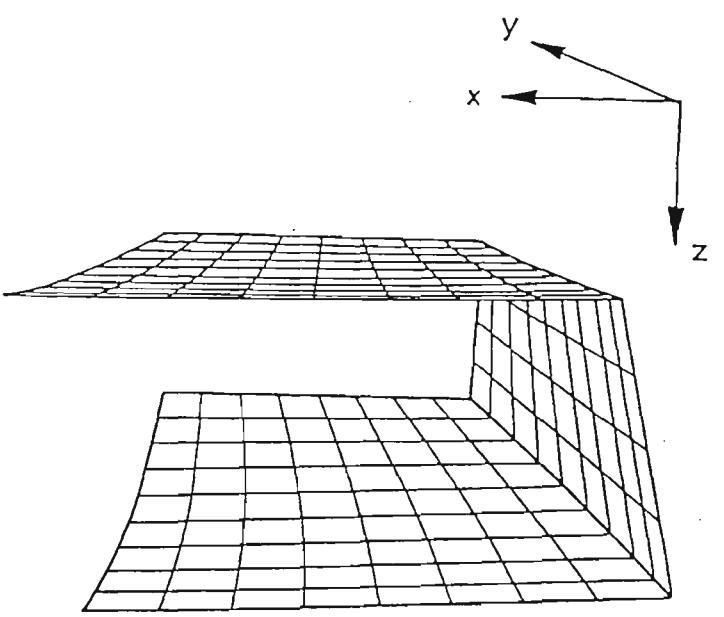

Fig. 3.7 Three-dimensional deflected shape of an open box girder; magnification factors: x 20, y 10 and z 5

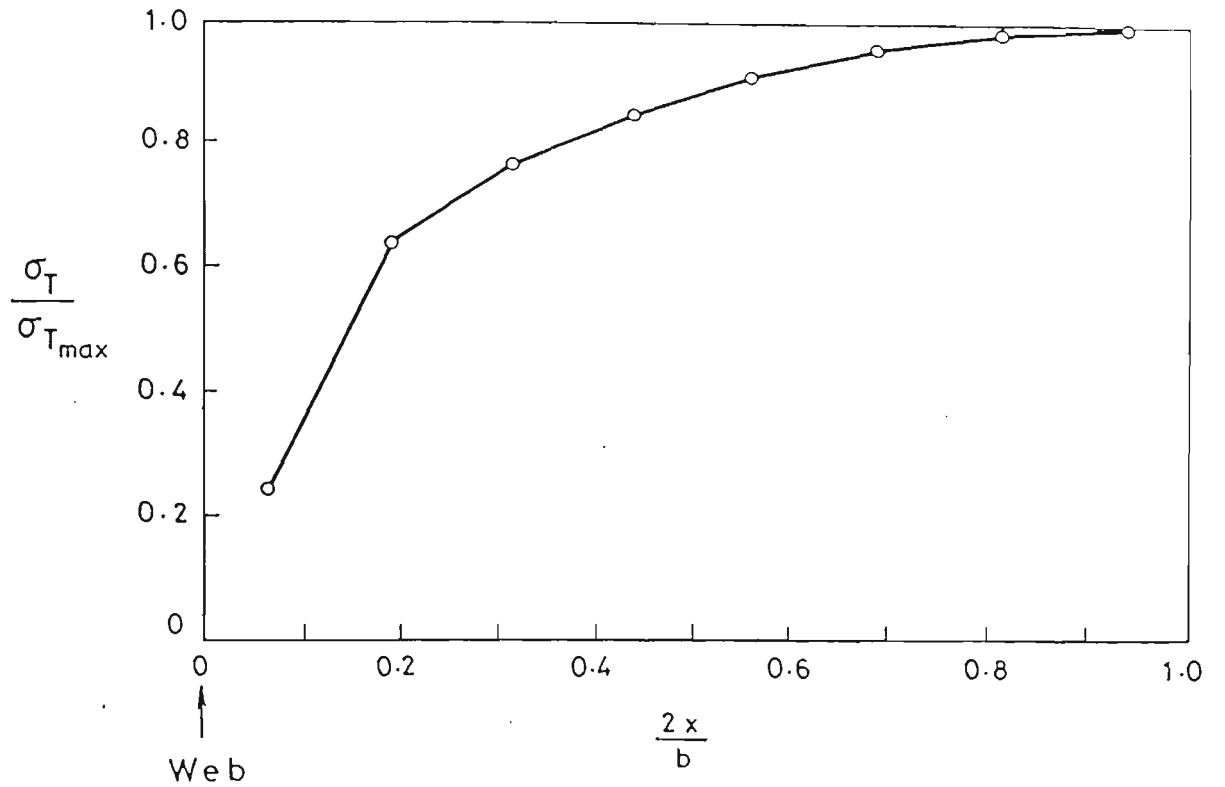

Fig. 3.8 Transverse membrane stress distribution across the upper flange of an open girder (mid-span)

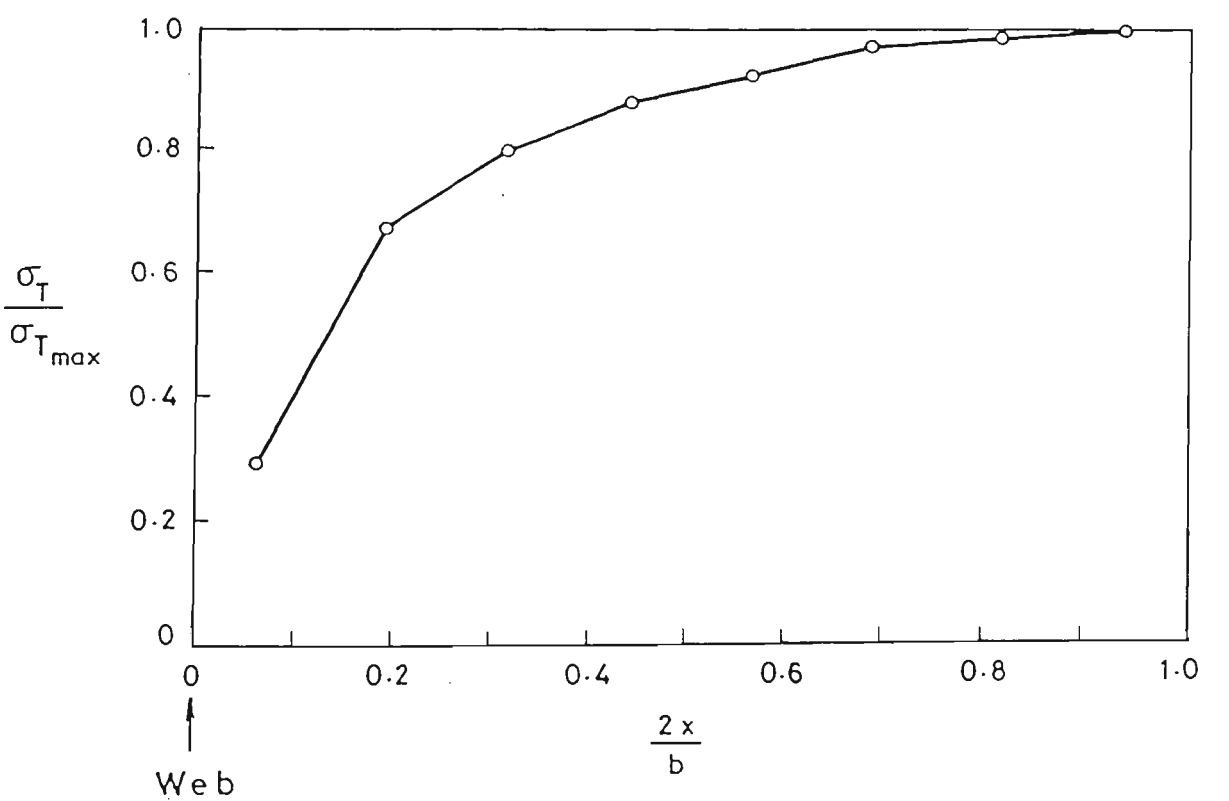

Fig. 3.9 Transverse membrane stress distribution across the cross section of the compressive flange of a closed box girder

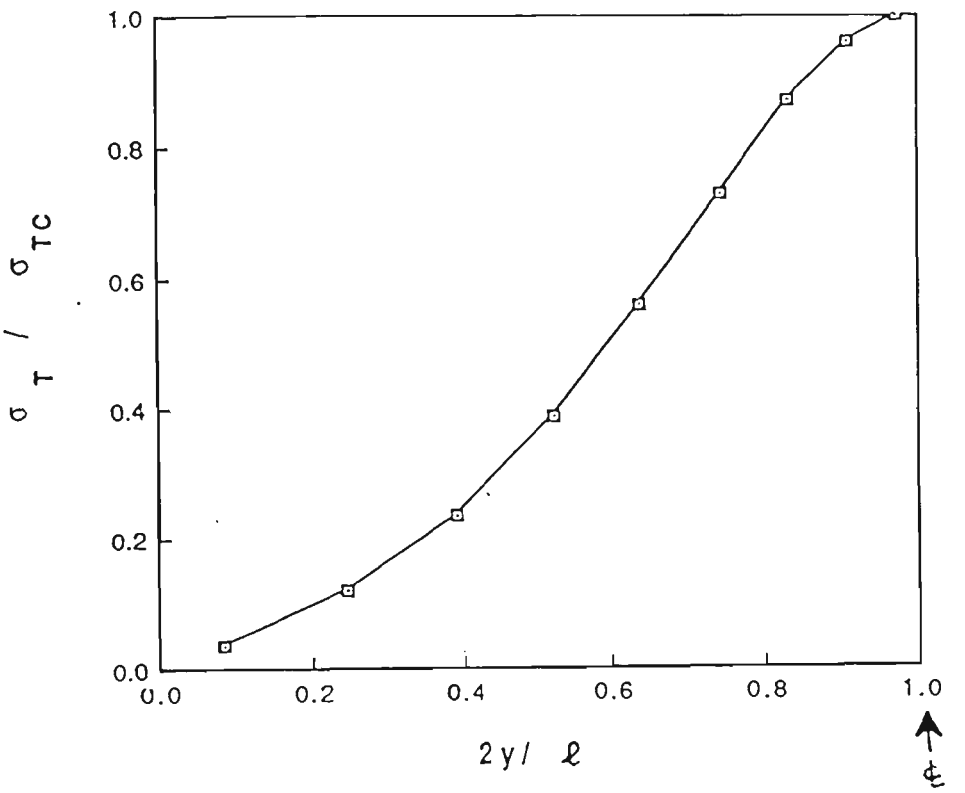

Fig. 3.10 Transverse membrane stress distribution along the centre-line of the flange

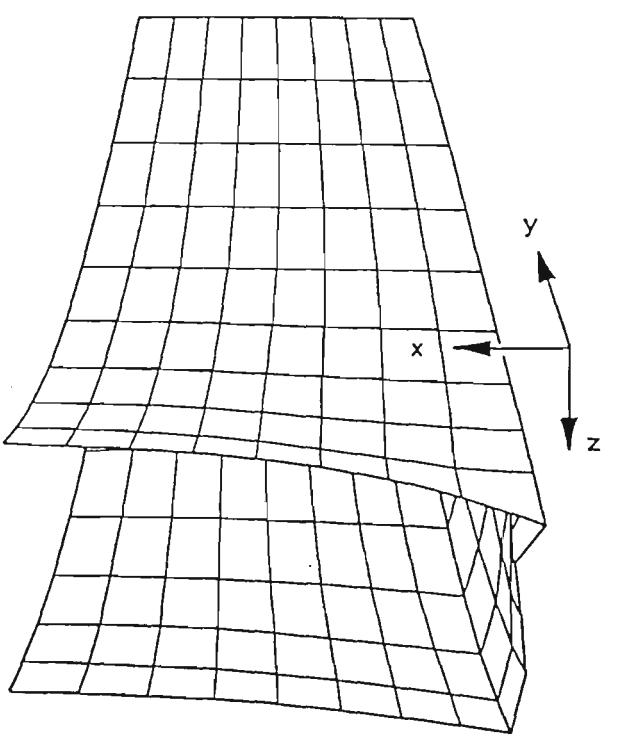

Fig. 3.11 Three-dimensional deflected shape of a box-girder; magnification factors: x 500, y 0 and z 100

Chapter 4

The Effect of Aspect Ratio on Transverse Stresses in Box Girders

4.1 Introduction

There now seems to be sufficient information available indicating that:

(i) Under the geometrical configuration and the loading condition considered in the previous chapter, the flange of a box girder is subjected to appreciable transverse membrane stresses.

(ii) A possible strong correlation between these transverse membrane stresses, which are determined from the finite element analysis, and the force calculated using a simple structural mechanics method of analysis exists.

The question arises as to how the distribution of these transverse stresses can be influenced by the change of geometrical configuration of the box girder. Also, the effect of geometrical configuration changes on the proposed correlation between the transverse stresses and the force determined by a

simple structural mechanics approach needs to be investigated in order to prove the validity of this proposal.

If the relation between the different parameters affecting the distribution and the magnitude of the flange transverse membrane stresses in a simple box girder is established, a simple procedure can be introduced to predict these stresses.

Bearing these objectives in mind, an extensive parametric study, using the finite element approach, is conducted. The details of this study is presented herein.

4.2 Elements of Investigation

a) Range of Parameters

The influence of varying two geometrical parameters is studied, namely, the width to length ratio (aspect ratio) b/ℓ and the depth to width ratio d/b. The range of variation of each of these parameters is chosen to represent the range normally encountered in practice; hence the practical extent and the significance of the problem can be explored.

The study covers an aspect ratio ranging between 0.1 to 1.0. The same range is investigated when considering the depth to width ratio. Fig.4.1 shows the cross section of the simple box girder which is the basis of this analysis, together with the external loading. All the elements of the box girder have the same thickness t.

As the analysis is conducted within a linear elastic frame of reference, the change in the slenderness ratio of the flange does not influence the results, and therefore this parameter has not been considered.

b) Modelling Technique

In all models considered for analysis a full interaction between the elements of the structure was allowed, as no restrictions were imposed on the six degrees of freedom (three translations and three rotations) of the nodes along the web/flange junction line. An end diaphragm of infinite in-plane stiffness but no out-of-plane stiffness was assumed at the simple supports.

In all cases considered, a double symmetry was assumed, and hence one quarter of the box girder was modelled. A concentrated load was applied at the mid-span on each web/flange junction, as shown in Fig.4.1. Young's modulus, E, was assumed to be 200 GPa, and Poisson's ratio, μ, was assumed to be 0.3 for the material.

The aspect ratio of the elements in the finite element models had a limited influence on the lateral force F_i (The lateral force F_i is defined as the integration of the membrane transverse stresses along the centre line of the flange over the side surface area of this flange).

For an extreme case where d/b=1, the number of elements down the web was increased from 4 to 8 elements. As a result of that F_i was reduced by a 1 per cent. In the longitudinal direction, for a b/ℓ ratio of 0.1 (long span), when the number of elements along half the span was increased from 9 to 18 elements, F_i was reduced by a factor of 6 per cent.

In all cases the mesh was biased to allow a fine discretization near the mid span where the central load was acting. The total number of nodes along half the span (due to symmetry) ranged between 10 and 20 nodes, 9 nodes were used across half the flange and the number of nodes down the web ranged between 5 and 9 nodes.

4.3 Numerical Results

a) Transverse Membrane Stress Distribution

The finite element analyses show that the flanges of a box girder, under the loading and boundary conditions described earlier, experience large transverse membrane stresses σ_T. These stresses are compressive in the upper flange and tensile in the lower flange. The influence of the aspect ratio, b/ℓ, and the width to depth ratio, d/b, on the distribution of these stresses along the side mid-surface of the box girder flange is displayed in Figs.4.2 and 4.3.

Fig.4.2 shows the influence of the aspect ratio on the stress distribution along the centre-line of the flange. It can be seen that for low values of the b/ℓ ratio the stresses are almost totally localized at the centre of the span. With increasing b/ℓ ratio the localized stress spreads more evenly towards the support. In all cases, the stresses at the support are equal to zero and have a maximum value at the centre. A comparison between Figs.4.2-a, b and c indicates that the pattern of the stress distribution remains almost unchanged for different values of the d/b ratio.

The influence of d/b ratio on the distribution of σ_T is examined further in Fig.4.3. The plotted results suggest an almost identical distribution of stresses

for a d/b ratio of 0.1 and 0.5. A slight difference is noted when considering a d/b ratio of 1.0. However, in general, the shape of the distribution is preserved. Hence, it can be deduced that the distribution of transverse membrane stresses along the mid-surface of a box girder flange depends principally on the change of the aspect ratio of the flange.

b) Shear Stress Distributions

The distribution of the shear stresses τ_e along the web/flange junction is shown in Fig.4.4. When considering a larger span for a given width ($b/\ell = 0.1$) the shear stress distribution is almost constant along the span length. A decay is noticed near the centre, and the rapid change of the stress distribution leads to a surface free of shear stresses at the mid-span.

For the shorter spans ($b/\ell = 1$) the results display, in general, the same pattern of stress distribution. However, the decay in the stress distribution starts earlier along the span length.

c) Static Equilibrium

As a further part of this investigation, the stresses determined by the finite element analyses are used to examine the static equilibrium of the flange. A cut is made around one quarter of the compressive flange so that it becomes completely detached from the structure (Fig.4.5). The aspect ratio of the flange in question is 0.5 and the d/b ratio of the model is 0.25.

At the simply supported end the flange is acted upon by shear stresses τ_s which have a maximum value at the web/flange junction and a value of zero at the centre. The side mid-surface, along the centre line of the flange,

experiences transverse compressive stresses σ_T which have a maximum value at the centre and a zero value at the support. The side surface, at the centre across the flange, is subjected to longitudinal membrane stresses σ_N which have a maximum value at the web/flange junction and a minimum value at the centre; a distribution which demonstrates the shear lag effect. The fourth side of the flange along the web/flange junction is subjected to shear stresses τ_e which have an almost constant value over the length and drop rather rapidly to zero at the centre.

The examination of these stresses shows that the integrated value of the stresses τ_s over the side surface at the support across the flange is almost equal to the stresses σ_T when integrated over the side mid-surface along the flange at the centre line. The error in this case was 0.4 per cent. Further, the longitudinal stresses σ_N, when integrated over the edge of the surface across the flange at the centre, are found to be almost equal to the force determined when integrating the stresses τ_e over the side surface along the web/flange junction; an error of 0.5 per cent was encountered in this case.

When considering the integral of the stresses acting on each of the four faces of the flange and taking a moment about any point in the plane of the flange, the result is almost zero. The error encountered in this calculation ranged between 1 to 1.5 per cent. It can be concluded, therefore, that the stresses determined by the finite element analyses satisfy the three conditions of static equilibrium in a plane.

4.4 Transverse and Longitudinal Stresses

In order to retain a sense of perspective as to how significant the transverse membrane stresses are, the ratio of these stresses to the associated

longitudinal membrane stresses at the centre of the flange (σ_{TC}/σ_{NC}) is calculated; the influence of the aspect ratio (b/ℓ) on this ratio is then examined.

Fig.4.6 shows how this ratio can be influenced by the change in the aspect ratio, which is achieved by changing the length ℓ while the width b remains constant.

For a high value of the b/ℓ ratio, the transverse membrane stresses reach a value which is several times that of the corresponding longitudinal membrane stresses. With the decrease of the b/ℓ ratio, the σ_{TC}/σ_{NC} ratio decreases. This effect is attributed to the increase of σ_{NC} with the increasing length ℓ. This increase, in turn, is a result of two factors: i) the decline in influence of the shear lag effect as the b/ℓ ratio decreases, which results in higher longitudinal stresses at the centre; ii) the increase of the length ℓ leads to an increase of the applied bending moment. Consequently, longitudinal stresses increase.

The value of transverse stress at the centre of the flange, σ_{TC}, is almost independent of the length ℓ and therefore remains, in general, unchanged as the b/ℓ ratio varies.

When considering shorter spans, the importance of transverse membrane stresses is apparent as these values are significant in comparison with the corresponding longitudinal membrane stresses. For larger spans, the importance of the transverse stresses, although small in comparison with σ_N, cannot be overlooked as the design of local transverse members (i.e. stiffeners etc.) are inevitably influenced by the existence of these stresses.

4.5 Effect of Rigid End Diaphragm

So far, the analyses have been conducted on the assumption of an end support diaphragm which had an infinite in-plane stiffness but zero out-of-plane stiffness. This assumption is achieved by the restraint of vertical and transverse degrees of freedom at the support. The assumption guarantees the condition of no- distortion of the cross-section at the support. It follows that the transverse membrane stresses, at the support, are equal to zero. In a practical situation the end diaphragm will have a finite in-plane stiffness, and this finite stiffness will have some influence on the distribution and magnitude of the transverse membrane stresses. It is important that this influence is investigated, so that the significance of the rigid end diaphragm assumption can be assessed.

An idealized model where the end diaphragm is assumed to have an infinite in-plane stiffness is analysed and compared with another model where the diaphragm is assumed to be a plate with a finite stiffness. The thickness of the diaphragm plate is varied and the influence of this variation on the distribution and magnitude of the transverse membrane stresses is noted. The models have a b/ℓ ratio of 0.5 and a d/b ratio of 0.25. All the models have the same cross-sectional dimensions.

Fig.4.7 illustrates the influence of the diaphragm stiffness on the distribution and magnitude of the transverse stresses along the centre-line of the girder. Values of σ_T/σ_C are given for a rigid diaphragm and for two elastic diaphragms with thicknesses t_d of 5 t_f and t_f, where t_f is the flange thickness. The value of σ_T near the centre is almost independent of the condition of the end diaphragm. At the supporting end, a diaphragm with finite stiffness allows the cross-section distortion to take place. Consequently, tensile transverse stresses

appear in the compressive flange. All the stresses are divided by σ_{TC} and are thereby normalised.

Fig.4.8 shows the effect of increasing the thickness of the diaphragm on the magnitude of σ_T at a station near the support where $2y/\ell$ equals 0.08. When the thickness of the plate diaphragm increases, a rapid decrease of the tensile transverse stresses is noted.

4.6 Stiffened Flange Behaviour

In this study attention has been focussed on the transverse membrane stresses of the flange of a simple box girder. The box girder is assumed to be isotropic with a uniform cross-sectional area (flanges and webs, each of constant thickness). In practice the flange of a box is usually stiffened using longitudinal stiffeners to prevent the local buckling of the compressive flange. It is therefore desirable to examine how the transverse membrane stresses can be influenced as a result of stiffening the flange in this way. In order to investigate the significance of the stiffeners, a model of a stiffened flange (Fig.4.9) was analysed using the finite element technique. The model has a b/ℓ ratio of 0.5, a d/b ratio of 0.25, and the depth of the stiffeners is 0.25 the depth of the web; the thickness of the stiffeners is the same as the thickness of the flange. These stiffeners are an extreme case, chosen to highlight and magnify the influence that the presence of the stiffeners might have.

Fig.4.10 shows the distribution of the flange transverse membrane stresses, along the centre line of the flange, of the stiffened and the unstiffened simple box girder. The two box girders have the same dimensions. The stresses are normalised with respect to σ_{TC} of the simple box girder. It is apparent that the

longitudinal stiffeners have very little influence on the distribution and the magnitude of the flange transverse membrane stresses.

Fig.4.11 shows the distribution of the normalised flange transverse membrane stresses across the flange at the centre. Once again the difference between stresses and the stiffened and the unstiffened flanges is insignificant.

On the other hand the distribution of the longitudinal membrane stresses (Fig.4.12) between the two cases, the stiffened and the unstiffened flange, shows a significant change, as stiffening the flange increases the shear lag effect. It can be deduced from the above discussion that the influence of the longitudinal stiffeners is limited and therefore can be ignored for the determination of the transverse membrane stresses.

4.7 Structural Mechanics Analysis

As discussed in previous chapters, a box girder can be thought of as an assembly of two symmetrical channels (Heyman 1982). Each channel is subjected to a torque which is introduced by virtue of the central load being offset transversely with respect to its shear centre. This torque induces a twisting movement. However, in the case of a box girder, this movement is restrained. Consideration of moment equilibrium can be used to deduce a fictitious force F_s which is necessary to keep the channel in the no-twist position and satisfy the imposed boundary conditions (Fig.4.13).

The analysis shows the value of the fictitious force F_s to be:

$$F_s = \frac{Pe}{2d} \qquad (4.1)$$

where e is the distance from the shear centre to the applied concentrated load.

It will be shown at a later stage that this fictitious lateral force can be used to aid in the prediction of the magnitude of the transverse membrane stresses acting on the longitudinal centre-line of the box girder flange.

4.8 Structural Mechanics and Finite Element Analyses

A lateral fictitious force F_s has been obtained using a simple structural mechanics analysis technique. Also, the membrane transverse stresses along the side mid-surface of the flange of a box girder have been determined as a result of finite element analyses. These stresses, when integrated, result in a lateral (transverse) force F_i over the half span of the girder :

$$F_i = 0.5 \int_A \sigma_T \, dA \qquad (4.2)$$

where $dA = t_f \times dy$

It follows that

$$F_i = \int_{y=0}^{y=b/2} \sigma_T \, t_f \, dy \qquad (4.3)$$

As the thickness of the flange t is assumed to be constant, and the membrane stress is constant throughout the depth, the integration is carried out with respect to the length, ℓ.

The fictitious force F_s can now be compared with the integrated force F_i for various b/ℓ and d/b ratios. Fig.4.14 shows, for different values of d/b ratio (1.0, and 0.1) the ratio F_i/F_s plotted against the b/ℓ ratio.

The plotted points suggest that, in the main, the value of the integrated force F_i is not dependent on the change of the length ℓ ,and, as such the value of F_i/F_s in most cases is not sensitive to the change of geometrical parameters. In fact, for a large practical range of b/ℓ ratios (0.1 to 0.5), the results suggest that F_i is effectively equal to F_s.

With an increasing b/ℓ ratio, there is a reduction in the value of F_i/F_s, which is attributed to the influence of the change in geometrical configuration. This problem will be dealt with at a later stage.

The results shown in Fig.4.14 suggest that the lateral force F_s, which is determined by a simple structural mechanics approach, may be used to predict with reasonable accuracy both the distribution and the magnitude of the transverse stresses along the longitudinal centre-line of a box girder flange.

4.9 Empirical Formula

A correlation between the lateral force F_s and the membrane transverse stresses, σ_T, along the centre-line will now be attempted. An empirical expression is investigated to represent the distribution of these stresses for the range of parameters discussed herein.

The distribution of the membrane transverse stresses along the longitudinal centre-line of the box girder flange, σ_T, is highly influenced by the change of the b/ℓ ratio. Change of the d/b ratio leads to an insignificant change of the distribution. The empirical expression is thereby simplified and becomes a function of the b/ℓ ratio only.

A curve fitting procedure for the results of the finite element analyses produced the following exponential relation, which represents the distribution of σ_T along the longitudinal centre-line of the flange in non-dimensional form:

$$\frac{\sigma_T}{\sigma_{TC}} = e^{-\alpha (1-2y/\ell)^{\beta}} \qquad (4.4)$$

where $\alpha = 1.97(b/\ell)^{-1.4}$ (4.5)

$$\beta = 1.6 + 0.5(b/\ell) \qquad (4.6)$$

The finite element analysis results were used to determine numerical values for α and β for different values of the b/ℓ ratio. Curve fitting exercises to these numerical values resulted in equations (4.5) and (4.6), as shown in Figs.4.15-a and b,which show the graphical representations of α and ß. When the b/ℓ ratio approaches zero, equation (4.5) indicates that α approaches ∞. In this case relation (4.4) suggests a localized concentration of stresses near the centre for a small value of the b/ℓ ratio. It is to be noted that equation (4.4) does not give a zero value at the support. However the value given, in most of the cases, is very small and has a little influence on the general pattern of the stress distribution. When considering the extreme case of b/ℓ=1.0, σ_T/σ_{TC} is equal to 0.14. It is also to be noticed that this equation represents, with a good degree of accuracy, the distribution of membrane transverse stresses near the centre where the influence of these stresses is more significant.

Figs.(4.16-a and b) represent a comparison between the finite element results and these predicted by the formula for two selected values of the b/ℓ ratio for a box girder. It is evident that the empirical formula predicts with a good degree of accuracy the distribution of the membrane transverse stresses along

the longitudinal centre-line of the box girder flange. The same figure also supports the view that the change of distribution of these stresses due to change of the d/b ratio, is very limited and hence can be ignored.

4.10 Prediction of Transverse Stresses

For any particular geometrical dimension and applied load P, the value of F_s can be calculated using simple mechanics principles as equation (4.1) suggests. Also, from Fig.4.14, it is known that $F_i \approx F_s$ (note that allowances can be made for the reduced force F_i when considering a high value of the b/ℓ ratio). Now, substituting F_s for F_i, equation (4.2) becomes:

$$F_S = 0.5 \int_A \sigma_T \, dA \qquad (4.7)$$

The r.h.s of equation (4.7) represents the integration of the transverse membrane stresses along the centre-line side surface of the box girder flange. The distribution of these stresses can be predicted using equation (4.4). Now, considering equation (4.7) and bearing in mind that the geometrical dimensions of the side surface along the flange longitudinal axis are known, σ_{TC} is the only unknown and hence it can be determined. The following equation, which is based on equation (4.4), represents the relation between the b/ℓ ratio and the numerical values of σ_{TC} :

$$\sigma_{TC} = 3.12 \, \Phi \, (b/\ell)^{-0.86} \qquad (4.8)$$

where $\Phi = \dfrac{Pe}{\ell t_f d}$

This relation is used to predict directly the value of the transverse stress at the centre of the flange of a box girder. Alternatively, Fig.4.17 can be used for the

same purpose.It is to be noted that equation (4.8) and its graphical representation (Fig.4.17) represent non-dimensional relations, and, therefore, are valid for any set of units.

As an example of the accuracy of the application of equation (4.8), Fig.4.18 illustrates the influence of the b/ℓ ratio on the parameter η, which is defined as the ratio of σ_{TC} as determined by the finite element analysis to the predicted value of σ_{TC} . The results are given for a d/b ratio of 0.1.

For low values of the b/ℓ ratio η is effectively equal to 1.0, a value which demonstrates the good agreement between the predicted values of σ_{TC} and those determined using the finite element technique. When considering high values of the b/ℓ ratio the values of η are reduced as a result of the influence of the change in geometrical configuration. For b/ℓ=0.1, η is equal to 0.67.

In order to account for the reduction of η when considering high values of the b/ℓ ratio, a non-dimensional parameter K_1 is introduced and equation (4.8) becomes:

$$\sigma_{TC} = 3.12\, K_1 \Phi (b/\ell)^{-0.86} \qquad (4.9)$$

where $K_1 = 0.2\,(b/\ell)^2 - 0.5(b/\ell) + 1.0$

and $$\Phi = \frac{Pe}{\ell t_f d}$$

When equation (4.9) is used the maximum difference between σ_{TC} obtained using a finite element analysis and σ_{TC} calculated from equation (4.9) is 5 per cent for the whole range of the b/ℓ ratios (0.1 to 1.0).

Overall, both the distribution and the magnitude of the membrane transverse stresses can be predicted, to a reasonable degree of accuracy, by using this simple technique. Such information is an aid for a designer in the initial design stage for a box girder.

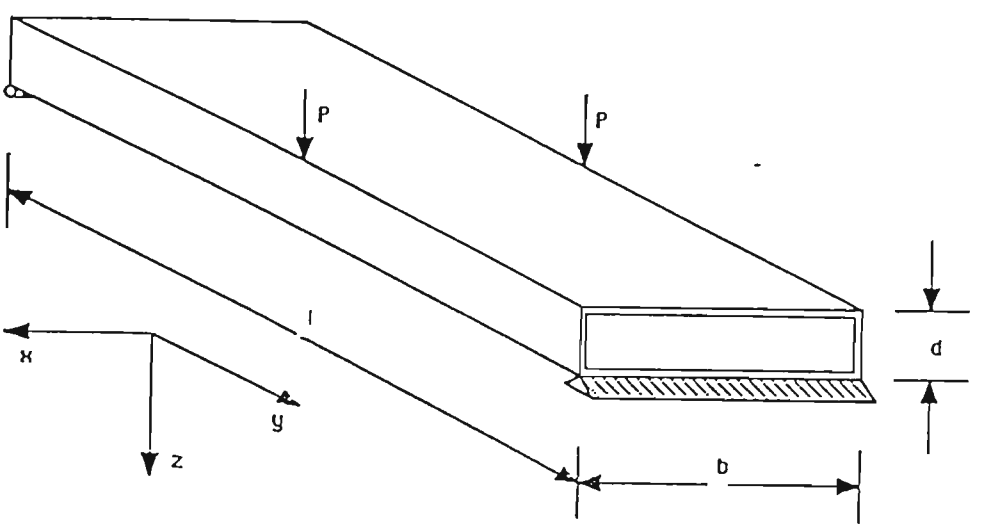

Fig. 4.1 Simple box girder with a rigid end diaphragms

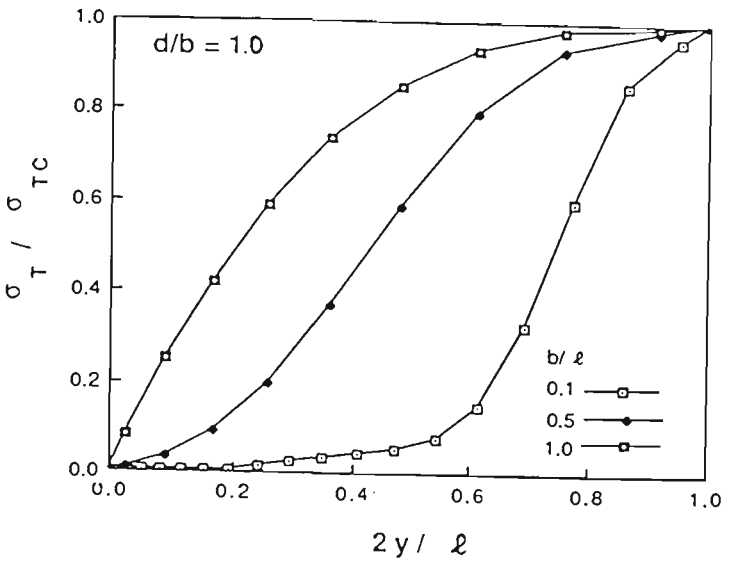

(a)

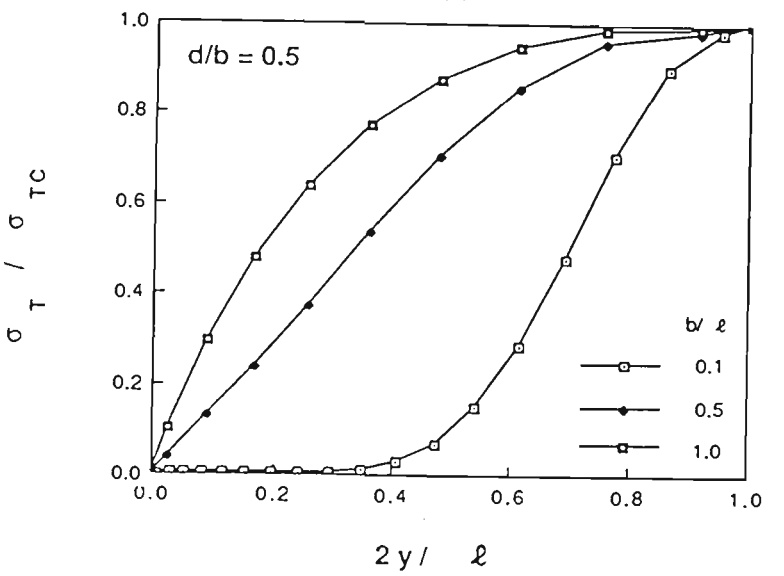

(b)

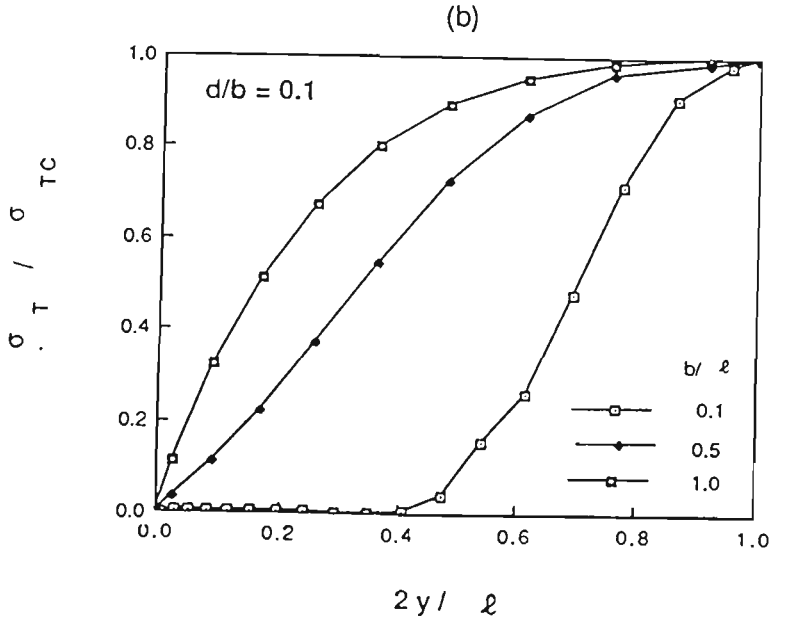

(c)

Fig. 4.2 The influence of b/ℓ ratio on the transverse stress distribution; (a) d/b=1; (b) d/b=0.5; (c) d/b=0.1

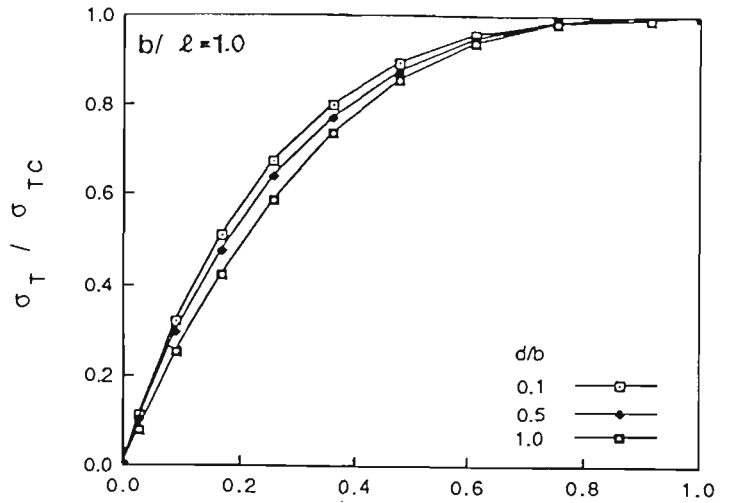

(a)

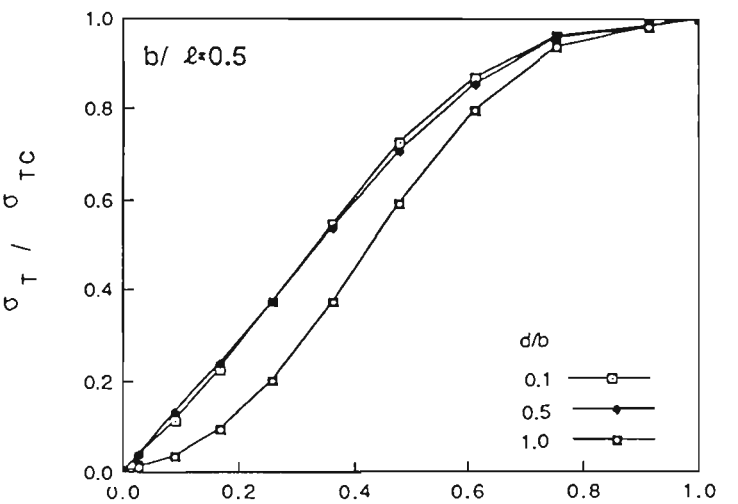

(b)

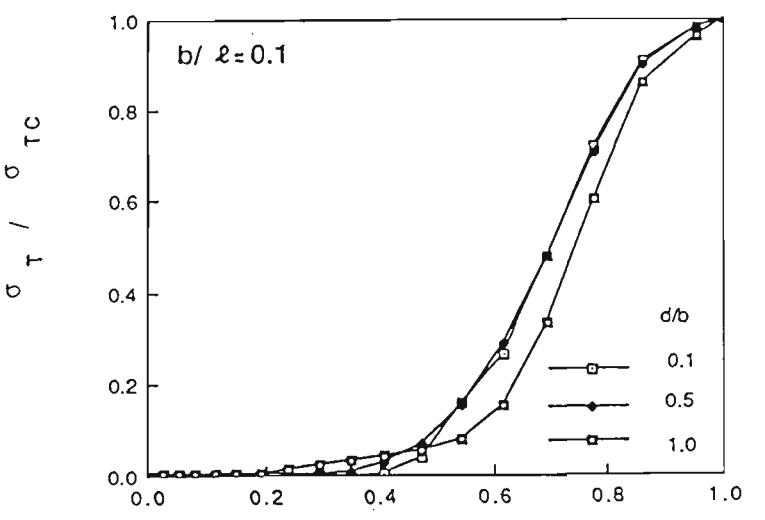

(c)

Fig. 4.3 The influence of d/b ratio on the transverse stress distribution; (a) b/ℓ=1; (b) b/ℓ=0.5; (c) b/ℓ=0.1

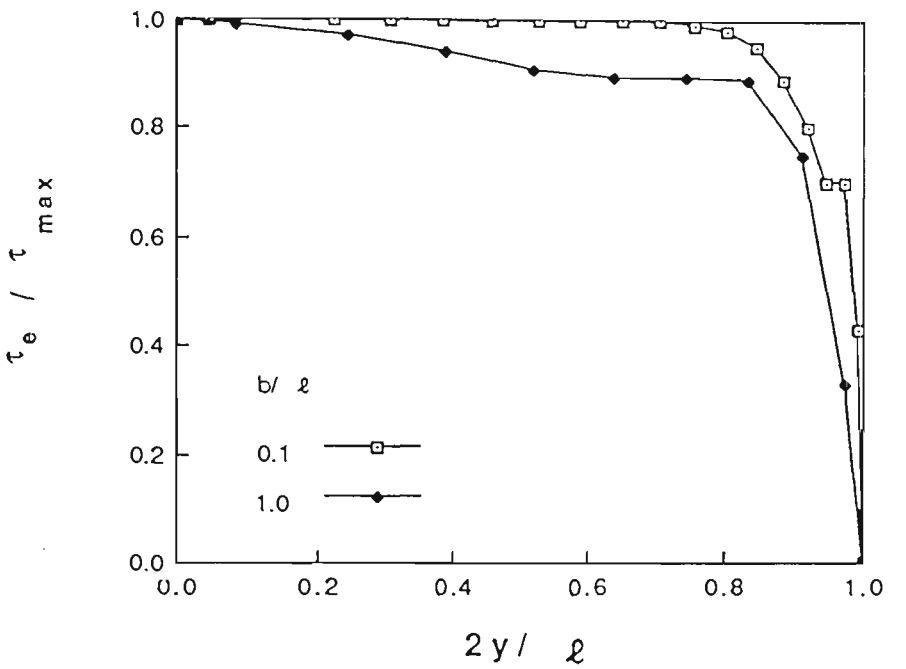

Fig. 4.4 Shear stress distribution along the web/flange junction

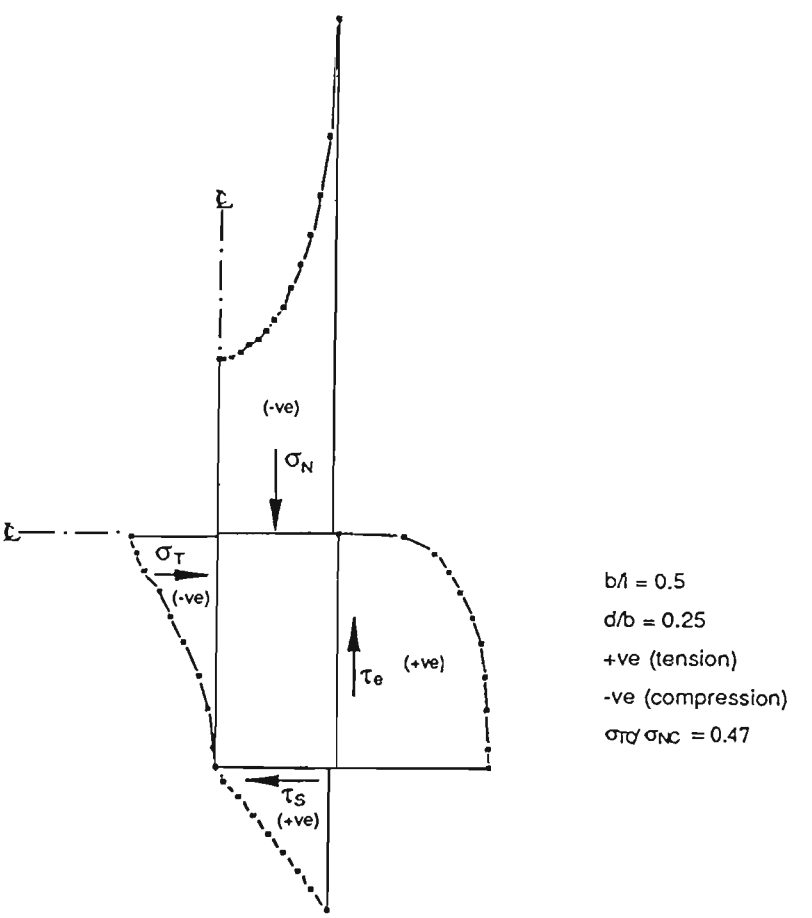

Fig. 4.5 Longitudinal, transverse, and shear membrane stresses on four edges of one quarter of the box flange

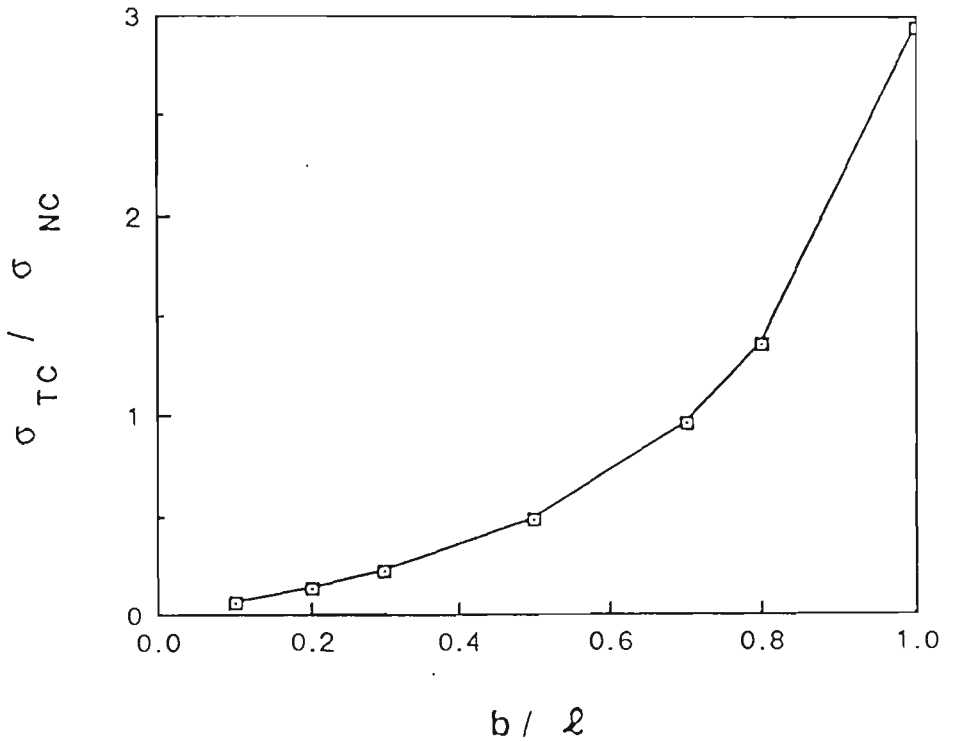

Fig. 4.6 The influence of b/ℓ ratio on the σ_{TC} / σ_{NC} ratio

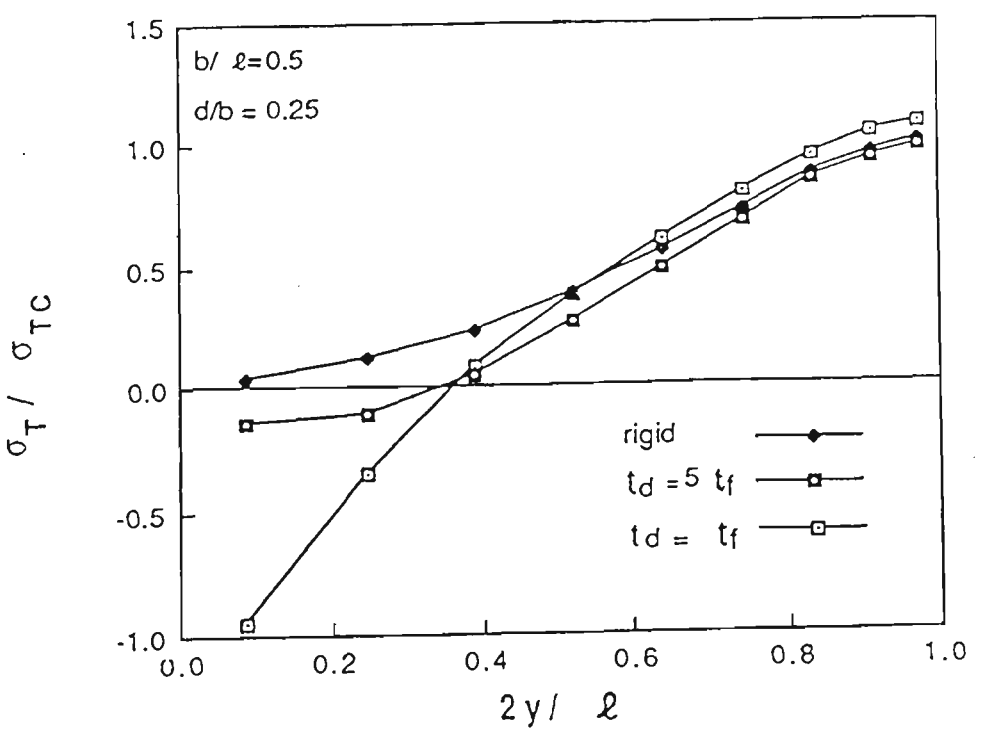

Fig. 4.7 The influence of the end diaphragm condition on the distribution of σ_T

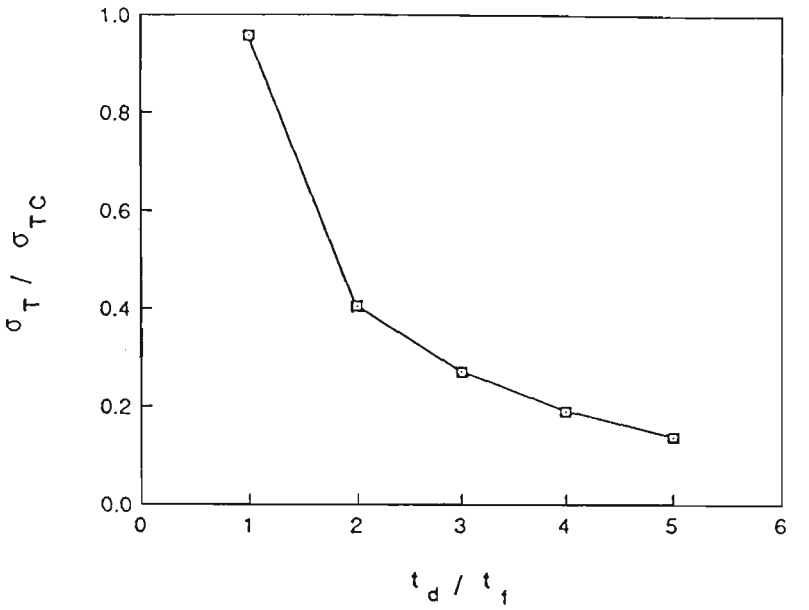

Fig. 4.8 The ratio t_d/t_f versus the transverse stresses at a station near the support

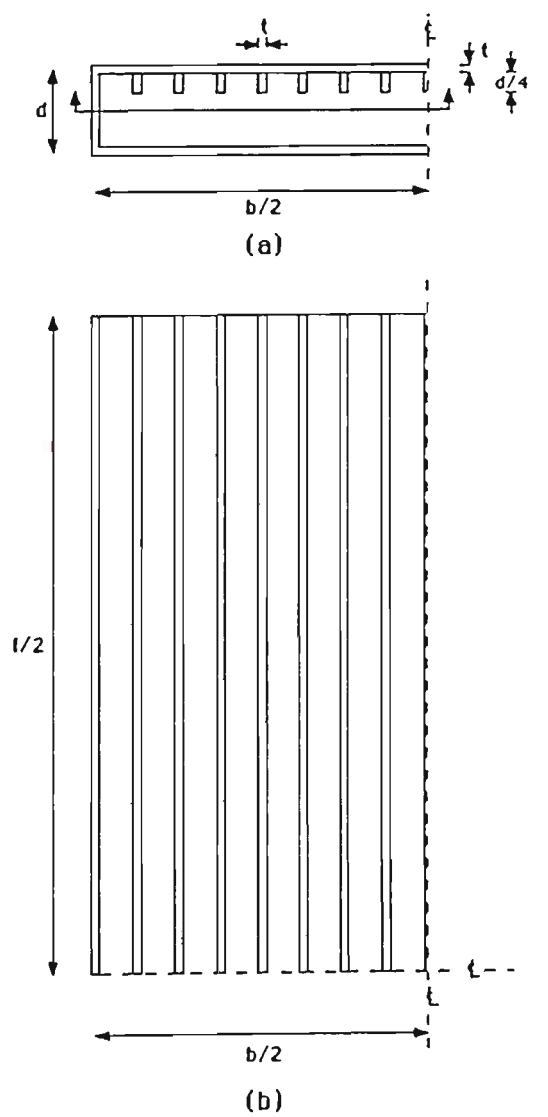

Fig. 4.9 Box girder with stiffened flange

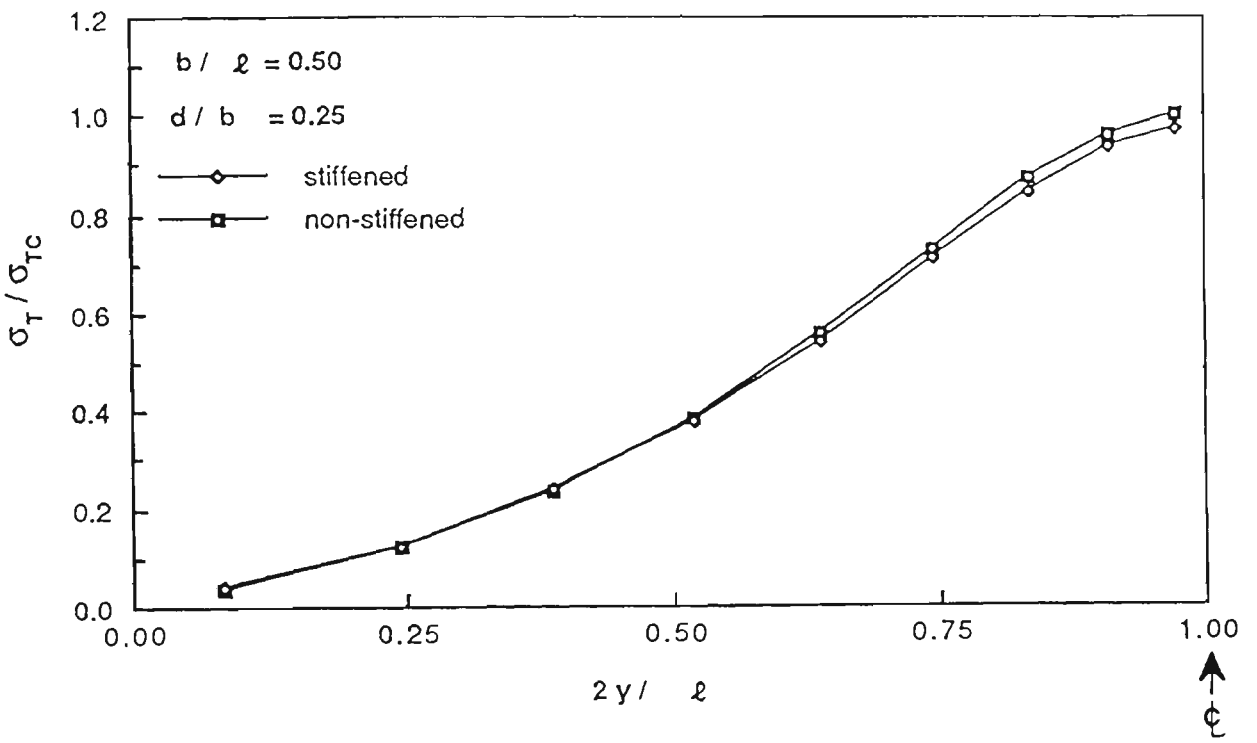

Fig. 4.10 Distribution of transverse membrane stresses along the centre line of stiffened and unstiffened compressive flange

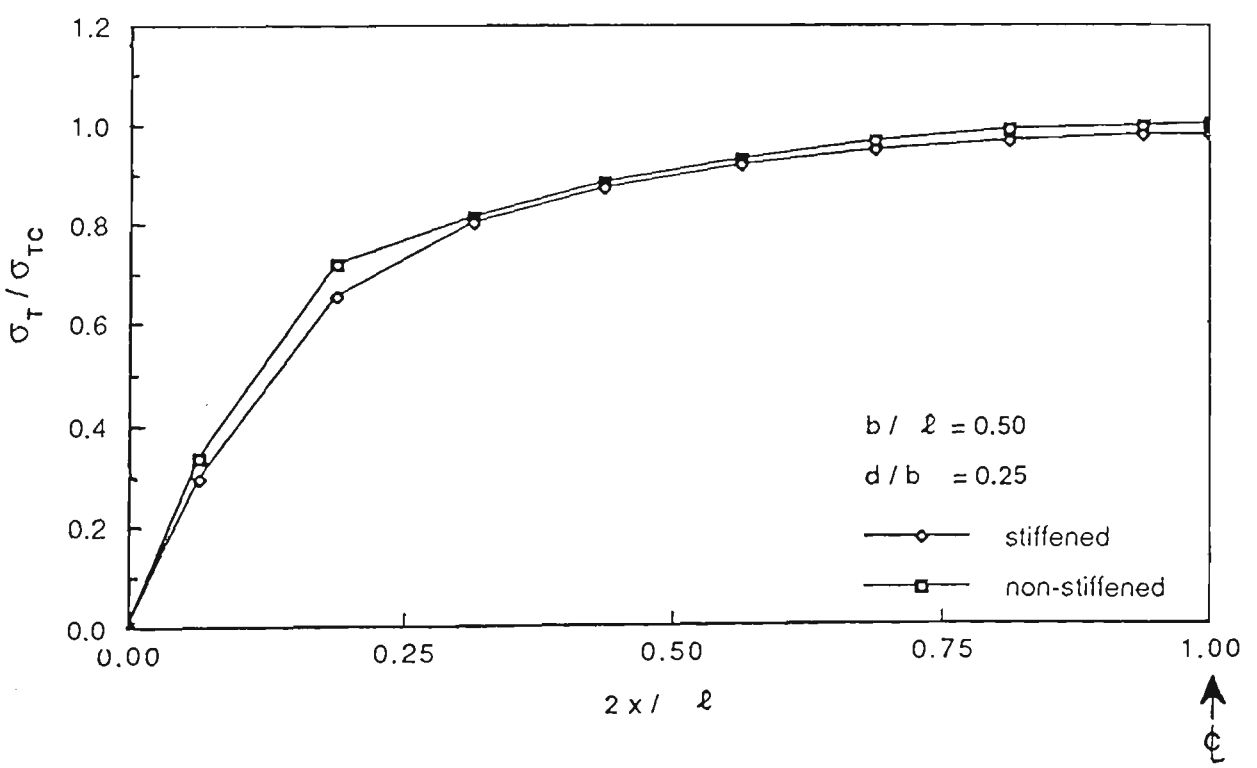

Fig. 4.11 Distribution of transverse membrane stresses across the centre of stiffened and unstiffened compressive flange

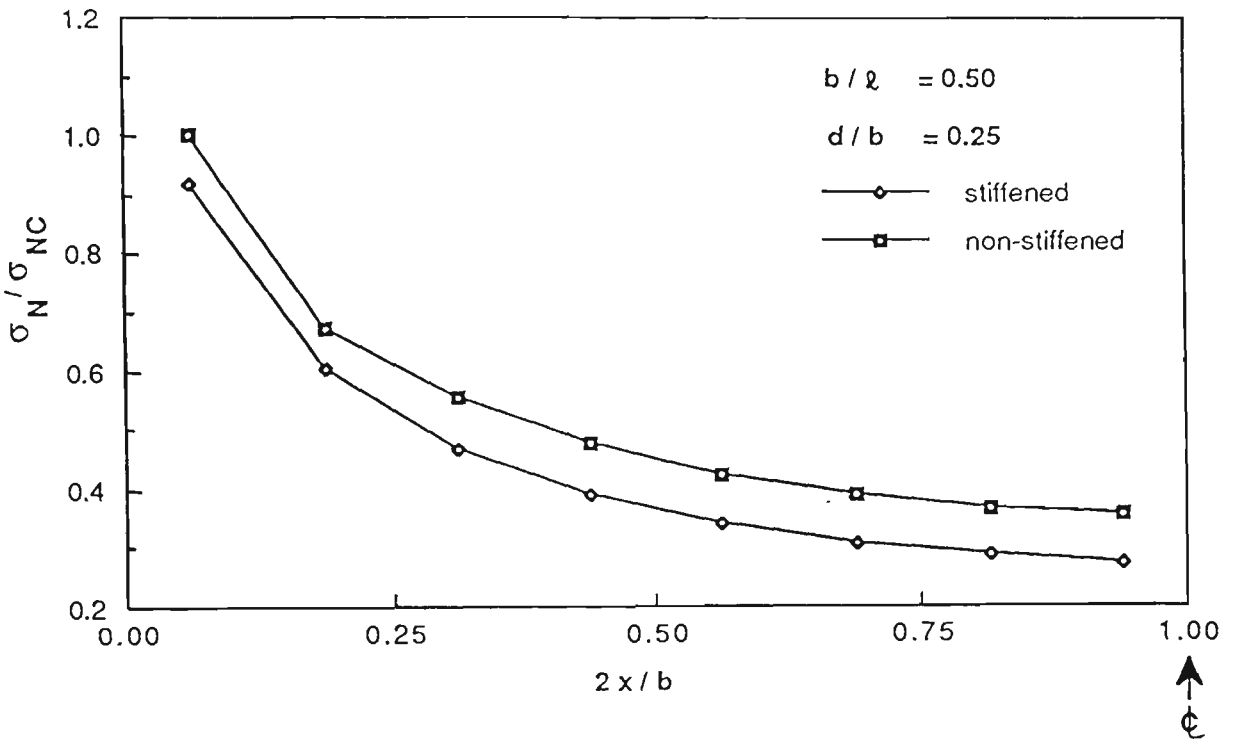

Fig. 4.12 Distribution of longitudinal membrane stresses across the centre of stiffened and unstiffened flange

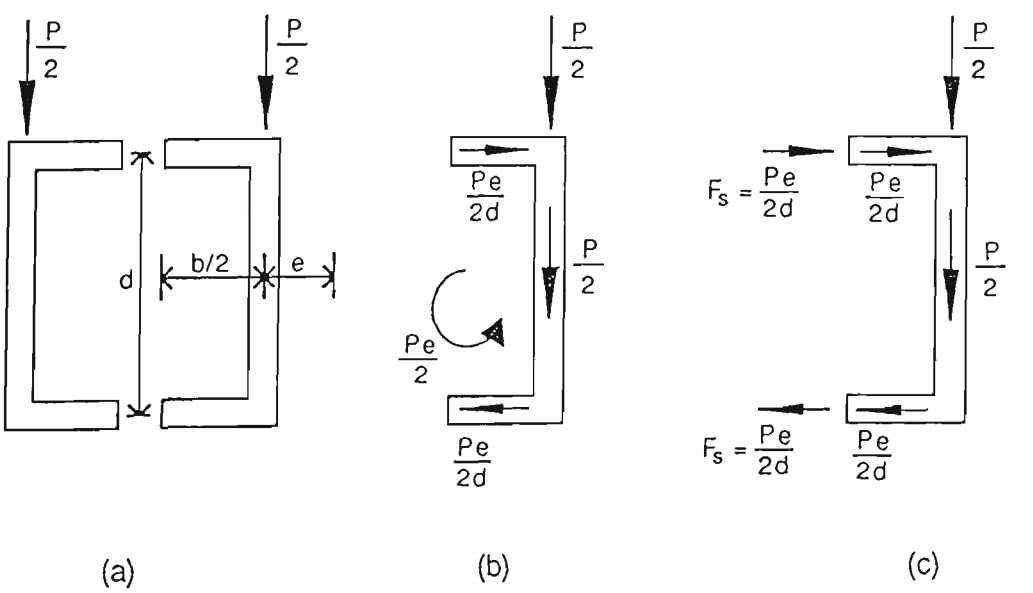

Fig. 4.13 Box girder; (a) section considered as two channels;
(b) forces acting on cross-section of unrestrained channel;
(c) forces acting on cross-section of restrained channel

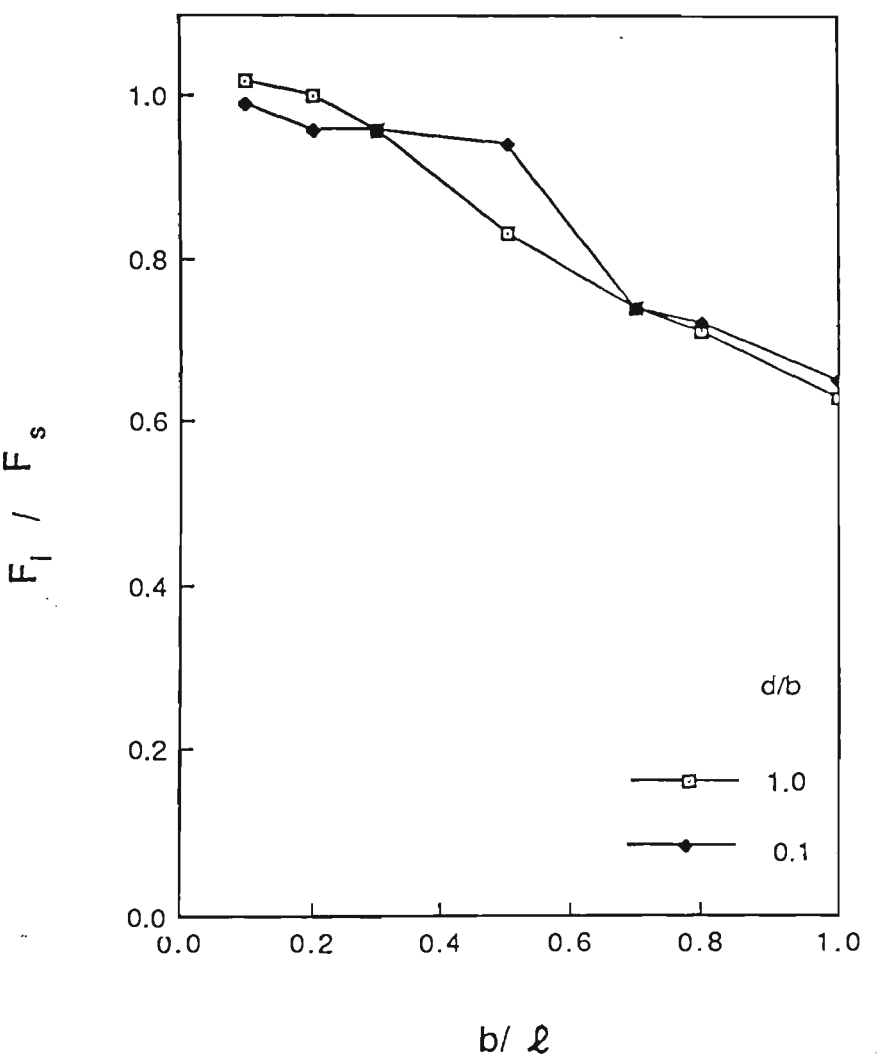

Fig. 4.14 Correlation between F_s and F_i versus b/ℓ

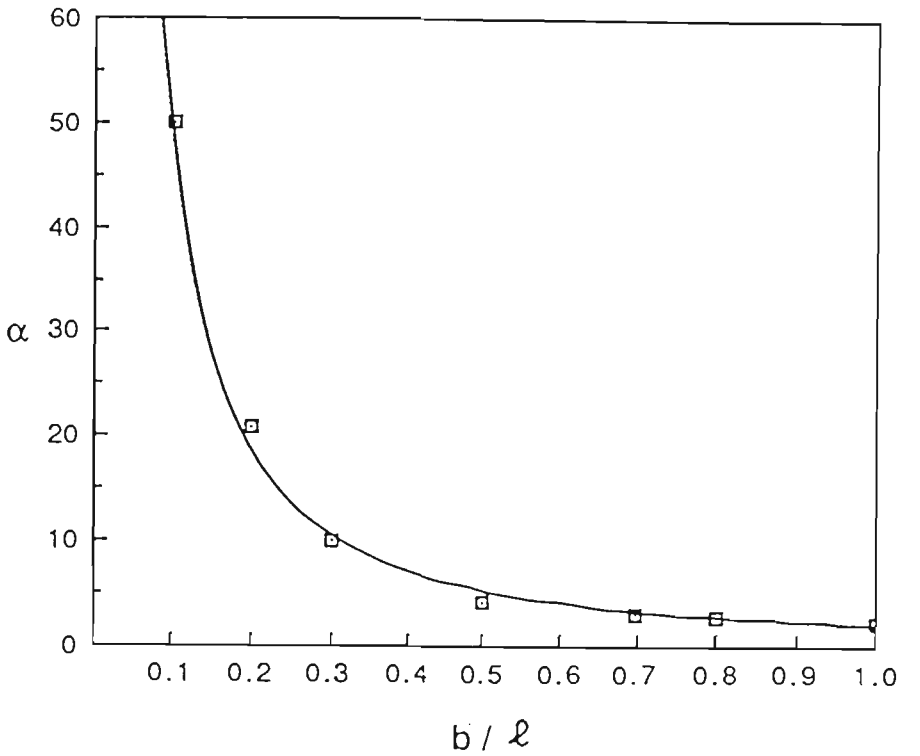

(a)

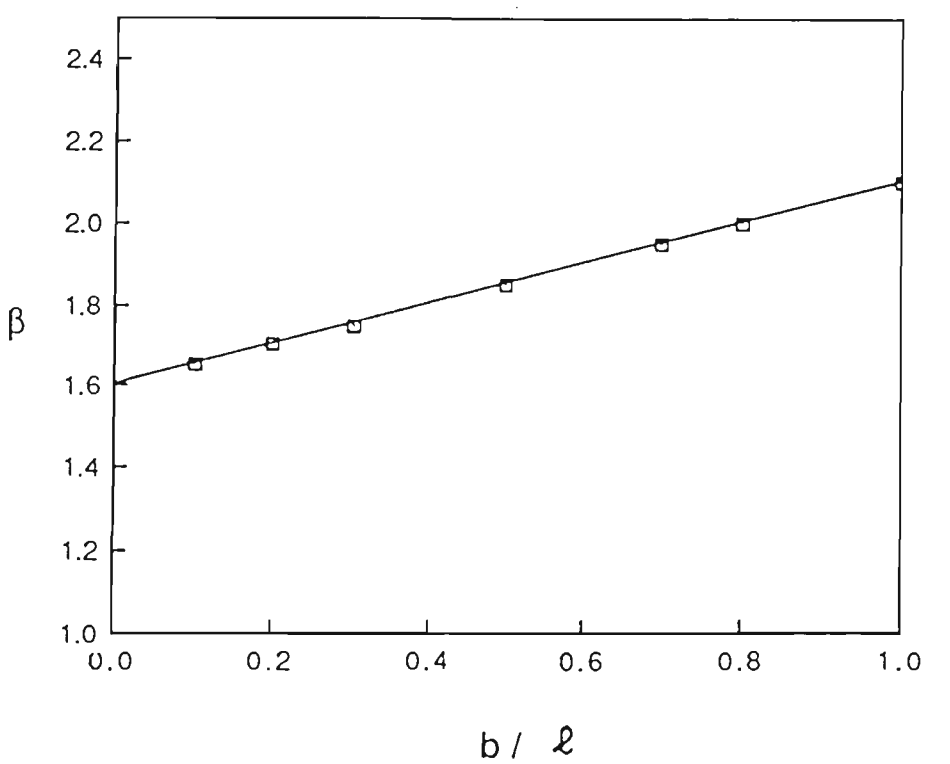

(b)

Fig. 4.15 Graphical representation of empirical parameters; (a) α; (b) β; versus b/ℓ

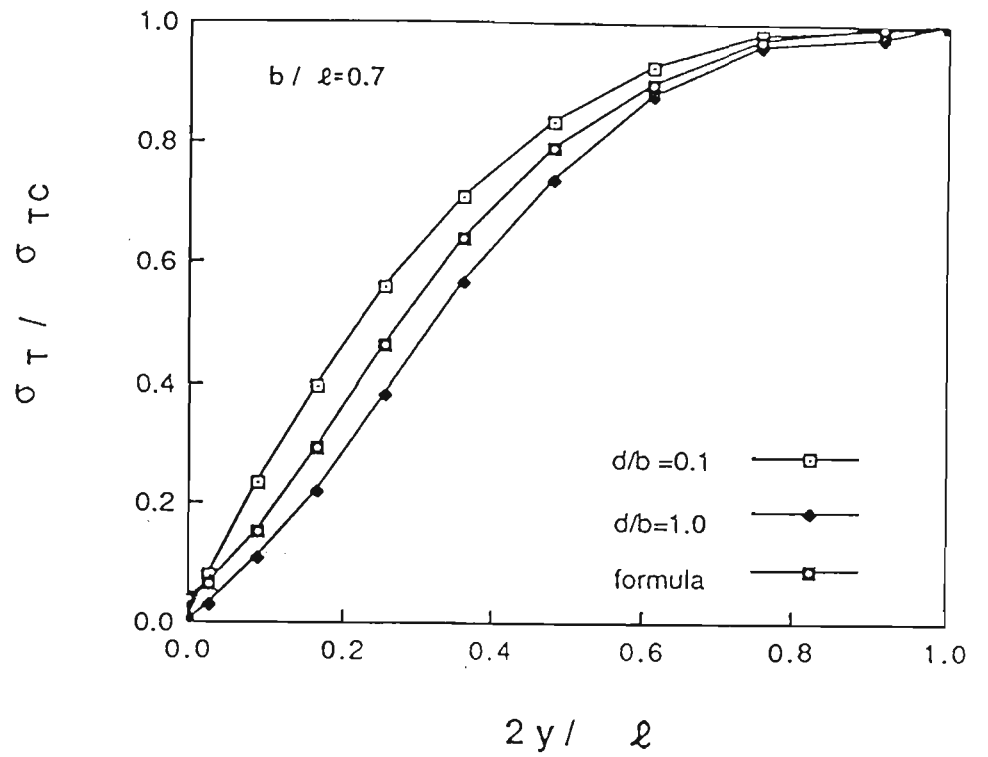

(a)

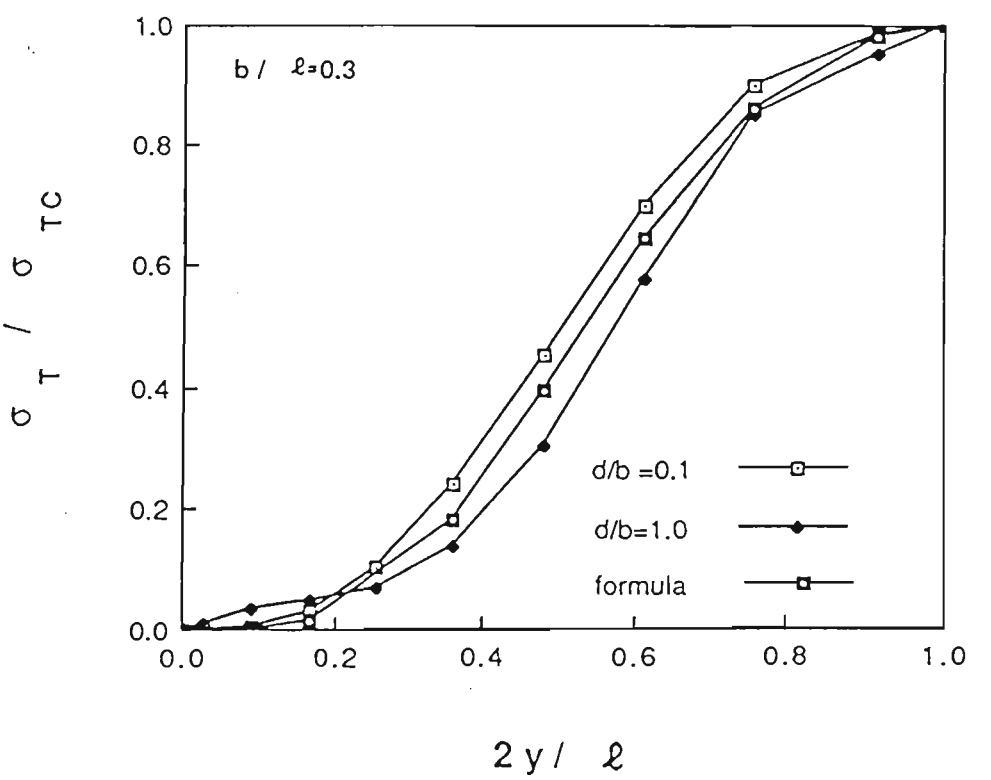

(b)

Fig. 4.16 Distribution of transverse stresses; comparison between finite element and empirical results; (a) b/ℓ=0.7; (b) b/ℓ=0.3

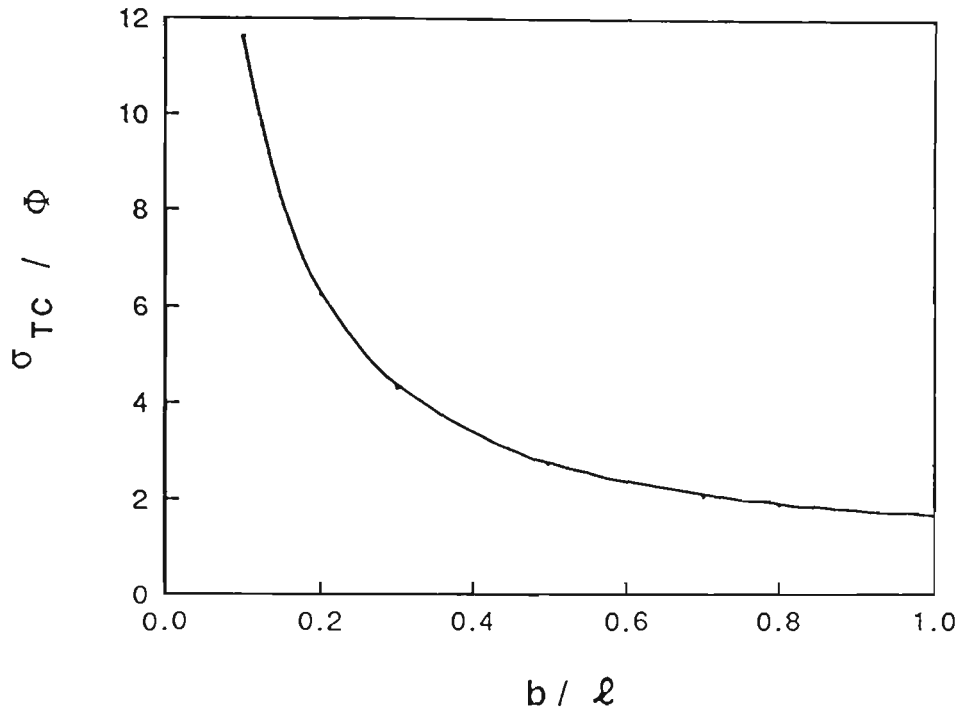

Fig. 4.17 Prediction of σ_{TC} for different values of b/ℓ ratio

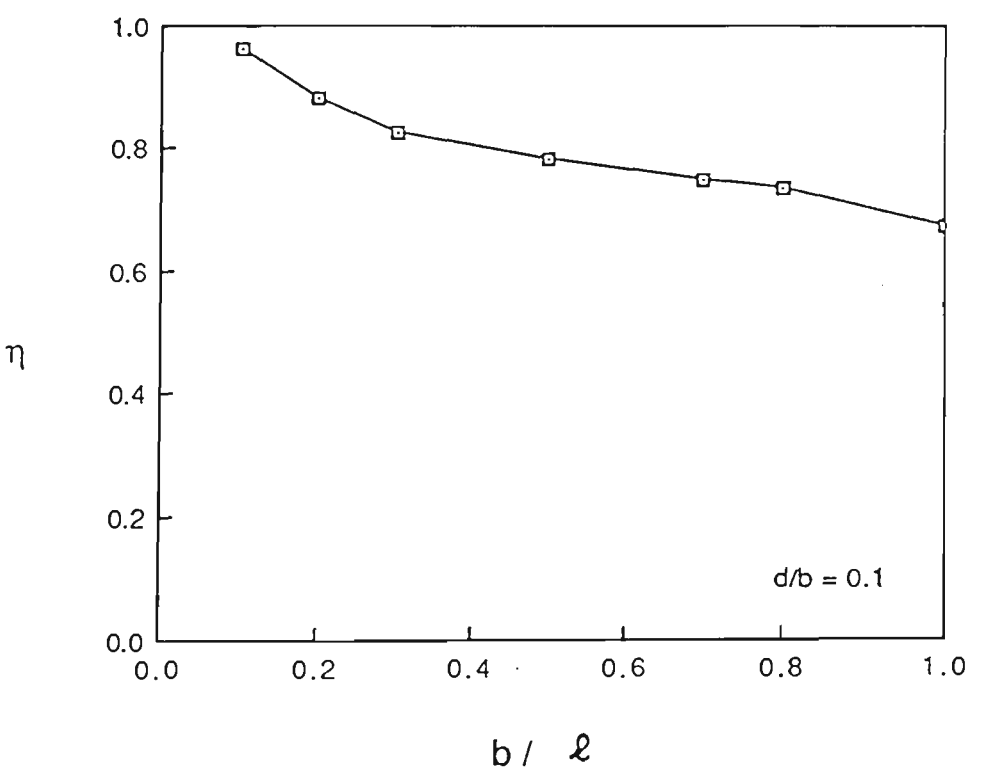

Fig. 4.18 The influence of b/ℓ ratio on the parameter η for d/b = 0.1

Chapter 5

Transverse Stresses in an I-Beam Girder

5.1 Introduction

In the preceeding chapters, the lateral membrane stresses in the flange of a simply supported box girder, under a central concentrated load, have been investigated. As a result of the investigation the influence of the aspect ratio on these stresses has been identified. An attempt to quantify this influence has resulted in the introduction of simple formulae which can be used to predict the magnitude and the distribution of these stresses.

During the investigation, it has been noticed, when considering the finite element analysis results of a simply supported I-beam girder under central concentrated load (Fig.5.1), that the flanges of the I-beam deformed laterally (Fig.3.5). This deformation was associated with transverse membrane stresses. These stresses were tensile in the compressive flange and compressive in the tensile flange.

In order to understand the lateral deformation behaviour of an I-beam section, certain lines of enquiry are pursued. First, the shear stress distribution in an I-beam section is observed.

Fig.5.2-a shows the shear stresses to be zero at the free edge of the I-beam flange and to increase linearly to reach their highest value, in the flange, at the web/flange junction. The shear stresses continue to increase down the depth of the web and reach a maximum value at the neutral axis of the cross-section. Fig.5.2-b displays the shear stress distribution in a channel section. The similarity between the distribution of shear stresses in the channel section and that of the I-beam suggests that an I-beam can be thought of as an assembly of two channels placed back to back.

It is to be noted that the distribution of shear stresses down the depth of the web of the I-beam (Fig.5.2-a) is represented by two identical diagrams, on the right an the left of the I-beam, each represents half the value of the actual stresses. This procedure facilitates the illustration of the similarity between the I-beam and the channel sections. The value of the shear stresses , in the web of the I-section, is obtained by adding the two diagrams together. It is also to be noticed that the thickness of the web of the I-section is assumed to be twice the thickness of the channel web.

Fig.5.3-a shows a cross-section through the centre of the I-beam girder (Fig.5.1). The I-beam is divided into two channels each is acted upon by one quarter of the total load. If the two channels are separated apart each of them will have tendency to twist. This tendency is the result of the vertical load line of action being offset a distance e from the shear centre of the channel.

Now to bring the two channels back together so they form the original I-beam cross section, there must be a lateral force which keeps the channels in the no-twist-position. This lateral force, as illustrated in Fig.5.3-c, is tensile in the compressive flange and compressive in the tensile flange. This fictitious force F_s can be calculated from equation (4.1).

The resemblance is apparent of the lateral deformation behaviour of the two channels, each of them representing half of a box girder (Fig.4.13), with the two halves of an I-beam, each of which is a channel (Fig.5.2). This resemblance suggests that it may be possible to extend the simple analysis approach, by which the transverse membrane stresses are determined in a box girder, to evaluate these stresses in the flange of an I-beam girder.

5.2 The Analysis of Lateral Stress in an I-Beam Girder

An extensive parametric study, using the finite element technique, was conducted in order to investigate the transverse membrane stresses in the flanges of an I-beam girder. The analysis employs a four-noded flexural extensional quadrilateral shell element (MacNeal, 1978).

5.2.1 Geometrical Configurations

The objective of the study is to investigate the influence of geometrical configurations on the magnitude and the distribution of flange transverse stresses. Special attention is given to the effect of the aspect ratio (the width to length ratio) which varies between 0.1 to 1.0. Also, the influence of the change in the depth to width ratio is studied. The change in this ratio covers the range between 0.1 to 1.0. The thickness of the I-beam web is assumed to be twice the thickness of the flanges (the I-beam will be looked at as an assembly of

two channels having the same thickness). Both the compressive and the tensile flanges have the same thickness t.

The wide range of geometrical configurations enables observation of the change of the behaviour patterns, and thereby allows its significance to be assessed.

5.2.2 Analysis Assumptions

The I-beam girder is assumed to be simply supported at both ends and subjected to a concentrated load at the centre (Fig.5.1). The lateral and vertical degrees of freedom are restrained at each of the simply supported ends. This restriction simulates the assumption of an end rigid diaphragm which does not allow in-plane deformations. The question of how realistic this assumption is, will be considered during the investigation.

No restrictions are imposed on the six degrees of freedom of all the nodes along the web/flange junction line. This assumption leads to a full interaction between the flange and the web.

In line with the previous finite element study of box girders, this study assumes linear elastic behaviour. Young's modulus, E, is assumed to be 200 GPa, and Poisson's ratio, μ, is assumed to be 0.3 for the I-beam material.

The number of nodes along the span is increased up to 37 with the decrease of the aspect ratio; a similar increase of the number of nodes across the web occurs when the d/b ratio increases. For d/b equal to 1.0, 9 nodes are employed. The number of nodes across the width of the flange remains

constant (17 nodes) as the flange width remains unchanged during the change in the parameters.

The change in both the aspect ratio and the depth to width ratio is achieved by changing the length and the width respectively.

Due to the assumption of double symmetry, only one quarter of the I-beam girder is modelled. The modelling technique employs a biased mesh towards the area of stress concentration near the applied central load.

5.3 Finite Element Results

5.3.1 Lateral Membrane Stress Distribution

(a) Stress Distribution Across the Flange

Fig.5.4 shows the distribution of the transverse membrane stresses across the flange of the I-beam section at the mid-span. The finite element stresses are calculated at the centre of the element and are shown as marked dots. These stresses have a value of zero at the free edge of the flange and this value increases when moving towards the web/flange junction (x is measured from this junction). The maximum value of the transverse stresses at the centre σ_{TC} is extrapolated. The extrapolation is achieved by a curve fitting procedure of the finite element results employing a polynomial of the third degree. This procedure is dictated by the rapid increase of the stress near the web/flange junction.

A comparison between Fig.5.4-a and Fig.5.4-b shows that the change of the aspect ratio has very little influence on the distribution of the transverse

membrane stresses across the flange of an I-beam girder. All the stresses are divided by σ_{TC} and are thereby normalised.

(b) Stress Distribution along the Span

Figs.5.5-a, b, and c show the distribution of the transverse membrane stresses along the web/flange junction line, for different values of the b/ℓ and the d/b ratios. The distance y is measured from the simply supported end. The transverse stress is equal to zero at the support; its value increases when moving towards the centre. This pattern of stress distribution is observed in all models within the considered range of the b/ℓ and the d/b ratios. The decrease of the aspect ratio results in a greater stress concentration at the centre; for an aspect ratio equal to 0.1, the transverse membrane stresses are almost totally localised at the centre (Fig.5.5-c). The depth to width ratio however, has a very limited influence on the stress distribution. For a d/b ratio ranged between 0.1 to 0.5, the analyses show an almost identical distribution of stresses, for the same value of aspect ratio. When the d/b ratio is equal to 1.0, the stress concentration, towards the centre of the girder, is slightly increased over that for lower d/b ratios

It is to be noted that some irregularities occur in the distribution of transverse membrane stresses along the web/flange junction line, in form of a drop or an increase of stresses just before the centre. These irregularities are unnoticeable for low values of the aspect ratio (b/ℓ= 0.1). When Poisson's ratio is reduced to zero these irregularities disappear and a smooth distribution of transverse of stresses is displayed (Fig.5.6). It can therefore be deduced that these irregularities can be attributed to the aspect ratio influence and Poisson's effect. Overall these irregularities are limited in their magnitude and, therefore, do not upset the general pattern of the distribution of transverse

stresses; neither do they have a significant influence on the predicted magnitude of these stresses.

From the above discussion it can be deduced that the aspect ratio has a great influence on the distribution pattern of the transverse membrane stresses along the web/flange junction line of an I-beam girder. It can also be deduced that, within the range of parameter investigated herein, the depth to width ratio has an insignificant influence on the distribution of these stresses and, therefore, can be ignored.

5.4 Evaluation of Transverse Stresses

5.4.1 Distribution of Transverse Stresses

The study of the pattern of distribution of transverse membrane stresses along the web/flange junction of an I-beam girder, which was obtained from the finite element analysis, reveals the similarity of this distribution with the distribution of the transverse membrane stresses along the centre-line of a box girder flange. An attempt is made to use the formula, which was introduced earlier to predict the distribution of transverse stresses in box girders (equation 4.4), to evaluate the distribution of transverse membrane stresses in the flange of an I-beam girder.

Figs.5.7-a, b, and c show the stress distribution predicted by the formula compared to the stress distribution obtained from the finite element study of the I-beam girders. The stresses are divided by σ_{TC} (the value of transverse membrane stresses at the centre of the flange) and are thereby normalised. The full range of parameters is presented; b/ℓ and d/b ranged between 0.1 to 1.0.

The comparison shows that the formula can predict, with a good degree of accuracy, the transverse membrane stress distribution along the web/flange junction-line.

5.4.2 Magnitude of Transverse Stresses

Now that the distribution of the transverse membrane stresses can be obtained, using equation (4.4), the magnitude of these stresses can be evaluated if the value of σ_{TC} is determined. Equation (4.8), which was used to predict the value of σ_{TC} in the flange of a box girder, is used to determine the value of σ_{TC} in the flange of an I-beam girder.

Fig.5.8 shows the parameter η, which is defined as the ratio of σ_{TC}, determined using the finite element analysis, to σ_{TC} predicted by equation (4.8). The values of σ_{TC} predicted appear to be in good agreement with those determined using the finite element analysis. A drop in the value of η is noted for high values of the b/ℓ ratio. This effect is attributed to the change in geometrical configuration.

In order to account for the reduction of η when considering high values of the b/ℓ ratio a non-dimensional parameter K_2 is introduced and equation (4.8), which predict the maximum transverse stress σ_{TC}, becomes:

$$\sigma_{TC} = 3.12\, K_2 \Phi (b/\ell)^{-0.86} \qquad (5.1)$$

where $K_2 = 0.19\,(b/\ell)^2 - 0.52(b/\ell) + 1.15$

and $\Phi = \dfrac{Pe}{\ell t_f d}$

Applying equation (5.1) the maximum difference between σ_{TC} obtained using finite element analysis and σ_{TC} calculated from equation (5.1), is 6 per cent for the whole range of the b/ℓ ratios (0.1 to 1.0).

It is to be noted that the equation (5.1) is the same as equation (4.9) with K_1 in the former is replaced by K_2 in the latter.

Now, it can be deduced that the validity of the formulae, which predict the distribution and the magnitude of the transverse membrane stresses in box girders, can be extended to cover the prediction of transverse membrane stresses along the web/flange junction line of I-beam girders. It can also be deduced that the aspect ratio is the principal factor influencing the distribution of these stresses.

5.5 End Diaphragm Effect

The finite element study has been carried out assuming that at the simply supported ends the lateral and vertical displacements are restrained. This assumption is used to simulate the effect of a diaphragm, at the simply supported ends, which has infinite in-plane stiffness but no out-of-plane stiffness. As a result of this assumption the lateral deformations are restrained and the transverse membrane stresses at the supports are equal to zero.

In order to examine how realistic this assumption is, the in-plane end rigid diaphragm, is replaced, in two models, by a plate with a finite stiffness. In the first model the thickness of the diaphragm is assumed to be equal to the thickness of the flange. In the second model the thickness of the diaphragm is changed to become five times the flange thickness. The transverse membrane

stresses, along the web/flange junction, which are determined as a result of the analysis of these two models, are then compared with the stresses determined when a rigid end diaphragm is assumed.

The three models, two with finite stiffness and one with infinite stiffness diaphragms, have the same cross-section dimensions. The span length is also identical in the three cases. The aspect ratio of the flanges is assumed to be 0.5, while the depth to width ratio of the cross-sections is assumed to be 0.25. Fig.5.9 shows the comparison between the transverse stresses in the three cases. All the stresses are normalised with respect to σ_{TC} determined from the analysis of the I-beam with a rigid end diaphragm.

The stresses near the centre, show very little difference for the three different models. This effect reflects the lack of sensitivity of the central stresses to the change in the boundary conditions at the supports.

At the support, the use of a finite-stiffness diaphragm allows lateral deformation to take place. These deformations are associated with transverse membrane stresses, which are compressive in the compressive flange and tensile in the tensile flange. The values of these stresses are reduced when the thickness of the plate diaphragm increases. Over most of the span length the distribution of transverse stresses, in the three cases, seems to follow the same pattern.

It can now been seen that, if a reasonable stiffening element is used at the supports, the formulae introduced earlier to predict the transverse membrane stresses along the centre of a box girder flange, can be used to estimate the stresses along the web/flange junction of an I-beam section with a reasonable degree of accuracy.

It is to be noted that the use of an end diaphragm to restrain lateral deformation has the effect of reducing the transverse membrane stresses at the simply supported ends. However, this procedure results in an increase of the shear stresses at these ends. In other words, the reduction of transverse membrane stresses, at the simply supported end, is associated with an increase of the shear stresses in this area. When an infinite rigid diaphragm is used the transverse membrane stresses, at the simply supported ends, are equal to zero and the associated shear stresses are increased to a high value. The plots in Fig.5.10-a and b illustrate this view.

The transverse membrane stresses are normalised with respect to σ_{TC} of the model with a thinner diaphragm ($t_f = t_d$), while the shear stresses are normalised with respect to τ_{max} of the model with of a diaphragm infinite in-plane rigidity.

5.6 Transverse Stresses in an I-beam Flange

Now that the transverse membrane stresses along the centre-line of a simply supported I-beam girder flange can be predicted using a simple procedure, the question arises as how significant these stresses are and in what way they may influence the general behaviour of the girder.

The ratio of the transverse membrane stress at the centre to the associated longitudinal membrane stress, Ω, can be taken as a measure of the significance of transverse stresses. It is to be noted that the distribution of longitudinal stresses across the flange of the I-beam girder is non-linear due to the shear lag effect.

This distribution is sensitive to the change in the aspect ratio. However, in all cases the maximum value of the longitudinal membrane stresses occurs at the web/flange junction (σ_{NC}). An examination of the change of the parameter Ω when changing the aspect ratio, will help to assess the importance of transverse membrane stresses.

Fig.5.11 shows that the parameter Ω is highly influenced by the change in the aspect ratio. The increase of the b/ℓ ratio is associated with an increase of Ω. For a b/ℓ ratio equal to 1.0, Ω is equal to –0.2. The relatively low value of Ω is attributed to the effect of shear lag which results in high longitudinal stress at the centre (σ_{NC}).

It is to be noted that the transverse membrane stress have an opposite sign to the corresponding longitudinal membrane stress. This sign change has the effect of reducing the actual yield limit of the I-beam flange, according to a yield criterion such as that due to Von Mises.

The effect of reducing the yield limit, under the condition of loading discussed herein, is not confined within the area of wide flange I-beams. This effect is principally governed by the change in the aspect ratio, and, therefore, it can be deduced that a conventional I-beam girder with a short span (high aspect ratio) can be subjected to a reduction of its yield limit.

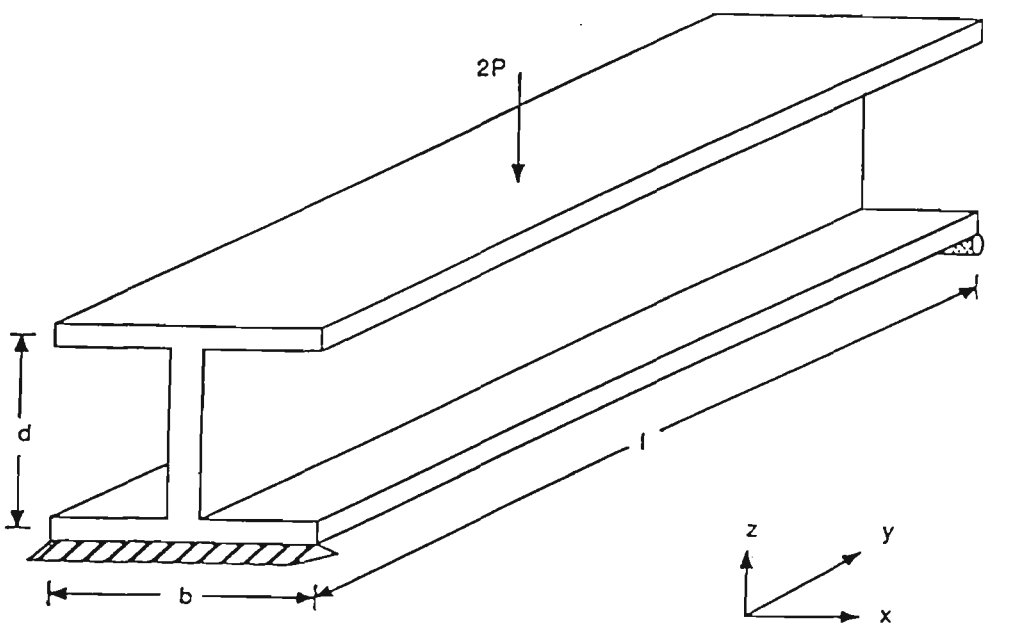

Fig. 5.1 Simply supported I-beam

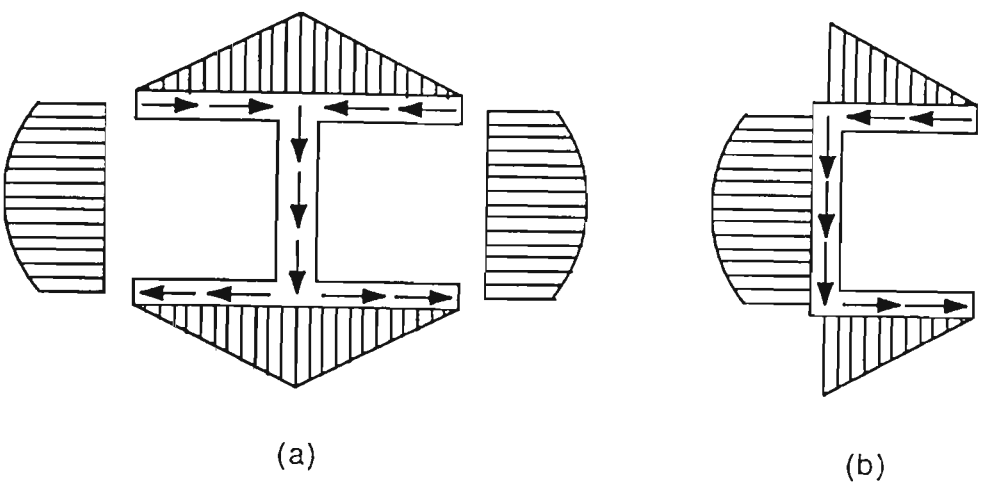

Fig. 5.2 Shear stress distribution

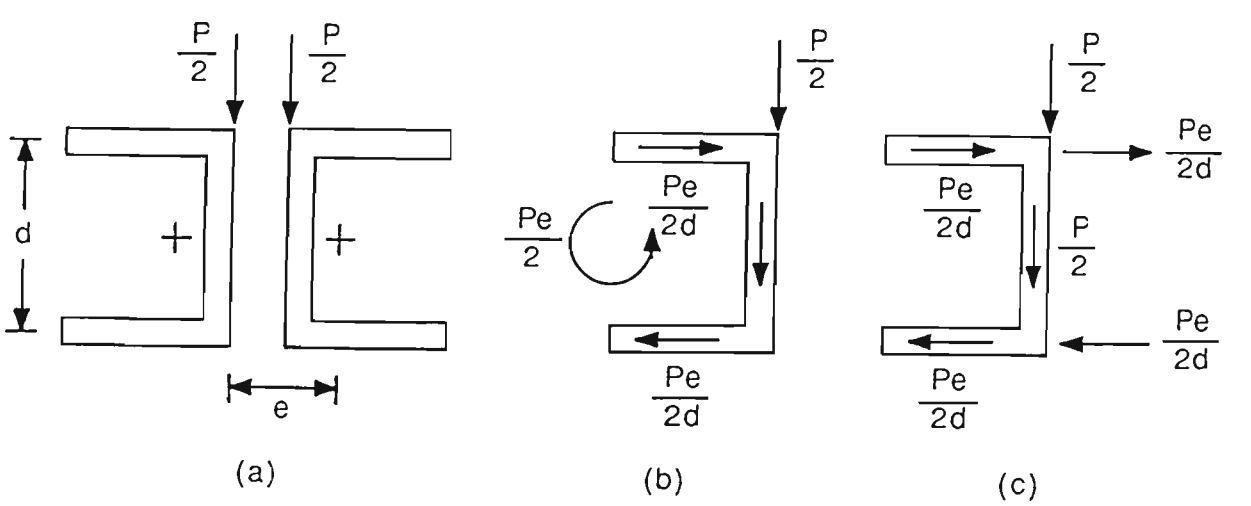

Fig. 5.3 I-beam divided into two channels

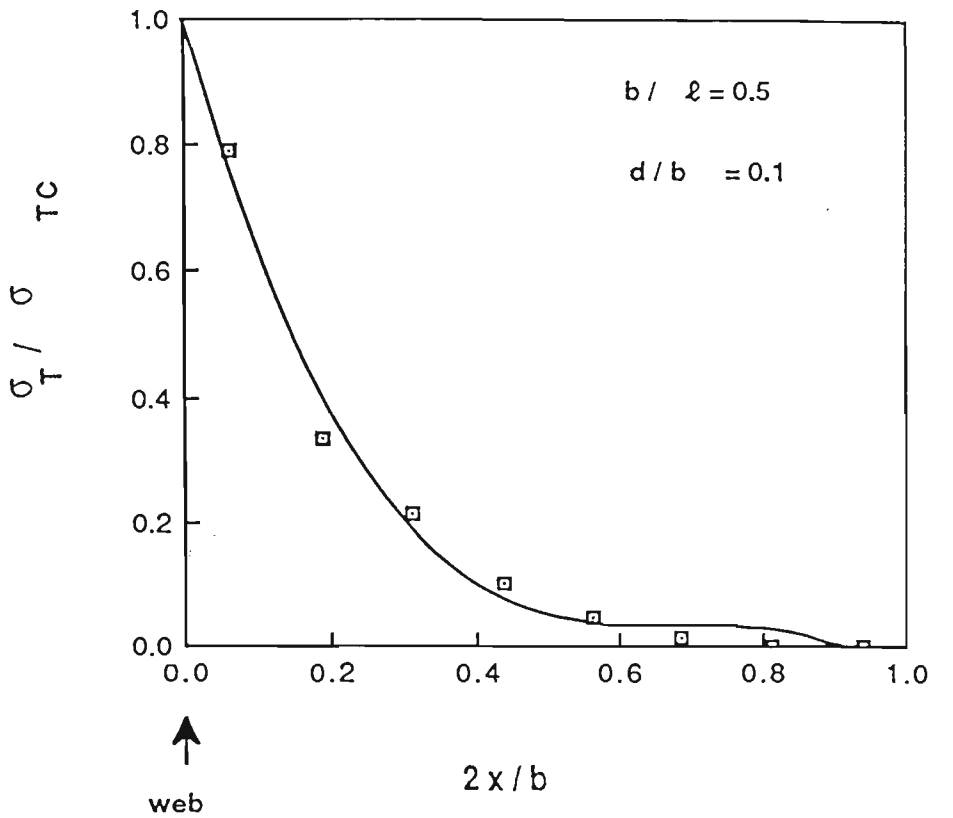

(a)

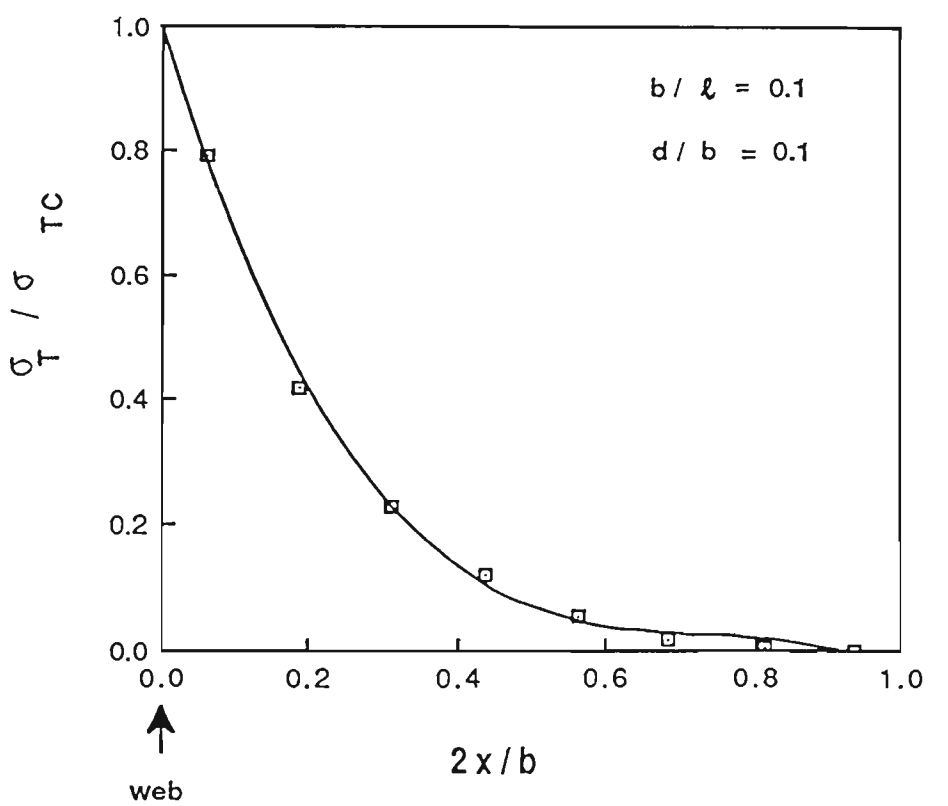

(b)

Fig. 5.4 (a) Distribution of transverse membrane stresses across half flange; (a) $b/\ell = 0.5$; (b) $b/\ell = 0.1$

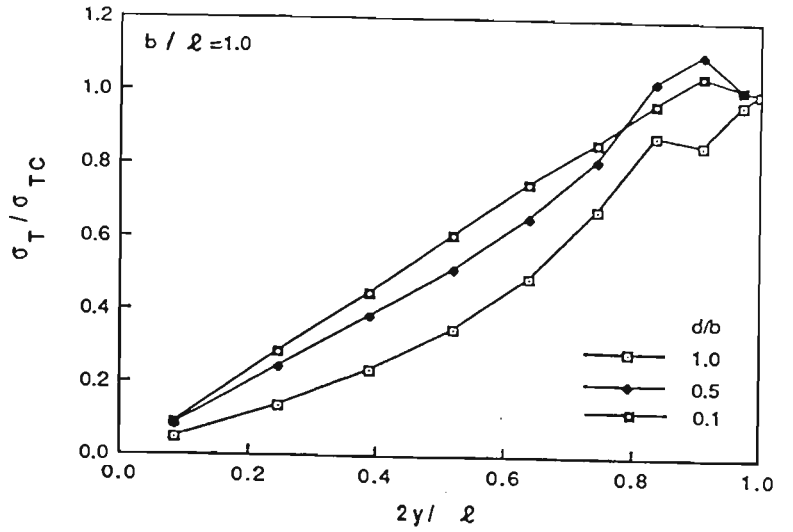

(a)

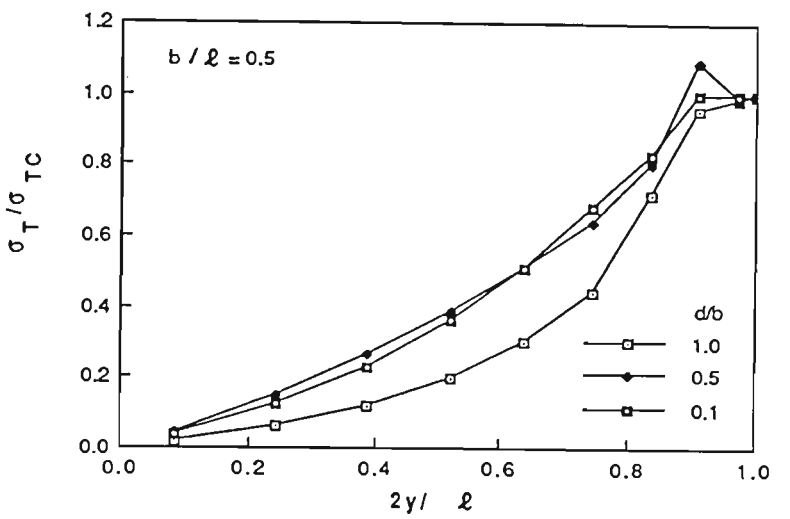

(b)

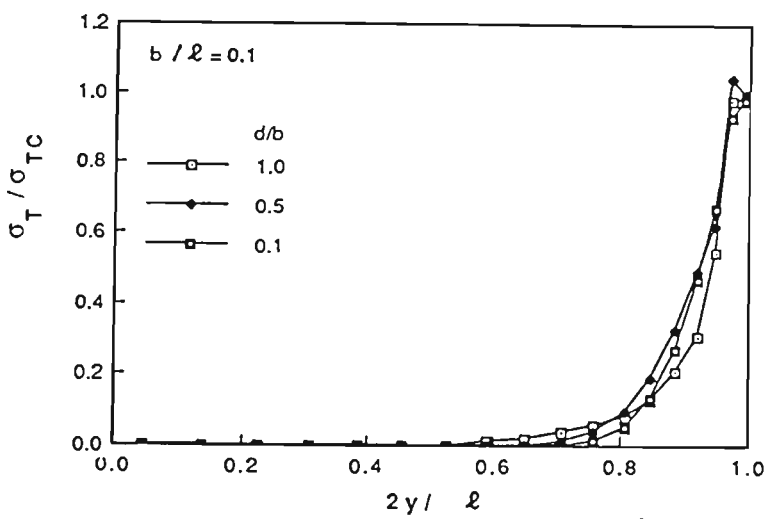

(c)

Fig. 5.5 Distribution of transverse membrane stress along web/flange junction line;
(a) b/ℓ = 1.0; (b) b/ℓ = 0.5; (c) b/ℓ = 0.1

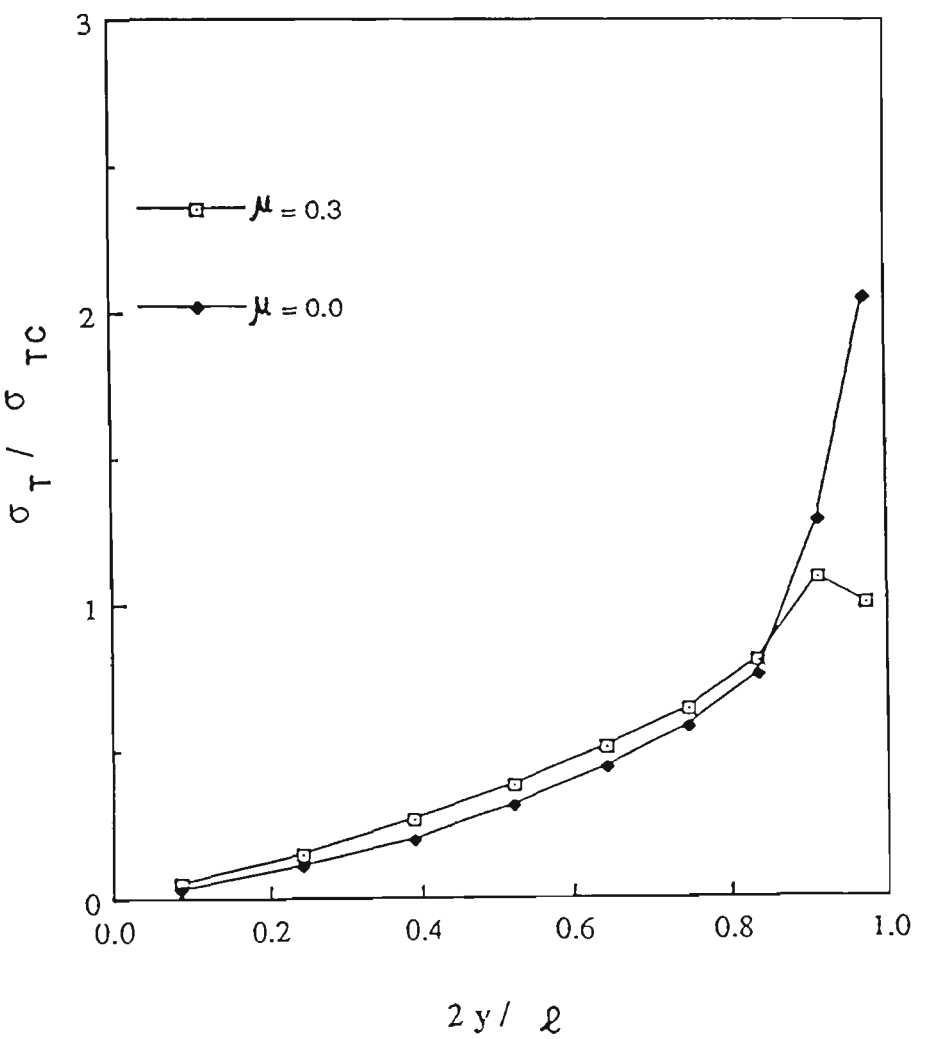

Fig. 5.6 The effect of Poisson's ratio on the transverse membrane stresses distribution along the web/flange junction of an I-beam

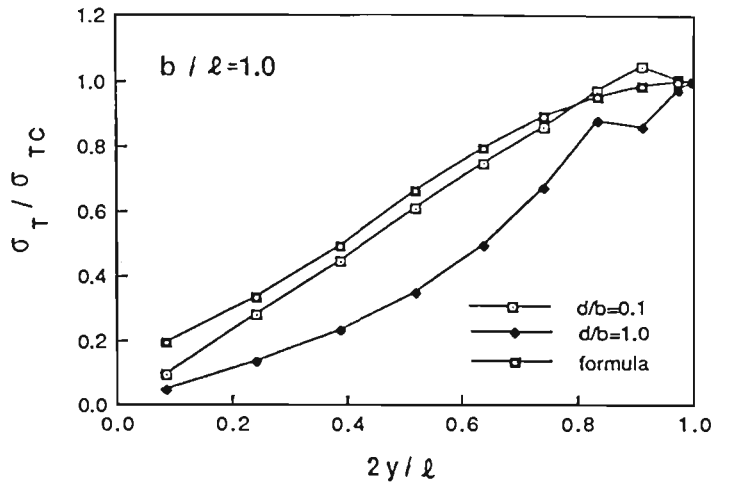

(a)

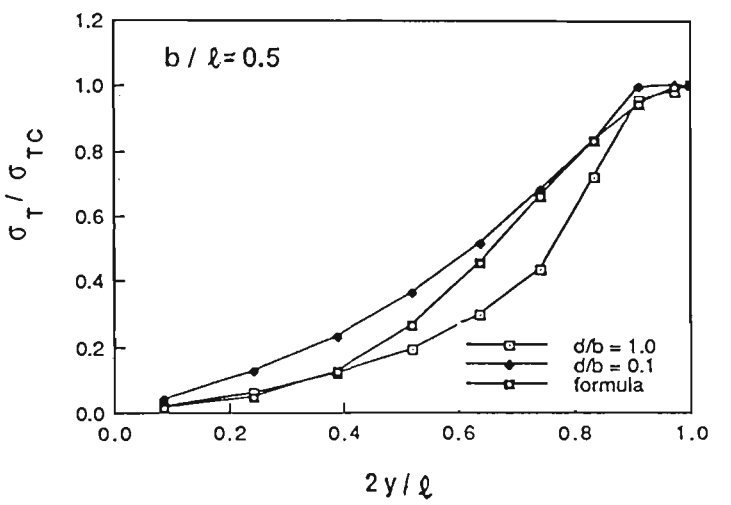

(b)

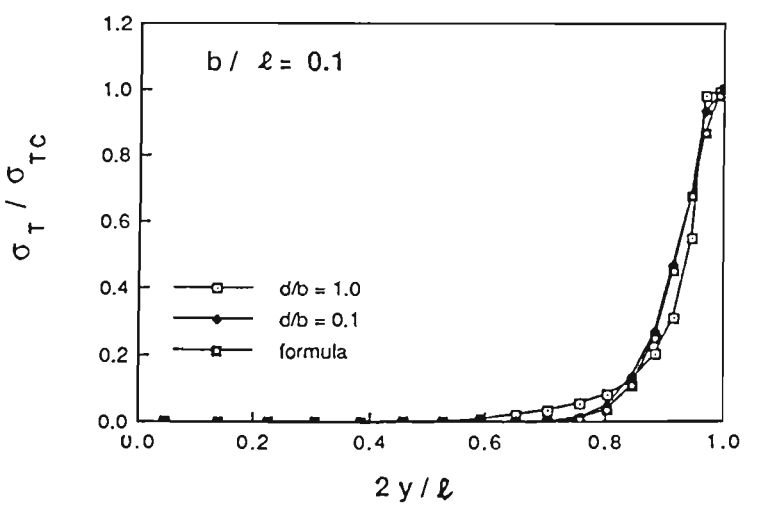

(c)

Fig. 5.7 Comparison of results from equation (4.4) with those from finite element analyses; (a) $b/\ell = 1.0$; (b) $b/\ell = 0.5$; (c) $b/\ell = 0.1$

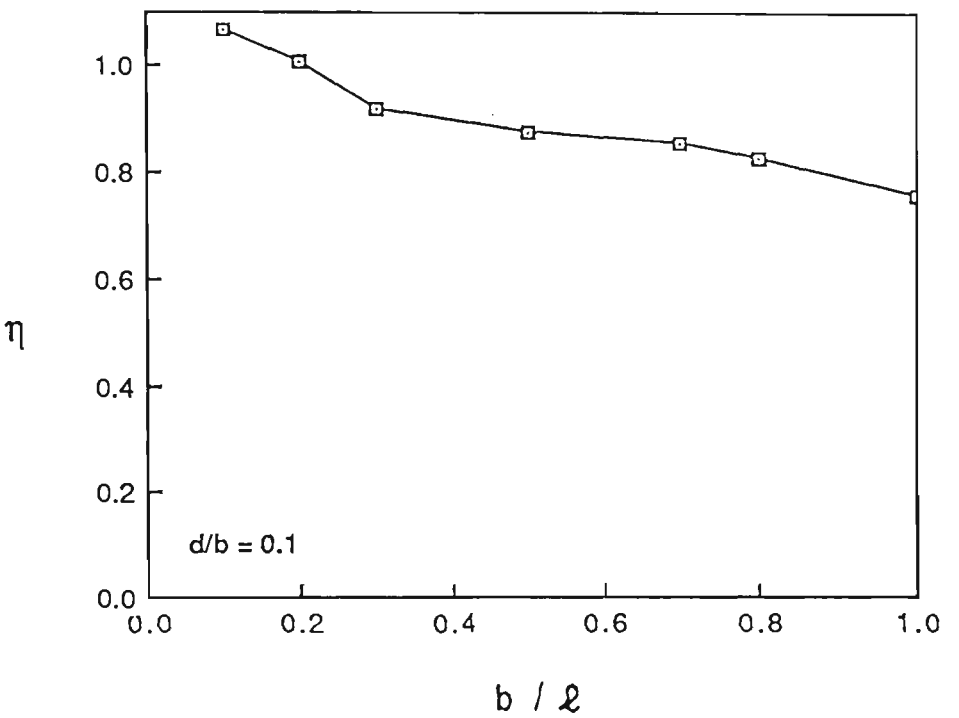

Fig. 5.8 Variation of η with aspect ratio b/ℓ

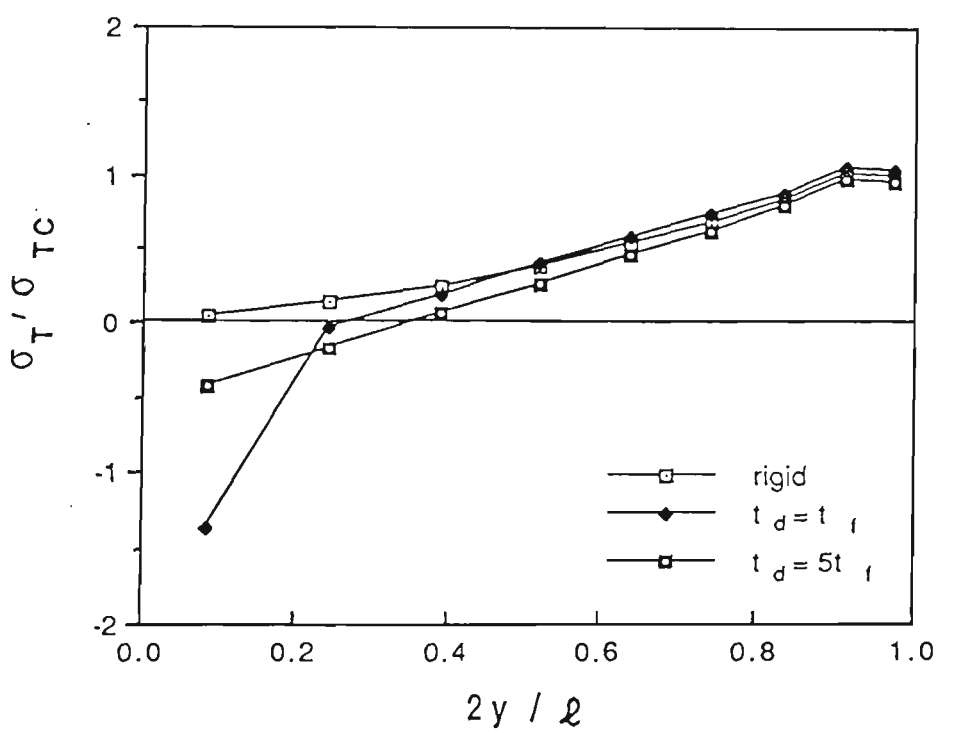

Fig. 5.9 The influence of rigid diaphragm on the distribution of transverse membrane stresses along the web/flange junction of an I-beam

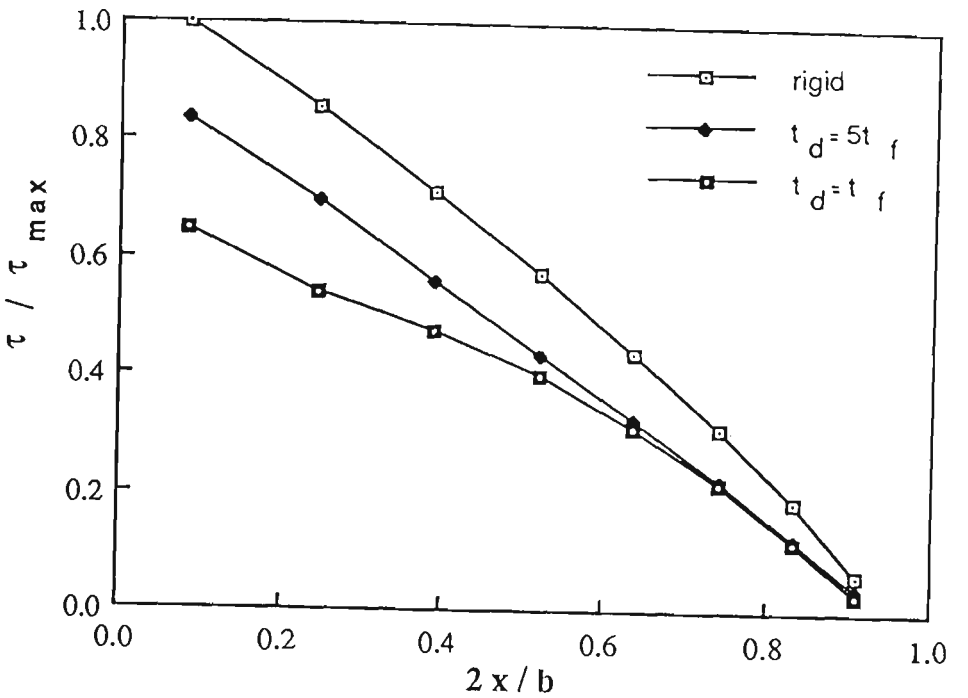

(a)

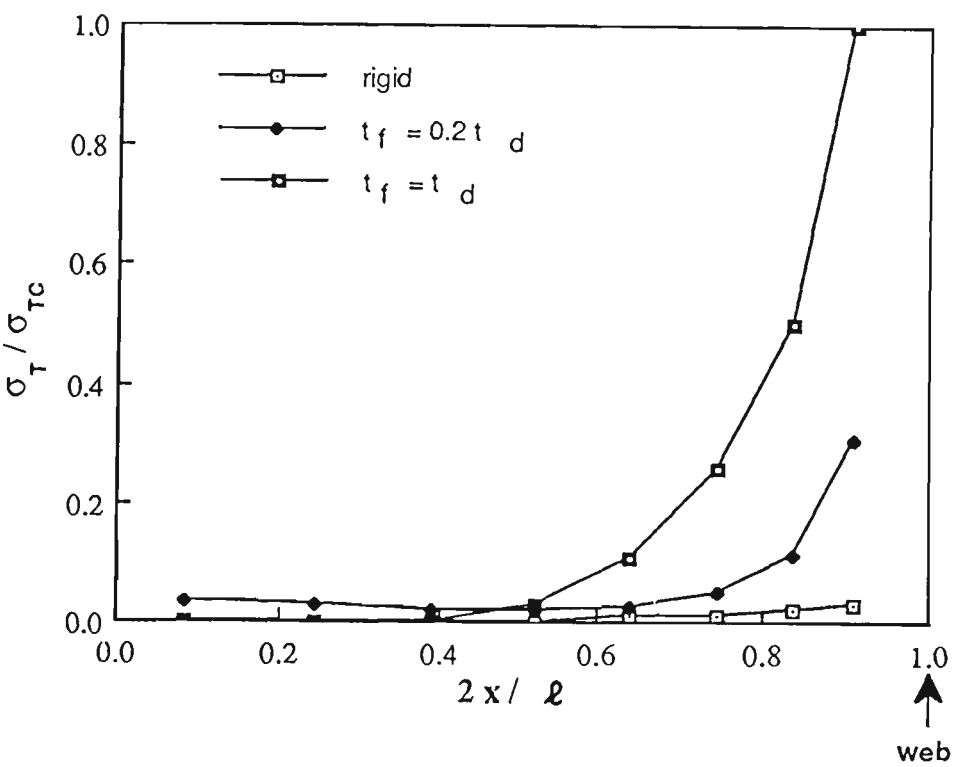

(b)

Fig. 5.10 The influence of rigid diaphragm on the distribution of stress (a) shear stress at the simply supported end; (b) transverse stresses at the simply supported end

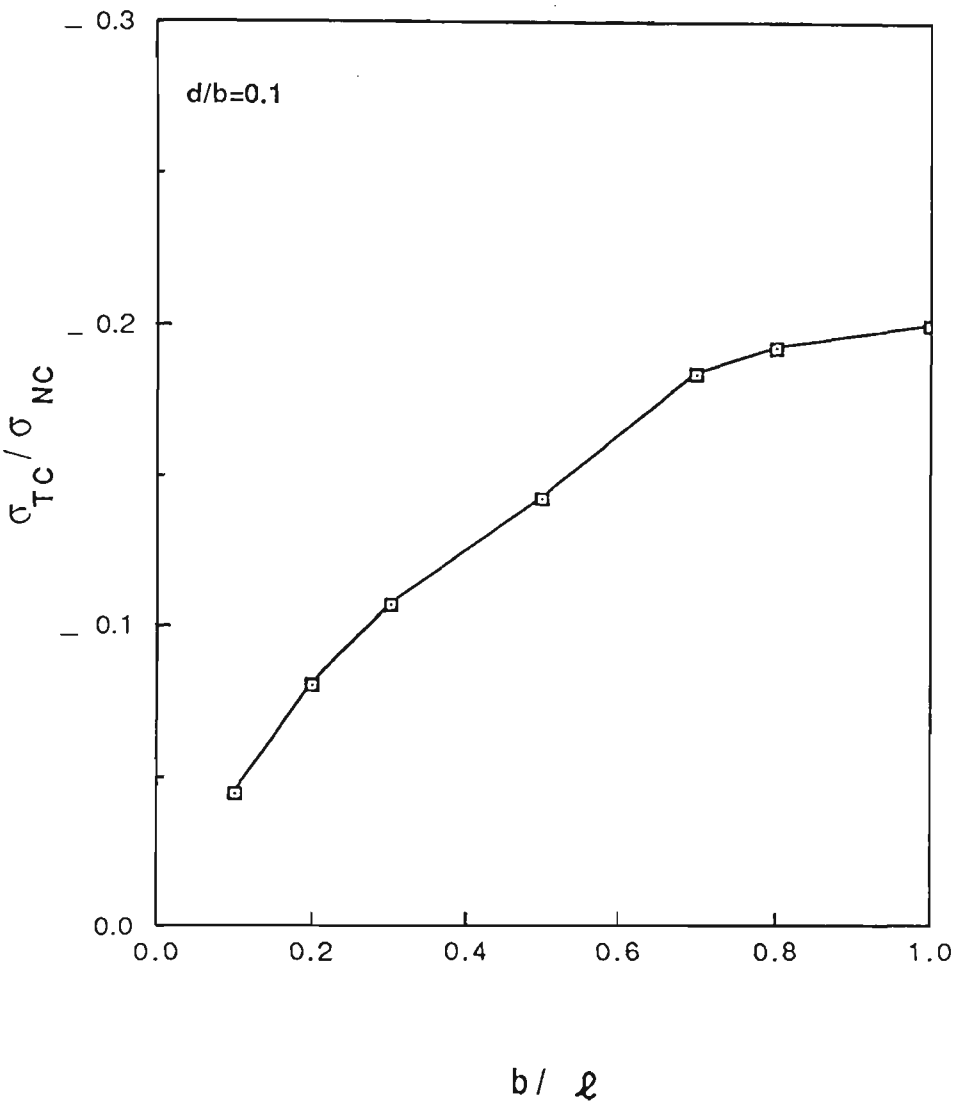

Fig. 5.11 Variation of $\Omega = \sigma_{TC}/\sigma_{NC}$ with aspect ratio b/ℓ

Chapter 6

Bending Lag in Box Girder Flanges

6.1 Historical review

When a box girder is subjected to flexural loading, the longitudinal curvature of the flange varies across its width causing a curvelinear distribution of flange-plate bending moment. This phenomenon is known as bending lag. Bending lag arises as a result of the finite torsional stiffness of the plate which creates reluctance to flexural rotation across the plate. Hence the phenomenon is termed "torsional lag" (Dowling, 1985) or "bending reluctance" (Chapman et al., 1971). This bending lag effect was first mentioned, by Chapman et al. (1971). They carried out an investigation on box girder bridges during which transverse distortion bending stresses were encountered under the flexural component of loading. These stresses were attributed partially to the longitudinal bending lag influence.

The bending lag influence was demonstrated again when the interaction between shear lag and stiffener-induced buckling in steel box girders was examined (Lamas et al., 1983). Investigation showed that a peculiar mode of failure occurred when buckling was developed in the longitudinal compression flange stiffeners located at the quarter width rather than those located near the web/flange junction. Bending lag was thought to be a contributing factor which can explain the observed mode of failure.

The increasing importance of bending lag as a factor in determining box girder behaviour dictates the need for more detailed studies to explore the different aspect of the phenomenon. Recently, a theoretical study into bending lag effect was conducted by Dowling et al. (1985).

Their analysis assumed the case of a double-web plate girder which was simply supported at each end, and the loads were applied to the webs (Fig.6.1). An idealisation of the behaviour of the cross section was assumed so that the flange could rotate in the transverse direction, independently of the web, resulting in zero transverse moment. However, the vertical deflection of the flange was assumed to follow that of the web.

Assuming small deflections the basic differential equation describing the behaviour was solved using trigonometric-hyperbolic series; the loads were modelled using Fourier series.

The effective width concept was adopted by Dowling as a suggested measure of bending lag. The bending lag effective width was defined as that width of the plate which could sustain a constant longitudinal bending moment equal to the maximum moment at the web/flange junction in the plate. Hence, the mathematical expression for this effective width is:

$$b_e = \frac{\int_0^{b/2} M_x \, dy}{[M_x]_{y=b/2}} \qquad (6.1)$$

Where b_e is the effective width, M_x is plate bending moment at distance y from the centre of the flange (Fig.6.1), and b/2 is half the flange width.

Fig.6.2 is a graphical illustration of the concept of bending lag effective width.

Another way to quantify the bending reluctance of the flange plate due to its finite torsional stiffness is to use the distribution of longitudinal curvature across the width of the plate. The effective width in this case is defined as that width which would experience a constant longitudinal curvature across the width of the plate equal to the maximum curvature. The mathematical definition is:

$$b_e = \frac{\int_0^{b/2} \partial^2\omega/\partial x^2 \, dy}{[\partial^2\omega/\partial x^2]_{y=b/2}} \qquad (6.2)$$

Where ω is the vertical deflection, x is the distance measured along the flange and y is the distance measured across the flange (Fig. 6.1).

It is to be noted that no consideration in this case has been given to anti-clastic curvature. Consequently, the value of 'b_e' obtained from equation (6.2) could be over estimated. It is preferable therefore, to use equation (6.1) to calculate the effective width.

The bending lag effective width is used in conjunction with the bending moment across the flange plate to quantify the bending reluctance of the

flange. In this case the flange is acting as a flexural member. In the case of a shear lag analysis, the effective width is used in conjunction with the overall bending of the girder. Hence, the flange is acting as a compressive or tensile member.

Based on the assumption that the web provides no rotational resistance to the flange and considering the overall equilibrium of the girder together with the bending lag effective width, Dowling introduced the following expression to evaluate the maximum bending moment of the flange plate 'M_{max}':

$$M_{max} = \frac{(1-D_1^2/D_xD_y)M}{2[EI/D_x+b_e(1-D_1^2/D_xD_y)]} \qquad (6.3)$$

where

$$D_1 = \frac{\mu Et^3}{12(1 - \mu)}$$

$$D_x = \frac{Et^3}{12(1-\mu_x\mu_y)} + \frac{Eth^2}{(1-\mu_x\mu_y)} + \frac{EI_s}{B}$$

$$D_y = \frac{E\,t^3}{12(1 - M_x\,M_y)}$$

Where M is the total applied bending moment at the sectin, E is Young's Modulus, I is the second moment of area of the cross section, I_s is the second moment of area of longitudinal stiffeners, B is the spacing of stiffeners, t is the thickness of the flange, and μ is Poisson's ratio.

In addition to the above formulae, the following two expressions were presented to estimate the longitudinal bending moment of the flange plate in the parts of the flange remote from the web/flange junction.

$$\frac{M_x}{M_{max}} = \{1.35\psi-0.36-(0.63\psi-0.73)[2y/b]^2-(0.62\psi-0.61)[2y/b]^4\} \text{ for } \psi > 0.225 \quad (6.4\text{-a})$$

$$\frac{M_x}{M_{max}} = \{-0.71\psi+0.1+(9.26\psi-1.62)[2y/b]^2-(6.96\psi-2.22)[2y/b]^4\} \text{ for } \psi \leq 0.225 \quad (6.4\text{-b})$$

where $\psi = b_e/b$

Fig. 6.3 shows how the effective width ratio ψ is influenced by the change in the flange aspect ratio (b/ℓ); for a larger aspect ratio the significant decrease in ψ is noticed. It was also concluded in the study that the web flexural stiffness had a very marked effect on the magnitude of the moment in the flange (Dowling and Burgess, 1985).

6.2 Linear and Non-Linear Analyses of Bending Lag in a Box Girder

The work which has been reviewed earlier provides sufficient and necessary information which helps to attain an appreciable insight into some of the elements involved in the bending lag effect on box girder behaviour. The aim of the present work is to investigation the assumption, which has been previously proposed, of no-flange-rotation restraint by the webs, and how this assumption can affect the bending lag of the flange assuming linear elastic behaviour. The effect of the aspect ratio on the bending lag influence has been also examined. The work is also extended to cover the nonlinear elastic response of box girders and its influence on the phenomenon of bending lag.

Figs. (6.4-a and b) show the simply supported box girder, which is the basis of this study, under central concentrated loads acting on the webs. The cross-section dimension is also shown. The lateral and vertical displacements are restrained at each simply supported end.

6.3 Linear and Non-linear Analyses.

In a linear analysis the assumption is that the deflection of the structure is too small to have a significant influence on the load carrying capacity, and as such a straight line can simulate the load deflection relationship. This assumption is known as the small deflection theory.

When considering a thin-walled structure it is found that, under working conditions, the plated elements of the structure undergo deflection which could reach several times the plate thickness. This increasing out-of-plane deflection leads to a considerable change in the geometrical characteristics of the overall cross-section. This change in geometry is associated with changes in the stiffness of the structure and its load carrying capacity.

If the structure were to undergo large out-of-plane deflections and if these deflections were not considered in a linear analysis, the deflection and the stresses predicted by this analysis could be considerably misleading. On the other hand, if these large deflections are considered, the analysis then becomes non linear. Account is then taken of buckling of the flange.

6.4 Computer Modelling

In the present analysis, both linear and non-linear techniques are used. The non-linear technique is employed to simulate the load-response history within the elastic range. This technique is formulated to allow for large element deflection under the condition that the change of the shape of the element is small. Small strain theory applies so that stresses are proportional to strain.

A major objective of the study is to quantify the extent to which the non-linear elastic behaviour or the elastic buckling phenomenon influences the overall behaviour of box girders. As the existence of stiffeners enhances the local buckling strengths, and therefore reduces the effect of buckling, stiffeners are not considered herein. Furthermore, a high (b/t) ratio of 100, which is within the range of practical use, is employed in order to magnify the effect of elastic buckling.

No consideration was taken of both initial out-of-plane deflections, residual stresses, and material non linearity, as these factors increase the complexity of the problem and may cloud the final interpretation of the original aim.

The web/flange interaction behaviour is examined for two cases: i) An idealised case where the flange is assumed to be connected to a web with high rigidity. This case is achieved by employing a modulus of elasticity of the web E_w which is ten times greater than the modulus of elasticity of the flange E_f. ii) A complete interaction between the flange and the web (The web and the flange have the same E) to simulate the actual behaviour.

The first assumption is introduced to examine the influence of web rigidity on the bending lag of the flange.

Both the compressive and the tensile flanges are assumed to have the same dimensions. The web thickness is assumed to be the same as the flange thickness.

The analysis employs the finite element method; a four noded modified isoparametric quadrilateral plate element is used (McNeal, 1978). The box girder is modelled using a fine mesh of 16 elements across the width of the

flange, 10 elements along the length and 5 elements down the depth of the web. Use is made of the double symmetry of the model; consequently, only one quarter of the box girder is considered for the analysis.

The existence of high stresses close to the concentrated load dictates the use of a biased mesh along the length of the girder; the segments near the end are 500% larger than those near the centre, as shown in Fig.6.5.

The nodal degree of freedom along the web/flange junction line, the three components of translation and the three components of rotation, were unconstrained thereby allowing the web/flange interactive behaviour to be investigated fully. The flange had a slenderness ratio (b/t) equal to 100. This ratio was considered the most critical parameter for practical problems (Lamas and Dowling, 1979). The material used was assumed to be mild steel with the modulus of elasticity E=200GPa.

6.5 Load Deflection Response

The non-linear relation between load and deflection was obtained by applying a low load first, then successively increasing the load and noting the corresponding deflection each time until reaching the maximum load. The maximum load P is defined herein as that which results in a zero membrane longitudinal stress at the central strip of the compressive flange for the non-linear analysis. The ratio P/P_u, where P_u is the elastic critical load, is then always close to 1.0, and hence P is associated with considerable out-of-plane deflection (Fig.6.6). From a practical point of view, this condition can be regarded as a limit state, such as the serviceability limit state which is outlined in the British Standard (1982). According to the British Code (1982) structural

steel work should be considered to have reached the serviceability limit state if either:

"(a) deformation has occurred in one of more components or connections such as to cause either excessive permanent deflection, or damage to finishes or to protetive coatings; or

(b) buckling of one or more elements has occurred to such an extent that the maximum stress exceeds the yield stress, and excessive deformation occurs due to spread of plasticity."

As the non-linear analysis did not consider failure based on a yield criterion, to allow the influence of full elastic buckling to be studied, the above definition of maximum load was essential in order to establish a limit state criterion.

6.6 Investigation of Bending Lag Effect

Bending lag is defined as the non uniform distribution of plate bending moment across the flange, with a maximum value at the web/flange junctions. The effect is attributed to the finite torsional stiffness of the flange (Dowling and Burgan, 1985).

In a simply supported girder, the compressive flange behaviour is of particular interest as it can be detrimental when considering the stability of the cross section. It is therefore of concern herein to investigate the bending lag effect in the compressive flange plate.

a) Linear analysis of an idealised cross-section

In order to examine the influence of web rigidity on the bending lag effect in a box girder flange, an idealised section, where the web rigidity was assumed to be ten times the flange rigidity, is considered for analysis. The analysis shows that the outer surface stresses of the compressive plate are greater than the inner surface stresses and both are compressive. Now, because of the difference in stresses, the plate is under bending moment and this moment acts on the transverse cross-section of the flange. This plate bending has a non-linear distribution across the girder, with the maximum value at the web/flange junction and a minimum value at the centre line.

It is interesting to notice (Fig.6.7) that the distribution of plate bending across the flange ($b/\ell = 0.4$) agrees well with the distribution obtained by using Dowling and Burgan's formula (1985).

The influence of the aspect ratio on the effective width ratio is illustrated in Fig.6.8. For a long span (low aspect ratio) the effect of bending lag is a minimum.

b) Linear analysis of a complete cross-section

For the same ratio of $b/\ell = 0.4$, a complete cross-section was examined, where the web rigidities were identical to those of the upper and lower flanges. For a particular model ($b/\ell = 0.4$), the analysis shows a dramatic increase in the non-linearity of the plate bending moment distribution across the girder (Fig.6.9). The change in the distribution, from that of an idealised case (Fig.6.7), demonstrates the effect of web rigidity not only on the magnitude of the bending moment of the flange (Dowling and Burgan, 1985), but also on the

magnitude of bending lag. A comparison between Figs.6.7 and 6.8 shows that when the web flexural rigidity decreases, the magnitude of the bending lag increases and the effective width ratio for plate bending, decreases. For the present example, the effective width ratio changed from 0.63 for the idealised case to 0.34 for a complete cross-section.

It is evident therefore that using a stocky plate as a web element in a box girder will reduce the effect of the bending lag. A comparison between Figs.6.7 and 6.8 confirms the earlier statement. A comparison between Fig.6.7 (Dowling formula) and Fig.6.8 (complete cross section) indicates that if the web-flange interaction is not fully considered (Dowling and Burgan, 1985), the bending lag effect may be underestimated.

Fig.6.8 shows the influence of the aspect ratio on the bending lag effective width ratio for the complete cross section. A similar effect to that of the idealised case is noticed where the effect of the bending lag is reduced when the aspect ratio increases.

Overall the impact of bending lag in the case of idealised cross sections is much less than for the complete cross section (Fig.6.8). However it is to be noticed that these results are for specific d/b value of 0.25.

c) Non-linear analysis of a complete cross section

The non-linear analysis shows the changes of stress associated with large out-of plane deflection, when approaching the critical load P. The central strip of the compressive flange undergoes a considerable amount of deflection. Consequently, tensile stresses at the inner surface are produced. Thus, the buckling behaviour of the central strip of the compressive flange results in

tensile stresses in the inner surface and compressive stresses in the outer surface. The strip near the edge has outer stresses higher than the inner stresses, and both are compressive.

Fig.6.10 shows the deflected shape of one quarter of the box girder as shown by the non-linear analysis of a complete cross section. The increasing deflection of the compressive flange, in comparison with the tensile flange, is apparent.

The changes due to buckling in the outer and the inner stresses lead to a negative bending lag, where the plate bending moment distribution across the compressive plate cross-section has a maximum value at the central strip and a minimum value at the edge (Fig.6.11). It becomes apparent that the definition of 'bending lag' given earlier, which is valid for linear analysis, cannot be extended to cover the result shown by the non-linear analysis. However, this result represents a more realistic picture of the stresses when reaching the maximum load capacity of the cross section, assuming that elastic buckling occurs.

6.7 Summary

The phenomenon of 'bending lag' has been explored within the scope of linear and non-linear elastic analyses for the flanges of a simple box girder.

The linear analysis of a complete cross section has shown that ignoring the web/flange interaction influence can lead to an underestimation of the bending lag effect.

The linear analysis has also shown that increasing the web rigidity of a box girder, in comparison of the rigidity of the flange, will reduce the effect of bending lag.

The non-linear analysis of a complete cross-section has shown that a negative bending lag is developed in the compressive flange, when elastic buckling occurs; the maximum plate bending moment then occurs at the central strip.

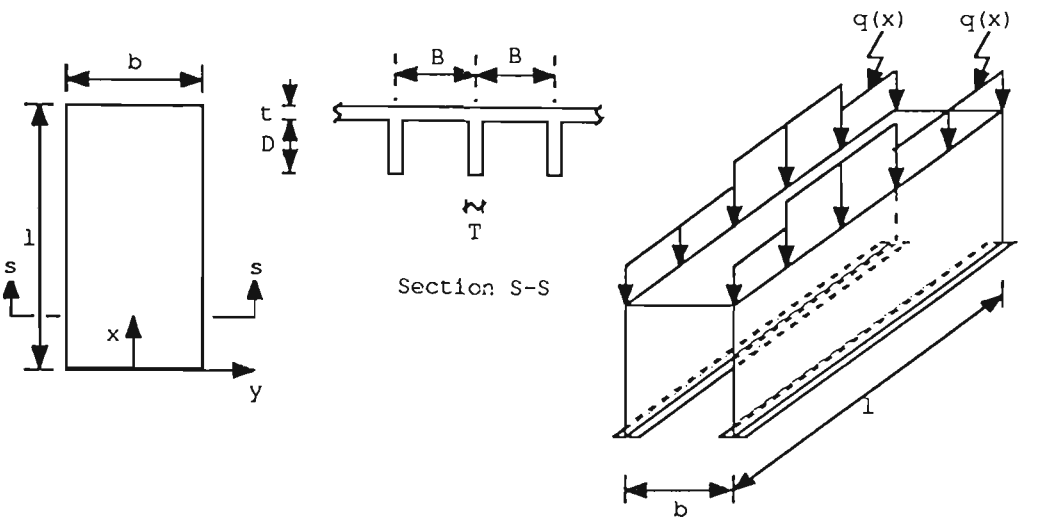

Fig.6.1 Girder plan view showing flange dimensions and axis. The longitudinal stiffener dimensions are shown (Dowling and Burgan, 1985)

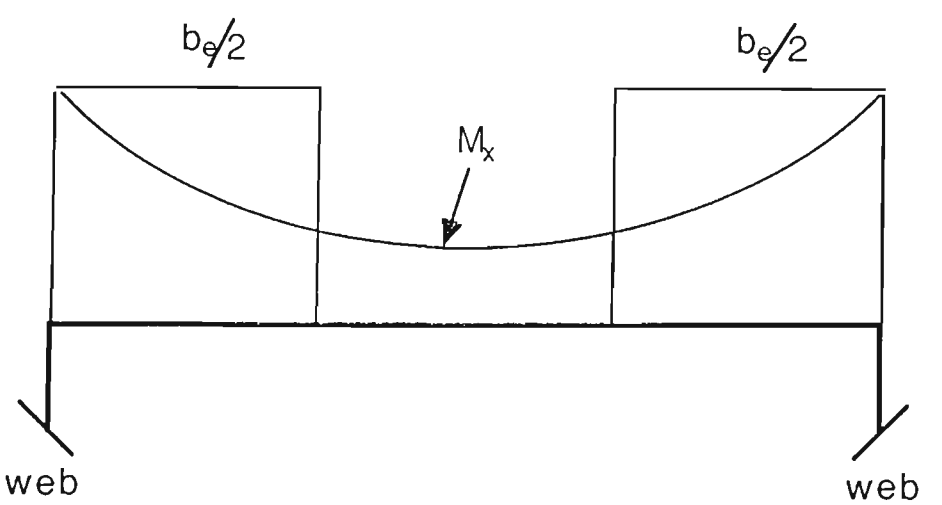

Fig.6.2 The bending Lag effective width concept (Dowling and Burgan, 1985)

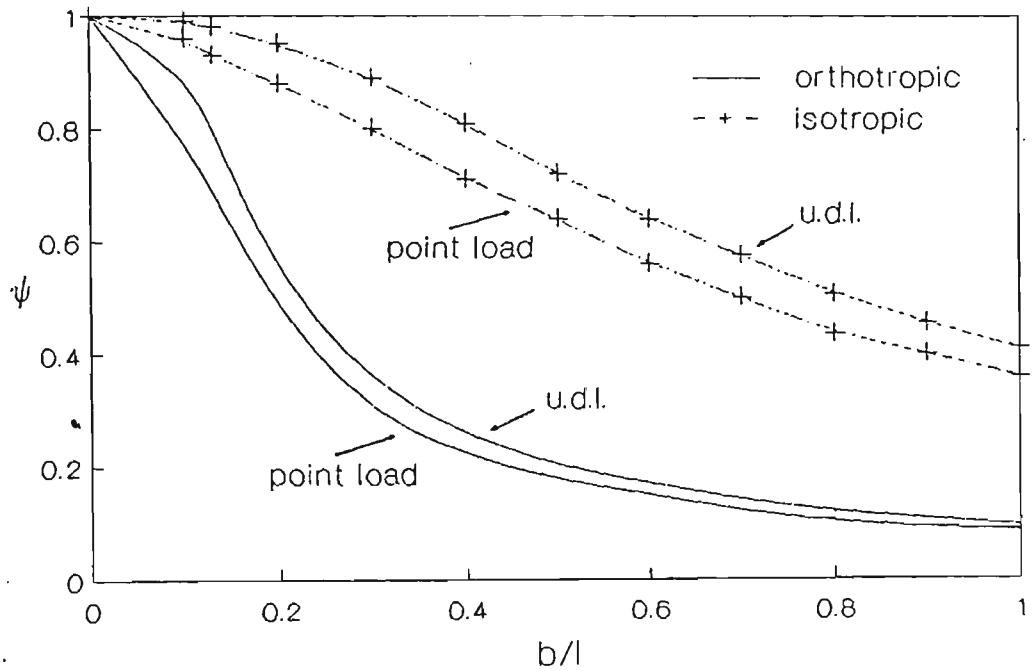

Fig.6.3 Variation of effective width with type of loading (Dowling and Burgan, 1985)

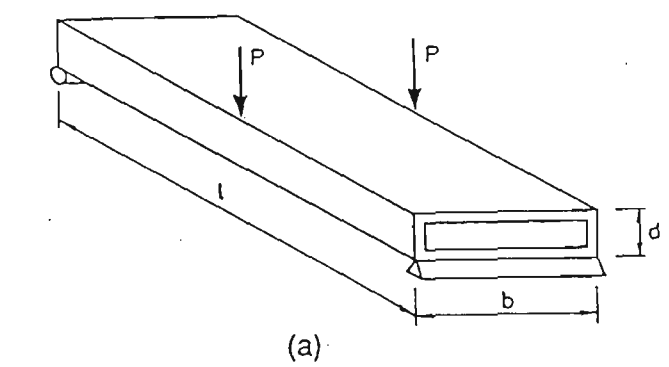

(a)

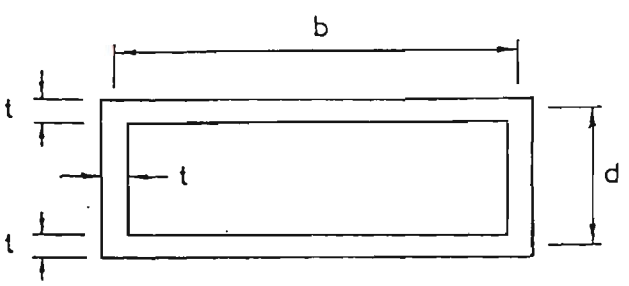

(b)

Fig.6.4 (a) Loading condition; (b) Cross-sectional dimensions of girder

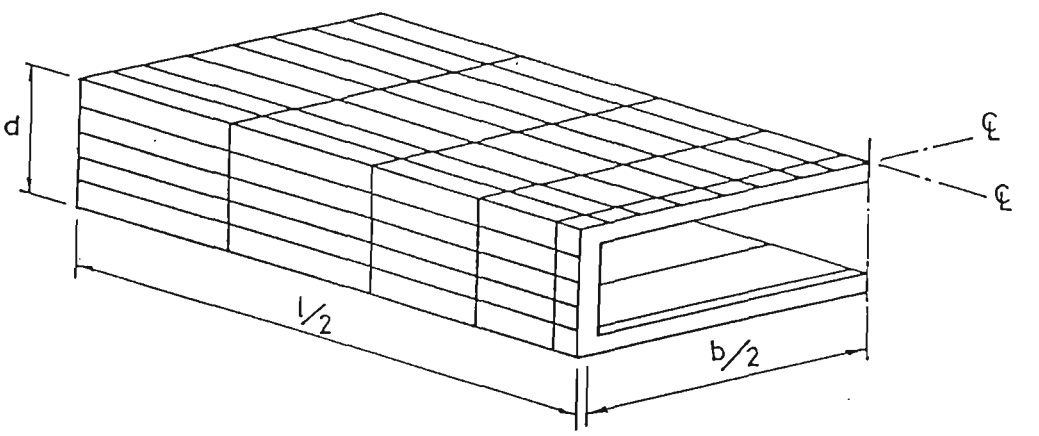

Fig.6.5 Finite element mesh for the numerical modelling

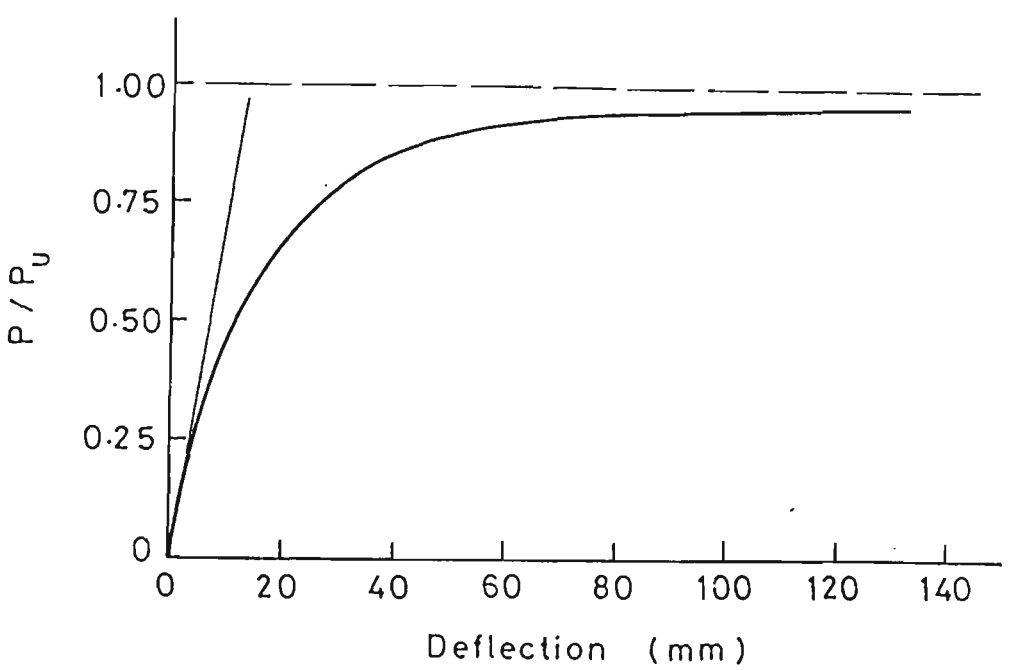

Fig.6.6 Typical load-deflection curve

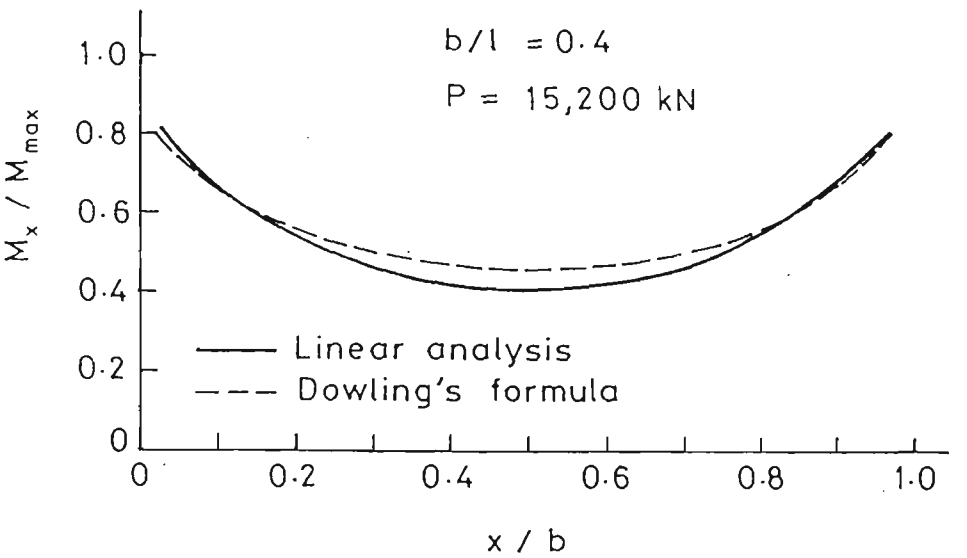

Fig.6.7 Distribution of plate bending moment across the compressive flange; idealised cross section - linear analysis

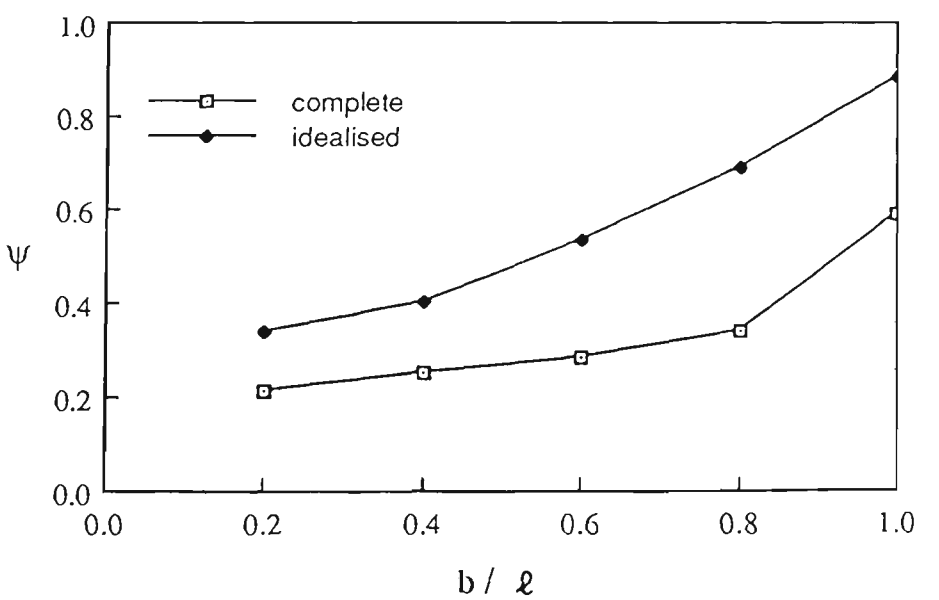

Fig.6.8 Effective width ratio - comparison

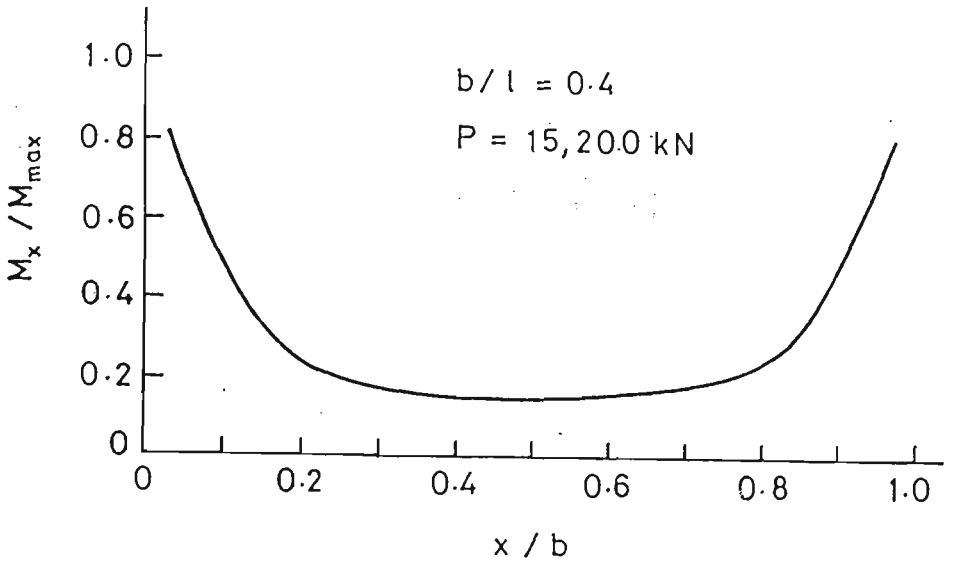

Fig.6.9 Distribution of plate bending moment across the compressive flange; complete cross section linear analysis

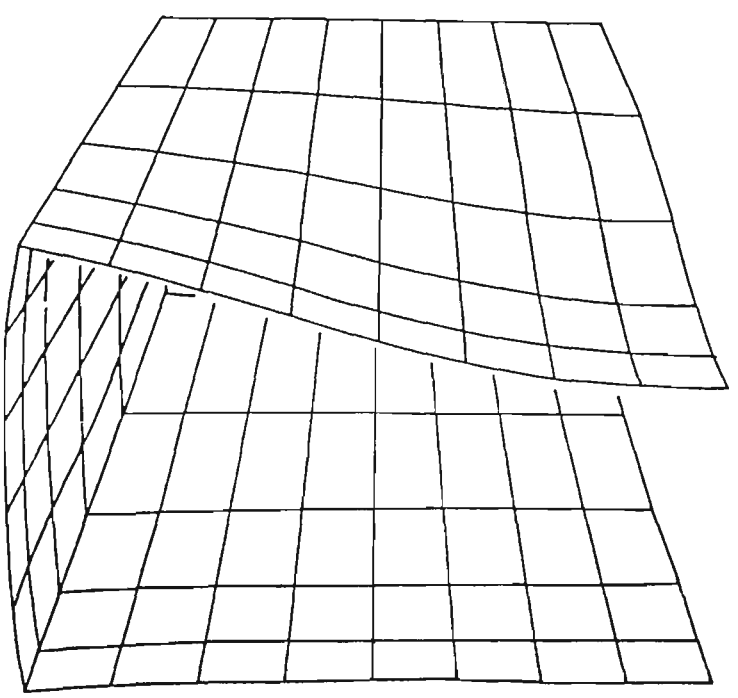

Fig.6.10 Deflected shape of box girder (original magnification x 5)

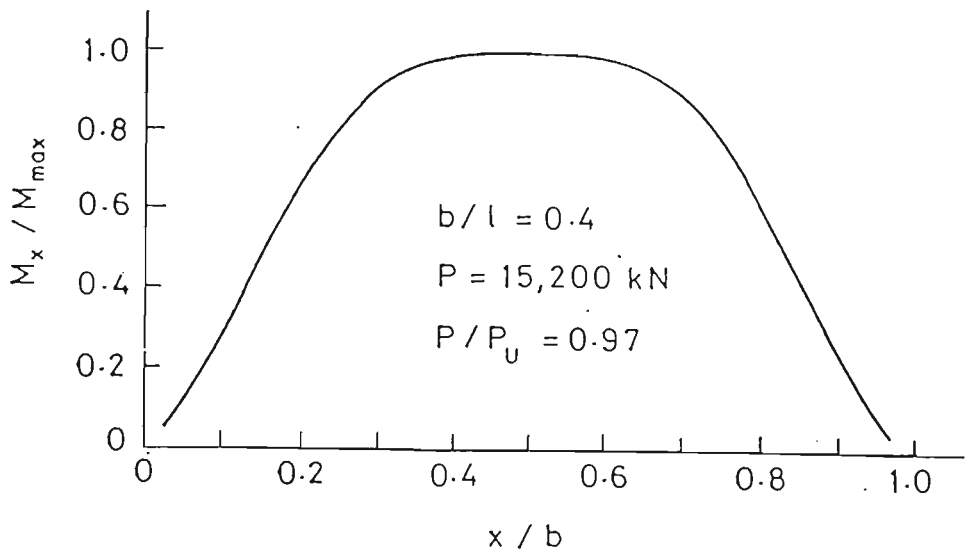

Fig. 6.11 Distribution of plate bending moment across the compressive flange; complete cross section non-linear analysis

Chapter 7

Profiled Sheeting

7.1 Introduction

Profiled sheeting is defined as sheeting which is formed longitudinally with regularly spaced shaping to give a corrugated or troughed cross section (Fig.7.1). Such sheeting has been used in the building industry for about one hundred years (Baehre, 1983). In the past, profiled sheets were considered as non-structural elements, and their design was based on semi-experimental work and subjective judgements.

Over the years, both analytical and experimental research work has focussed on the evaluation of profiled sheet behaviour under load, and an understanding of the variation of this load capacity with variation of the geometrical properties.

Huber (1914) established a method of stiffened plate analysis based on the analogy between a ribbed slab and an orthotropic plate. The corner stone in

the argument is that the ribbed slabs have different elastic properties in two orthogonal directions. This characteristic feature of a ribbed slab (stiffened plate) is shared by a corrugated sheet. Hence, the orthotropic theory of ribbed slabs developed by Huber was extended to cover the modelling of a corrugated sheet as an orthotropic plate.

Seydel (1931) performed some tests on buckling of corrugated plates. He employed the orthotropic plate model as proposed by Huber in order to determine the theoretical response. In Seydel's tests the corrugated sheet was subjected to edge forces. The results of these tests showed good agreement with the proposed model by Huber.

In a parallel development, Blodgett (1934), suggested four formulae by means of which the second moment of area, I, of a profiled sheet could be calculated. He assumed that the cross section of the corrugated sheet was composed of cycloidal arcs, parabolic arcs, circular arcs, straight lines and certain combinations of these. Each of his four relations corresponds to a certain profile shape. He assumed in his analyses that the profile bends about a neutral axis without distortion.

Wolford (1954) presented a set of formulae for quickly determining the second moment of area of profiled sheets. The formulae included Blodgett's formulae and additional expressions to facilitate conversion from ordinary dimensions to geometrical ratios. He assumed the profile to be of the arc-and-tangent type.

Abdel-Sayed (1970) made an attempt to evaluate the mechanical properties of profiled sheets of sine-wave form (Fig.7.2). He proposed the following relations:

$$D_x = \left(\frac{a}{2R}\right) \frac{E\ t^3}{12\ (1-\mu^2)} \tag{7.1}$$

$$D_y = E\ I_y \tag{7.2}$$

$$D_{xy} = \left(\frac{a}{2R}\right) \frac{E\ t^3}{12\ (1+\mu)} \tag{7.3}$$

Where D_x is the bending rigidity per unit width in the x direction (about the weak axis), D_y is the bending rigidity per unit width in the y direction (about the strong axis) and the D_{xy} is the torsional rigidity per unit width.

Considering that the ratio f/a, where f is the profile height and a is the wavelength of the corrugation, is small compared to 1.0, it is assumed that D_y can be approximated as:

$$D_y = 0.522\ E\ \left(\frac{f}{2}\right)^2 t \tag{7.4}$$

The relations proposed by Abdel-Sayed have been quoted by several authors such as Mang et al. (1976) and Davies (1978, 1979). Trahair et al. (1983) proposed an alternative set of relations to calculate the mechanical properties of profiled sheets. These relations were derived in a similar manner to those of Abdel Sayed. Briassoulis (1986) used finite element and energy analyses of a flat corrugated sheet to introduce improvements to the expressions proposed by Abdel-Sayed (1970). Zhang and Rotter (1988) used numerical studies to determine which of the early relations (Abdel-Sayed (1970), Trahair et al. (1983) and Briassoulis (1986)) furnished the best results. The study favoured Abdel-Sayed's prediction of the orthotropic bending rigidity of the sheeting.

The knowledge which has been gained through the understanding of the behaviour of these elements, has been implemented as sets of rules,

specifications and guide-lines in codes of practice. The simplistic design approach which prevailed in the early stages has been radically changed to comprehensive and extensive investigations which have impacted on recent codes of practice world-wide. (See for example, the Australian Standard AS 1538 - 1988, the Swedish Code for light-gauge metal - in English - 1982, the British Standard (1976), and the European recommendation for the testing of profile metal sheeting (1977)). These are examples of the new approach for testing and design.

The increase in research activities and the developments in the methods of research in the field of profiled sheeting has lead to a new building technology in which profile sheets are regarded as an integrated part of the structure, and are utilised to improve the overall structural performance. Hence new types of steel structures other than those based on conventional skeletal frameworks, girders or frames have been proposed (Baehre, 1983).

The successful future development of efficient integrated structural systems can only be achieved when full consideration is given to the behaviour of different structural elements under various loading cases and boundary conditions.

7.2 Present Research Work

Profiled thin plates are aesthetically pleasing, and efficient from the point of view of strength. They have a relatively high stiffness for in-plane and lateral loading, which is their striking characteristic. However, under certain loading conditions, local buckling can be a challenging problem for the designer of such structural elements.

The aim of this study is to report and explain an interesting phenomenon associated with the behaviour of profiled sheets under a laterally applied, static, concentrated load. During tests of profiled sheet type-A (Fig.7.3), it was found that initial failure, due to inelastic local buckling, occurred in shorter spans rather than longer spans under the same load level (Salaheldin et al., 1987). In identifying the various parameters that govern the performance of profiled sheets under such conditions, the study is divided into two parts.

The first part is focussed on the deflection behaviour of profiled sheets (type-A). The study includes testing of these type of sheets under concentrated load. Also, linear and non-linear finite element analyses of profiled sheeting models are conducted, and the finite element analysis results are assessed in the light of the experimental work. Through this part of the study the influence of the aspect ratio, $\lambda = b/\ell$ (Fig.7.1), on the behaviour of this type of profiled sheets is identified.

As the profile depth is a determining factor which affects the capacity and the performance of profiled sheets, the second part of the study is mainly focussed on an understanding of the effect of this parameter. The behaviour of profiled sheet type B (Fig.7.4), which has a relatively high value of profiled depth, is compared with the behaviour of profiled sheet type-A.

7.3 Research Work Stage I

7.3.1 Experimental Work

The geometrical configuration (profile and thickness) of the profiled sheets used is shown in Fig.7.3. The sheet material was high tensile steel with a modulus of elasticity E = 200 GPa, and a yield stress σ_y = 600 MPa. These

values were the average of the results obtained from three simple tensile tests of the material. As the width of the sheet was constant, the aspect ratio was changed by changing the sheet length. Two span lengths were examined namely, 1400mm and 900mm.

Simple supports were provided at each end of the profiled sheets which were subjected to a central concentrated load to obtain experimental values which could be compared with the results of computer analyses.

The concentrated loading system was designed in accordance with Australian Standard AS 1562-1980. The load was applied through a rubber pad of 102 mm diameter. The force was transferred to the rubber pad through a disc of steel (Fig.7.5) and was measured with a load cell.

The sheet was mounted on transverse channels, to which the sheets were fastened at four points at each support by means of screws (12mm diameter x 35mm length, hexagonal - neoprene washer) in a conventional manner (every second ridge).

The experimental deflections normal to the sheeting were measured by dial gauges graduated in 0.01 mm. Eleven gauges were located across the mid-span. The layout of the testing rig is shown in Fig.7.6.

7.3.2 Results and Discussion

(a) Test A - Span length = 1400 mm

Significant local out-of-plane deflections started to occur at a very early stage of loading. This type of distortion is expected due to the concentrated loading

used. As the load increased, a continuous flattening of the ridge under the load occurred.

A local plastic collapse mechanism developed at a load level of 2.1 kN at the central strip. The mechanism involved a localised folding of ridges adjacent to the flattened ridge. This mechanism was associated with the redistribution of stresses, where the region far from the concentrated load carried more stresses. Consequently, a more even distribution of longitudinal stresses across the corrugated sheet was achieved.

At a load level of 2.4 kN a global failure mechanism developed; the stiffness of the plate dropped off and this action was accompanied by rapid load shedding. A failure line occurred right across the sheet, with each ridge displaying a local plastic collapse mechanism. A detailed description of the mechanism will be presented at a later stage.

The results of deflection readings of the structural behaviour during the loading process for three stages of loading, namely, 0.2, 1.1, 1.8 kN, are shown in Fig.7.7-a. It can be seen with further increase of the load the concentration of the out-of-plane deflection decreases towards the centre (where the load is located), giving way to a more uniform deflected shape at a higher level of loading. In order to highlight this point, the deflected shape for each of these levels of loading was normalised, as shown in Fig.7.7-b.

The change in the deflected shape, which is associated with the increase of load level, influences the load carrying capacity of the plate due to the redistribution of the stresses over the cross section.

The point is made that non-uniformity of the stress distribution decreases, as higher levels of loading are applied, and therefore the efficiency of the corrugated sheet increases progressively.

(b) Test B - Span length = 900 mm

A local folding of the ridges adjacent to the flattened ridge formed at a very early stage of loading (0.6 kN). Although this local mechanism was formed, the corrugated sheet deformed further with increasing load carrying capacity until a global collapse mechanism was established at 4.0 kN.

The significant difference between the local buckling load and the over-all failure load, shows clearly that the former load does not indicate an upper limit to the load carrying capacity of the sheet, as a lengthy post-critical region exists. This behaviour is explained by the fact that once buckling occurs, the central strip, where the deflections are greatest, carries reduced load while the remaining parts of the sheet continue to resist the increasing loads. A significant internal stress redistribution occurs.

(c) General comments

In all models, the local collapse mechanism was initiated by some yielding occurring due to the increasing value of the stresses under the concentrated load.

For sheets with a large aspect ratio, $\lambda = b/\ell$, a local collapse mechanism occurs at an early stage of loading. Successive local collapse mechanisms formed in each ridge across the sheet as the loading increased. Upon formation of local buckling mechanism in the outermost ridges the carrying

capacity of the plate decreased rapidly. Simple overall folding of the sheet then occurred.

When the aspect ratio, λ, decreases the difference between the critical load, at which the first localised failure occurs, and the collapse load decreases.

It was noticed that the shape of the local failure plastic mechanism was identical for all models tested.

Although, the steel material used for the models tests was found to be brittle in tension, the overall behaviour of the laterally loaded sheet for a large aspect ratio, was classed as ductile in its load-deflection response. This finding can be explained by the change of geometry and the redistribution of stresses associated with the localised mode of failure.

For high values of λ, the permanent deflection caused by local buckling at an earlier stage of loading had very little influence on the total carrying capacity of the corrugated plate.

7.3.3 Computer Modelling

The computer models were specifically designed to study the effect of the aspect ratio, λ, on the response of corrugated sheet under a static concentrated loading applied laterally.

Both boundary conditions and the loading system, for all modes, were similar to those of the experimental work. Linear and geometric non-linear analysis were carried out, using a finite element method (McNeal, 1978) to simulate the

response of the sheet. The material was assumed to be perfectly elastic for these analyses.

A fine mesh was used with 51 elements across half the width of the sheet. The curved part at the ridge and the valley was idealised as a straight segment and the tangent part of the profile was divided into four segments as shown in Fig.7.8. The existence of high stresses close to the concentrated load dictated the use of a biased mesh along the length of the span. Because of the symmetric boundary conditions and loading, only a quarter of the plate was considered for analysis. The width of all models was constant and equal to 760 mm. The span, however, was varied to give an aspect ratio, λ, in the range between 1.08 to 0.27. The materials properties used in the analysis were assumed to have a modulus of elasticity E=200 GPa, a Poisson's ratio μ=0.3, and a thickness t = 0.45 mm.

Analyses were carried out for all models at two load levels, namely 0.6 and 0.8 kN. The experimental results showed that the former load was the critical load for the span of 900 mm.

7.3.4 Results and Discussion

Establishment of the validity of the results of the non-linear analyses was achieved by comparing them with the experimental results.

It can be seen from Fig.7.9 that the overall agreement between experimental and theoretical results is reasonably good. However, for position numbers (3 and 9) the difference between the two results is quite noticeable. But this difference is not of great significance as the value of the deflections at these positions are small.

Fig.7.10 shows the deflection at mid-span resulting from both linear and non-linear analyses. It is clear the result from the linear analysis is different from that from the non-linear analysis.

For a load level of 0.6 kN the linear and non-linear distributions of stress across the midspan of the profiled sheet are shown in Figs.7.11 and 7.12 for span lengths of 900 mm and 1400 mm, respectively. The results show that the corrugated sheet is subjected to varying non-linear distribution of stresses over the cross-section. This distribution is accompanied by a substantial out-of-plane deflection. A rapid decay of stresses is seen when moving away from the point of load application. The rate of decay is high for high values of λ (smaller span).

It is seen from Fig.7.11 that the non-linear analysis furnishes a maximum value of longitudinal stresses of almost 600 MPa. Knowing that the actual average material yield stress, in simple tension test, is 600 MPa, and that local plastic buckling was observed during the experimental work at a load level 0.6 kN, it appears that the non-linear analysis can predict the stresses of the plate to a good degree of accuracy. This observation assumes that buckling is likely when the yield stress is reached.

It is also noticed that for low values of λ (span length = 1400 mm), the maximum stresses derived by the non-linear analysis are less than those given by the linear analysis. For high values of λ the reverse applies. The significance of this point can be appreciated when considering the influence of the aspect ratio on the value of the maximum longitudinal compressive stresses at the same level of loading. Fig.7.13 shows this relation within the linear and the non-linear range. It is seen that the result of the linear analysis is misleading as it shows that the deflected shape does not agree with the

experimental results. The non-linear analysis shows that for the span length of 900 mm (λ = 0.84) the maximum longitudinal stresses are much higher than those obtained for a span length = 1200 mm (λ = 0.63).

It can now be seen that the ability of the sheet to distribute the stresses evenly, and hence to increase its efficiency and strength, is a function of the aspect ratio.

Fig.7.14 shows the relation between the aspect ratio and maximum longitudinal stresses at a load level of 0.8 kN. A comparison between Figs.7.13 and 7.14 shows that the maximum longitudinal stresses are highly influenced by the interaction of two factors: the increase of internal forces resulting from the increase of the span length, and the influence of the aspect ratio on the distribution of the internal stresses.

7.4 Research Work Stage II

In this part the deflection behaviour of profiled sheet type-B is studied. A comparison between this behaviour and the behaviour of profiled sheet type-A is conducted, together with stress-strain analyses of both types of sheetings. The analysis confirms the results obtained from the load-deflection study obtained experimentally.

7.4.1 Instrumentation and Test Procedure

The experimental work was conducted using a concentrated load and the testing rig described earlier (Figs.7.5 and 7.6).

A low voltage digital transducer was used to monitor the central deflection. The output was fed directly into an x-y plotter so that a continuous trace of the load-deflection curve was obtained. This procedure enabled the deflection associated with the onset of localised plastic collapse mechanisms to be observed.

In measuring the strain, uniaxial electrical resistance strain gauges were used. The gauges were bonded to both the inner and the outer side of the upper flange of the sheet, near the centre (Fig.7.15). The gauges could not be positioned exactly at mid-span because of the existence of the central load and the expected localised failure mechanisms.

The strain readings for each loading sequence were recorded using a computer-based automatic data acquisition central system. The data were processed and stresses at the strain gauge locations were calculated.

Prior to any load application, the strain gauge readings were checked. The models were loaded incrementally to collapse. The loading was applied by a hydraulic jack in series with a load cell. The central deflection was measured simultaneously using the transducer.

7.4.2 Load-Deflection Analysis

The load-deflection relations for the two types of profiled sheets, type-A and type-B, were observed. The span length was varied to allow for observation of the aspect ratio influence on the behaviour. Another factor which may influence the behaviour is the depth of the profiled section. This factor was examined when the results of profile sheet type-A were compared with the

results of profile sheet type-B. For each case considered herein, three tests were conducted. The difference between the three test results is within 6%.

(a) Profile Sheet Type-A

A transducer was used to obtain a continuous load deflection curve for simply supported profile sheets type-A with span lengths equal to 1400 mm and 900 mm respectively. The aim was to confirm the earlier results regarding the aspect ratio influence on the structural behaviour (Salaheldin et al., 1987).

Fig.7.16 shows the critical load (the load at which the first local plastic collapse mechanism is formed) to be 2.05 kN. The sheet reached a maximum load of 2.5 kN after which several local collapse mechanisms occurred; a failure line formed across the middle of the span and the sheet totally collapsed.

The load deflection relation is represented by a smooth continuous curve. The formation of each local plastic mechanism in each rib is associated with a small drop in the load capacity. The area of influence, which is defined as the area affected by the load and which participates significantly in the bearing capacity of the sheet at a particular load level, is found to be relatively large.

Testing the shorter span (900 mm) lead to a different pattern. Fig.7.17 displays the load deflection curve for profiled sheet type-A. The plotted results displayed an irregular load-deflection relation. The first collapse mechanism occurred at 0.55 kN. At the early stages of loading the observation of the deflected shape indicated that the area of influence was small in comparison with the area of influence of the large span; the formation of early local collapse mechanisms lead to the belief that the small area of influence is associated with a high longitudinal membrane stress concentration.

Although the sheet suffered a local collapse at an early stage of loading, the global collapse came at a much later stage (4 kN), indicating the ability of the sheet to resist the increasing load despite the local failure.

(b) Profile Sheet Type-B

Fig.7.18 shows the load-deflection curve for sheet type-B. The sheet is simply supported with a span length of 1400 mm.

The load-deflection curve seems to be reasonably smooth. Slight load drops are associated with the formation of each local collapse mechanism across the mid-span. The area of influence is small and the concentration of membrane stresses is high. This concentration of stresses is the reason for the early local collapse mechanism which occurred at 0.6 kN. The disadvantage of stress concentration, as a result of the increased profile depth of type-B, seems to overshadow the advantage of strength gained as the profile depth increased. When testing profiled sheet type-B with span length of 900 mm, the load-deflection is found to be irregular, with large drops in the load level associated with the formation of each local collapse mechanism (Fig.7.19). The first local collapse mechanism occurred at a load level of 1.0 kN. It can now be deduced that the influence of the aspect ratio on the behaviour of a sheet with a high profile depth (type-B) when considering the critical load P_c is limited.

7.4.3 Stress Distribution Analysis

The longitudinal stress distribution across the width of both profiled sheet type-A and profiled sheet type-B were recorded. The tests were carried for high and low values of the aspect ratio. A schematic diagram of the strain gauges arrangement is shown in Fig.7.20. Two strain gauges were placed at each

position, on the inside fibre and the other on the outside fibre. The mean value was used to determine the stresses. A review of these tests is presented with particular attention being paid to the influence of profile depth and aspect ratio on the redistribution of the stresses at different stages of loading.

(a) Profiled Sheet Type-A - Test 1

A long span of 1500 mm length was tested. The distribution of stresses across the width was observed at four distinctive stages of loading. These stages of loading are numbered as shown in Fig.7.21 which displays the central load-deflection curve for this test.

Fig.7.22 shows the longitudinal stress distribution across half the width of the sheeting. At the first stage of loading the stress distribution seems to be concentrated near the centre. While the three inside ridges experienced compressive stresses, with a maximum value near the centre, the outside ridge experienced a small magnitude of tensile stresses.

The second stage of loading shows an increase of the magnitude of stresses. It also shows a more even distribution of stresses, as the ridges away from the centre experienced relatively high values of compressive stresses.

Stage 3 shows a drop in the stresses near the centre (gauge No. 1, Fig.7.20), where the stresses dropped to almost half the values at the previous stage. This decrease of the stresses near the centre is due to the formation of a local collapse mechanism just before reaching stage 3. The two ridges near the edge (No. 3 and No. 4, Fig.7.20) experienced an increase in the stress.

At the final stage there was a general reduction in the stress across the width with the exception of the outermost ridge which experienced a slight increase in compressive membrane stresses.

The test confirmed the fact that for a small aspect ratio the redistribution of stresses across the profiled sheet is increased with increase of load. Thus a profiled sheet (Type-A) with a long span can sustain a high value of concentrated load without suffering from any sign of local failure. On the other hand a profiled sheet with a short span suffers local failure at an early stage of loading due to the concentration of stresses.

(b) Profiled Sheet Type-A - Test 2

A relatively short span of 990 mm was tested. Fig.7.23 shows the central load-deflection curve and the four stages of loading. Fig.7.24 shows the distribution of longitudinal stresses, across the sheeting for each stage of loading.

The first stage of the stress recording was considered just before the first collapse mechanism occurred. The stress distribution at this stage shows a high concentration of stresses towards the centre. The two outside ridges (No. 3 and No. 4, Fig.7.20) did not share in resisting the load at this stage. As a result of this concentration of longitudinal stresses an early local plastic mechanism was formed.

The second stage of data recording took place after the load collapse mechanism formed. It shows the longitudinal stresses at the ridge near the centre (No. 1, Fig.7.20) decreasing. The adjacent ridge experienced

increasing localised compressive stresses and the outside ridge (No. 4, Fig.7.20) experienced limited tensile stresses.

Another collapse mechanism occurred before the data recording of stage 3, which shows a drop in the membrane stresses of the second ridge from the centre (No. 2). The drop is expected as the stresses were affected by the second mechanism. Further decrease of the stresses near the centre (first ridge) is noticed. The stresses in the two outside ridges (No. 3 and No. 4, Fig.7.20) are increased.

The final stage of loading was associated with a reduction of stresses across the sheeting as more local collapse mechanisms occurred in the ridges. The test demonstrates that the relatively small span (large aspect ratio) limited the ability of the profiled sheet to redistribute the stresses across its width, leading to an early localised failure.

(c) Profiled Sheet Type-B - Test 1

A type-B long span sheet (ℓ = 1400 mm) was tested under a concentrated load. Figs.7.25 and 7.26 show both the load-deflection curve and the change of the distribution of longitudinal stresses, through different stages of loading, near the middle cross section of the sheet, respectively. The numbers in Fig.7.25 correspond to these stages of loadings. The stress distribution at these stages of loading is detailed in Fig.7.26.

Fig.7.25 shows a small drop in the load deflection curve at a very early stage of loading, before the first recording of the stress distribution. The collapse mechanism was so localised in its influence that the recorded stress

distribution at stage 1 did not seem to be affected by it. It is to be noted that the strain gauges were not placed at the centre (Fig.7.15).

The first stage of stress distribution shows more concentration of longitudinal membrane stresses towards the centre than those encountered when profiled sheet type-A were considered. A comparison between Fig.7.26 and Fig.7.22 supports this view.

Stage 2 (Fig.7.26) shows the load to be resisted only by the first and the second ridge from the centre. It also shows that ridge No. 1 experiences much higher longitudinal stresses than ridge No. 2.

Immediately after the second stage of loading, there was a drop in the local deflection curve which was associated with the formation of the second local collapse mechanism at a position adjacent to the first mechanism and further away towards the edge.

The stress distribution record of stage 3 shows an expected drop on the first ridge. It also shows a higher concentration of stresses at ridge No. 2. The stresses on the last two ridges contribute little to the load carrying capacity. Stage 4 of the loading cycle is a repeat of stage 3 as more local ridge collapse mechanisms were formed. The second strain gauge from the centre, furnished an unrealistic record. This record was a result of the damage of the strain gauge due to the formation of the local collapse mechanism.

The test proves that increasing the depth of the sheeting leads to more localised concentration of stresses. This concentration of stresses causes early localised failure (Fig.7.25).

(d) Profiled Sheet Type-B - Test 2

The profile sheet had a length of 900 mm. The length was chosen to achieve the same aspect ratio encountered when testing type-A (shorter span). Figs.7.27 and 7.28 display the load-deflection relation and the corresponding distribution of stresses across the width of the sheeting. The load-deflection curve shows a significant drop in the load level associated with the formation of the local collapse mechanisms in the ridges. The stress distribution diagram shows an increase in the concentration of stresses in comparison with type-A, which is attributed to the increase in profile depth, as can be seen when Fig.7.26 is compared with Fig.7.28.

Table 7.1 Critical and Failure Loads for Profiled Sheets

Profile type	ℓ (mm)	P_c (kN)	P_f (kN)
Profile Type-A	1400	2.10	2.50
	900	0.60	4.00
Profile Type-B	1400	0.60	3.55
	900	1.00	6.50

Table 7.1 summarizes the results when comparing the behaviour of type-A with type-B. Particular attention is focused on the influence of the span length ℓ (which represents the aspect ratios, as the width is constant) on the first critical load P_c and the final collapse load P_f.

When the profile depth is shallow (type-A) the sheet with a small span length (900 mm) suffers early local deformation (P_c = 0.6 kN). However, a reserve of

strength is evident as the value of P_f is equal to 4 kN. The sheet with the long span (1400 mm) has a great ability to redistribute the stresses without any plastic deformation, which reflects the effect of the low aspect ratio on the behaviour. As a result of this redistribution of stresses the values of P_c and P_f are very close (2.1 kN and 2.5 kN).

With the increased profiled depth (type-B), a normal "beam" behaviour dominated, where P_c for the shorter span (900 mm) is greater than P_c for the longer span (1400 mm). The same pattern of behaviour can be seen when considering the failure load P_f which has a value of 3.55 and 6.5 kN for the longer span (1400 mm) and the shorter span (900 mm), respectively.

Overall, the analysis confirmed the earlier results, as it proved the dominating influence of the aspect ratio on the redistribution of stresses in the shallow profiled sheets. It also proved that the increase in the profiled depth limits the influence of the aspect ratio on the redistribution of the longitudinal stresses. Each of the ridges of the profiled sheet (type-B) reflects the pattern of a "beam" behaviour. Consequently severe concentration of stresses exist and lead to early permanent deformation in the form of local collapse mechanisms in the ridges.

7.5 Local Plastic Mechanisms

When testing profiled sheet type-A and type-B identical local plastic mechanisms occurred for each type.

Fig.7.29-a and b shows the pattern of local plastic failure which occurred when testing profiled sheet type-A. A Z-shape deformation can be observed. The shape has two troughs almost transverse. These troughs are joined near the

top of the ridge by a short failure line (plastic line). It is this plastic line that allow the mechanism to be developed.

It is believed that the deformation started after reaching the plastic limit of the material, as the original shape of the cross section is expected to prevent elastic buckling.

Fig. (7.30-a and b) display the plastic mechanism encountered when testing profiled sheet type-B. The slenderness ratio of the profiled components together with the high yield stress of the material suggested that elastic local buckling in the upper part of the sheeting (the compressive part) occurred before the final plastic buckling. The increasing effect of the elastic local buckling leads to the yield of the material. However, the corner of the profiled sheet, where the flange meets the webs, restrains the structure against forming a collapse mechanism. The web/flange junction region has to undergo in-plane plastic deformation to create a yield region which links the yielded part of the flange with that of the web and thus allowing a mechanism of failure to be developed (Fig.7.30-b).

The critical load, where the first local collapse mechanism occurs, can be predicted with a good degree of accuracy using the finite element technique, as discussed earlier. However, an alternative method to determine the critical load and the post yield behaviour of profiled sheet type-B, where elastic buckling occurs, is to picture the complex mechanism of failure as the sum of a number of simple basic mechanisms. The deflections of these simple basic mechanisms are compatible with that of the actual complex mechanism (Murray and Khoo, 1981). A detailed study of the application of this method in the case of the local plastic mechanism for profiled sheet is beyond the scope of the present work.

7.6 Design Criteria for Profiled Sheeting Under Concentrated Load

As it has been demonstrated, in some cases, the performance of profiled sheeting under concentrated load can be critical. In these cases, the aspect ratio has a significant influence on the behaviour of the sheeting. For large aspect ratios (short spans) the sheeting performance under concentrated load is the governing design factor.

The British Standard (1976) specifies that for roofs between 0 and 45 degrees pitch, allowance should be made for a load of 0.9 kN acting vertically on a square with a 125 mm side measured on the roof slope. For roofs greater than 45 degrees pitch the standard recommends that no allowance need be made for a concentrated load. As for failure criteria, the British Standard states that "failure of a sheet should be deemed to have occurred when it reaches a state of collapse or becomes cracked to an extent that would make it unfit for use. Sheets could, for example, be considered to have become unfit for use, as demonstrated in the tests, when large permanent deformation occurs".

The Australian Standard AS1562-1980 states that for roofs with slopes less than 35 degrees a test concentrated working load of 1100 N shall be applied. For roofs with slopes greater than 35 degrees the concentrated working load is reduced to 450 N. For the ultimate loading test the test load is 2200 N and 1100 N for roofs with slopes not greater than 35 degrees and greater than 35 degrees, respectively.

In all cases the concentrated force shall be applied through a circular loading pad with a diameter of 102 mm. In the case of the ultimate load test the Australian Code specifies that the load shall be sustained and despite any

permanent deformation that may occur, the sheeting shall remain substantially in its proper position.

When the working load test is considered the code stresses that "no de-indexing, unclipping, permanent local deformation, fracture or failure of any part of the sheeting or failure of the fastening shall occur".

In comparison with the British Standard (1976), the Australian Standard (1980) seems to be conservative. It specifies a higher concentrated test load than that recommended by the British Standard. The Australian Standard also specifies a smaller area over which the concentrated load is applied than that recommended by the British Standard. Further, the significance needs to be re-assessed of the initial local failure as it occurred during the testing of the profiled sheets, and the corresponding critical load. The following paragraphs will highlight this point.

7.7 Concluding Discussion

The performance of profiled steel sheets has been investigated under static concentrated loads. Two basic profiled sections have been examined, profiled sheet type-A and type-B, with the former having a lower profiled depth than the latter.

In particular, overall deflections are considered in the non-linear range. Associated with this range is the onset of inelastic local buckling in the ridges of the profiled sheeting. The investigation indicates when this local buckling is likely to occur, and the manner in which it is affected by the aspect ratio of the sheeting.

The test results indicate that the sheeting is deemed, according to the Australian Standard Code (1980), to fail with the onset of permanent local buckling. Moreover, the problem is compounded, when considering type-A profiles, as the results indicate that this local buckling limit is reached in shorter spans rather than larger spans, for the same applied load. The investigation of the behaviour of type-B has led to the realisation of the profile depth influence on the redistribution of longitudinal stresses. The concentration of these stresses increased when the profiled depth increased.

In an attempt to summarise the results and the implications of this study, a review of these results is presented with particular attention being paid to the factors controlling the longitudinal stress distribution. The implications of the study is then presented.

When considering the performance experimentally of profiled sheets with a relatively shallow depth (type-A), it was found that the aspect ratio has a marked effect on the behaviour of the sheets. For higher aspect ratios (shorter spans) a local plastic failure mechanism was formed at an early stage of loading. However, a considerable post buckling strength was available. The initial local permanent buckling was associated with a drop in the load-deflection curve, and this drop was more significant for higher aspect ratios. This drop also reflected a local reduction in the carrying capacity of the sheet in the most heavily stressed area, and was associated with transverse redistribution of stresses, after which the sheet was able to regain its capacity to resist the load. The next local failure occurred at the two adjacent ridges away from the centre line, and another drop in the load-deflection curve was observed. The global collapse occurred after all the ridges, across the mid-span, collapsed locally (Fig.7.31).

For higher aspect ratios (shorter spans) the ultimate load was several times the critical load at which the first local permanent buckling occurred. Hence it can be deduced that the local failure, in this case, is principally an aesthetic one.

The deformability of the sheeting plays an important part in the redistribution of stresses. For low aspect ratios the sheeting is capable of achieving a considerable re-distribution of stresses. The critical load, in this case, is close to the ultimate load.

When examining the behaviour of profiled sheet type-B, which had a relatively higher profile depth, the influence of the aspect ratio on the critical load seemed to be insignificant. The increasing depth of the sheeting seemed to increase the concentration of longitudinal stresses near the centre. Therefore, for lower values of the aspect ratio (longer spans), the strength, which is assumed to be gained as a result of increasing the profile depth, seems to be overshadowed by the poor redistribution of stresses. This poor redistribution leads to local permanent failure. This effect was demonstrated when the sheet (ℓ=1400 mm) first failed locally at a load which is 0.54 the specified service load limit (1.1 kN).

The Australian Code AS1562-1980 is considered to be conservative when compared with the British Standard (1976). While the latter states that a roof sheeting at a slope less than 45 degrees should be able to sustain a load of 0.9 kN, on an area of 125 mm x 125 mm, the former states that the service load should be 1.1 kN acting on a circular area of a diameter of 102 mm. The Australian Standard (1980) also states that no plastic buckling should take place under service load. It can now be seen that the limit to useful loading of

profiled sheets, as stated in the Australian Standard, is based on aesthetic considerations rather than conventional limit states.

This investigation has fostered an atmosphere in which a more rational approach can be proposed for the structural quality control of profiled metal sheeting than is currently set down in the Australian Standard.

It is proposed, as a result of the study, that when the performance of profiled sheeting, under concentrated load, is sensitive to the change in the aspect ratio, this effect should be reflected in the design table proposed by the manufacturer. Thus consideration of the aspect ratio effect as a limit should be incorporated.

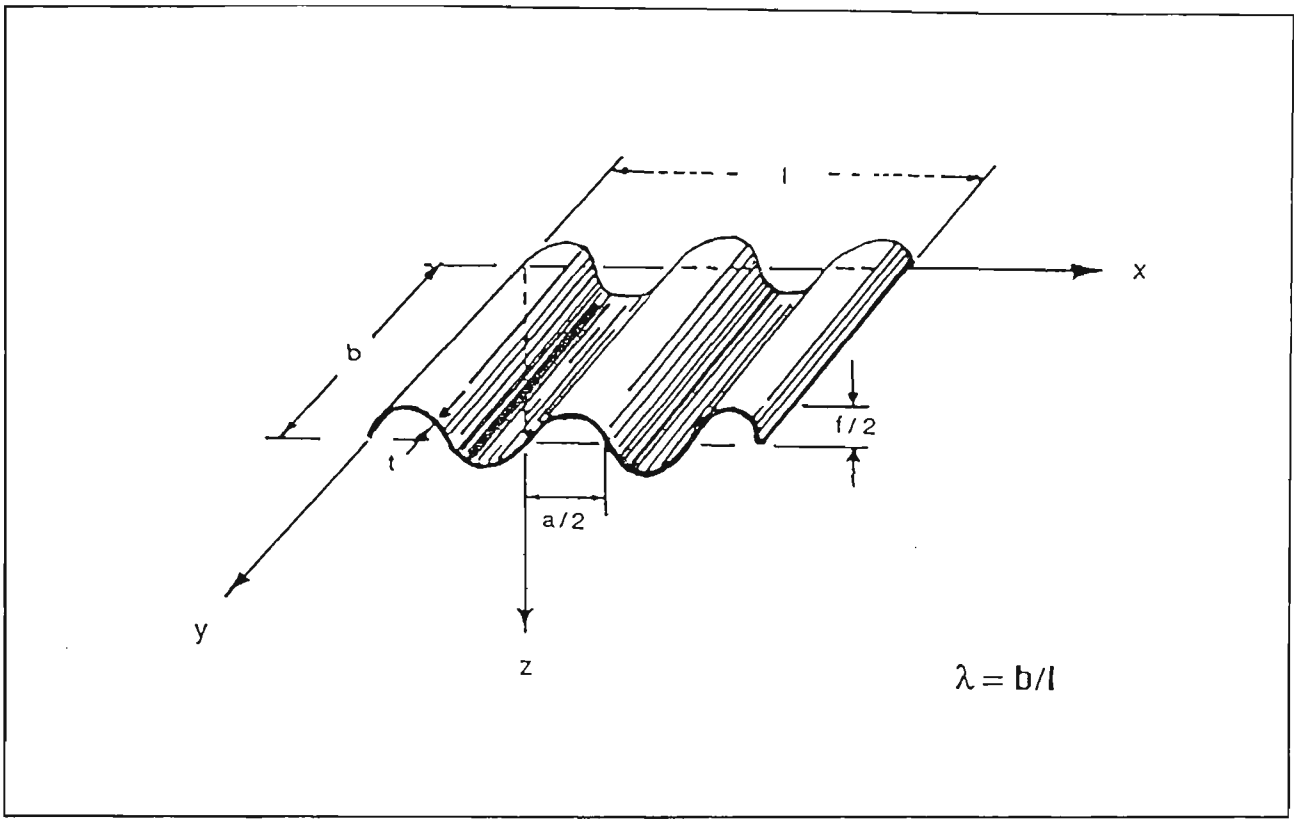

Fig. 7.1. Profiled sheet.

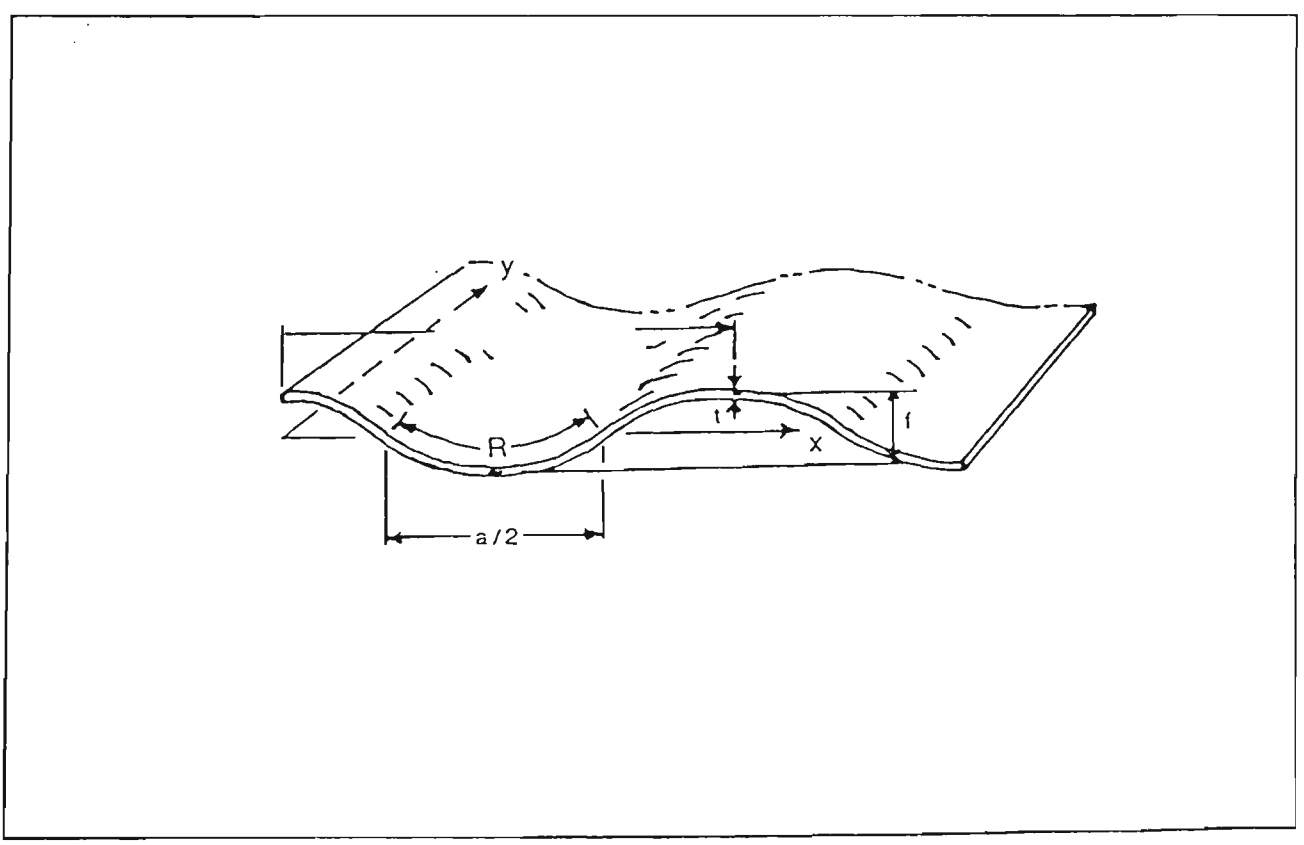

Fig. 7.2. Geometrical dimensions of profiled sheet.

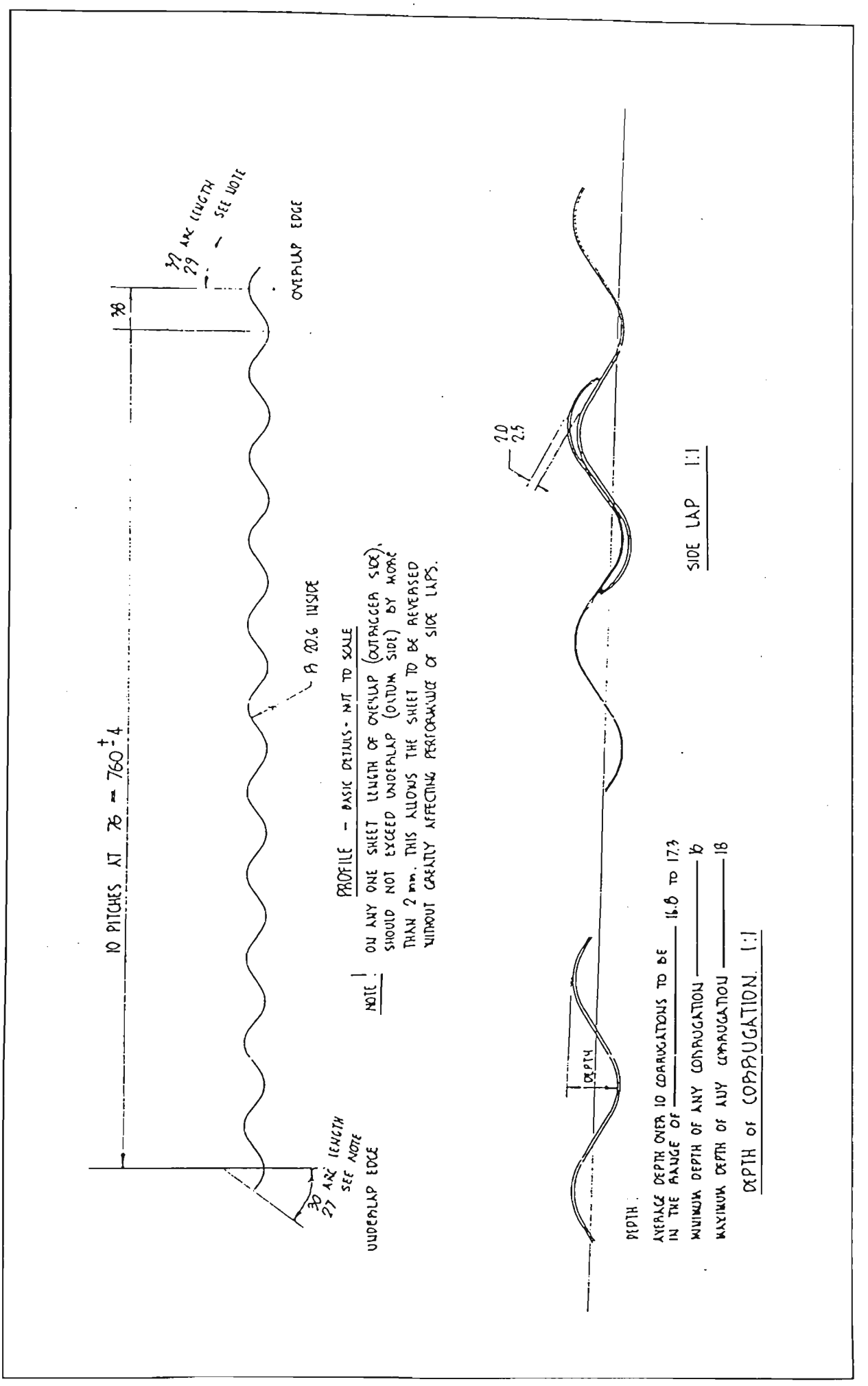

Figure 7.3. : Profiled sheet type-A.

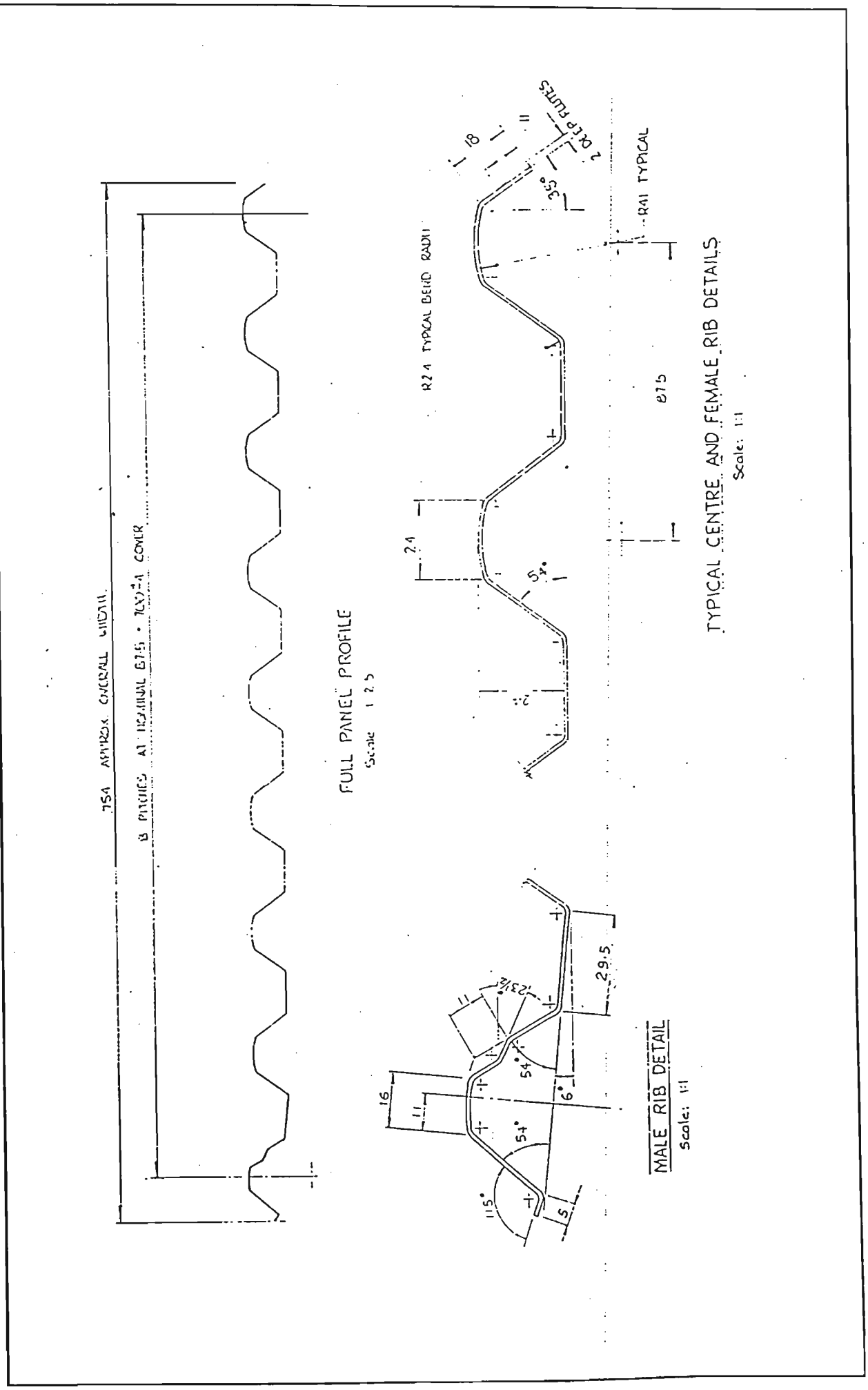

Figure 7.4. : Profiled sheet type-B.

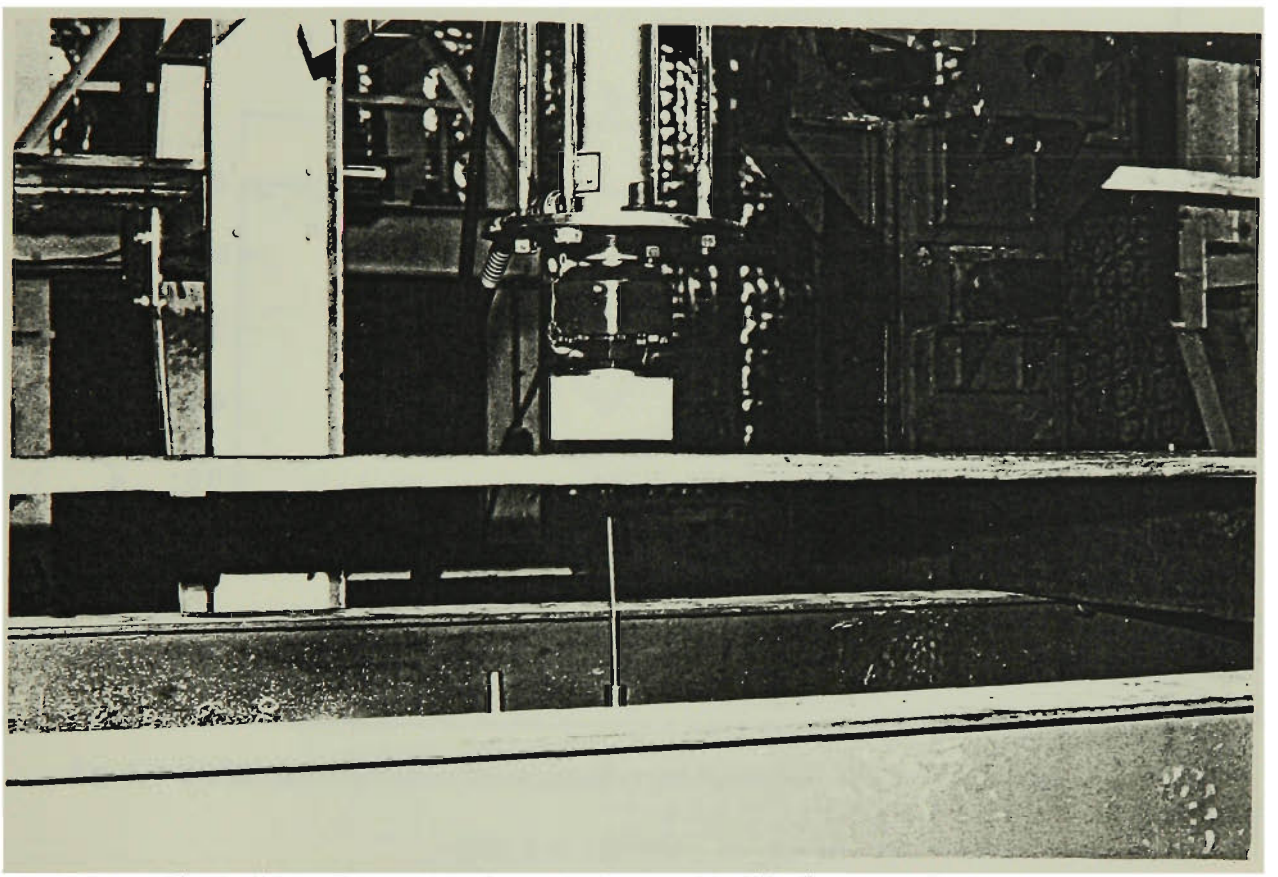

Fig. 7.5 Loading system in accordance with AS 1562 - 1980

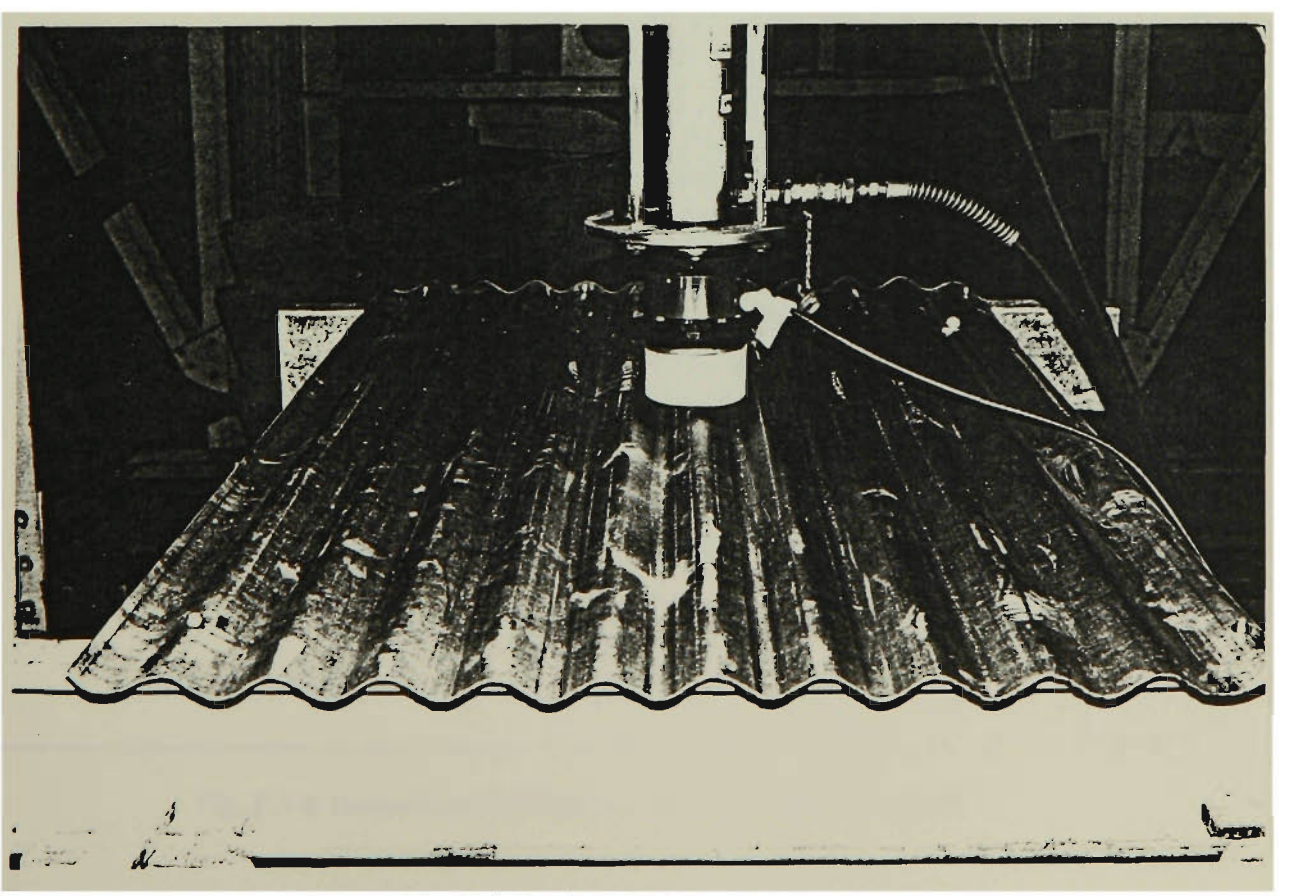

Fig. 7.6 Testing rig; layout

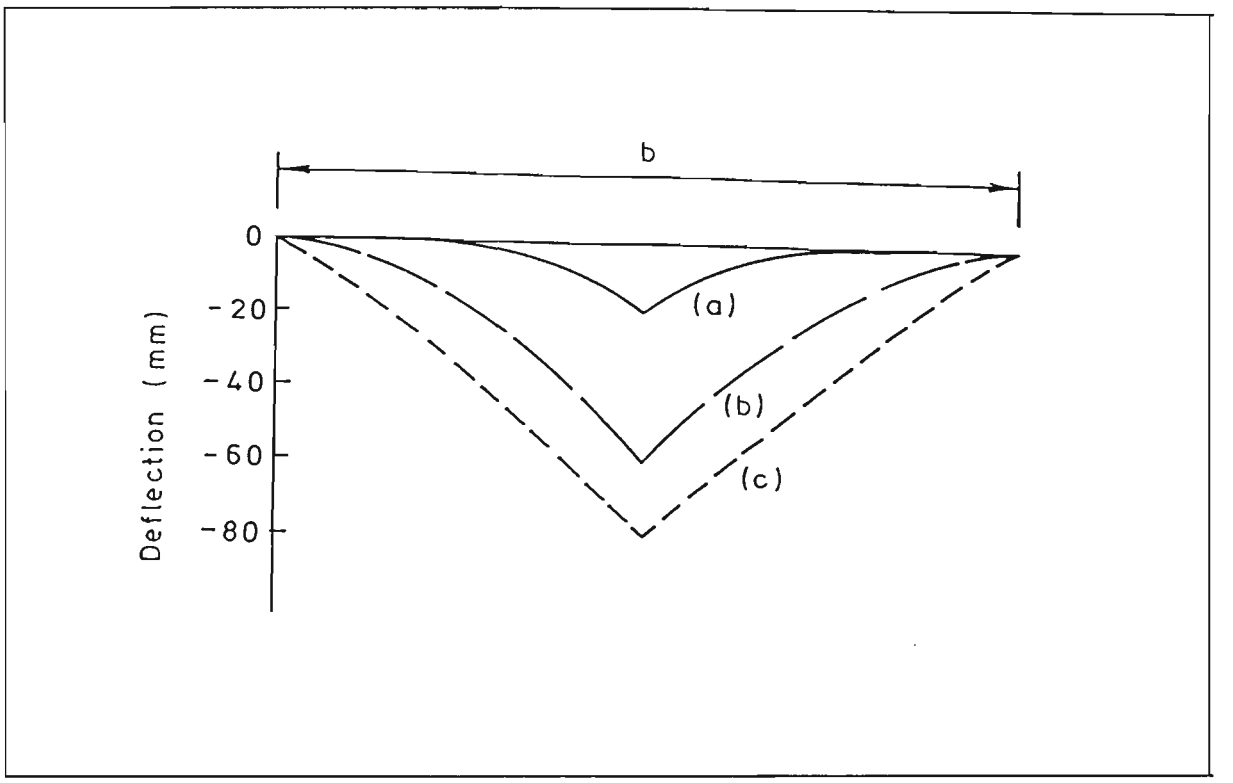

Fig. 7.7-a Mid-span deflection (ω) of cross section for three stages of loading

(0.2, 1.1, 1.8 kN)

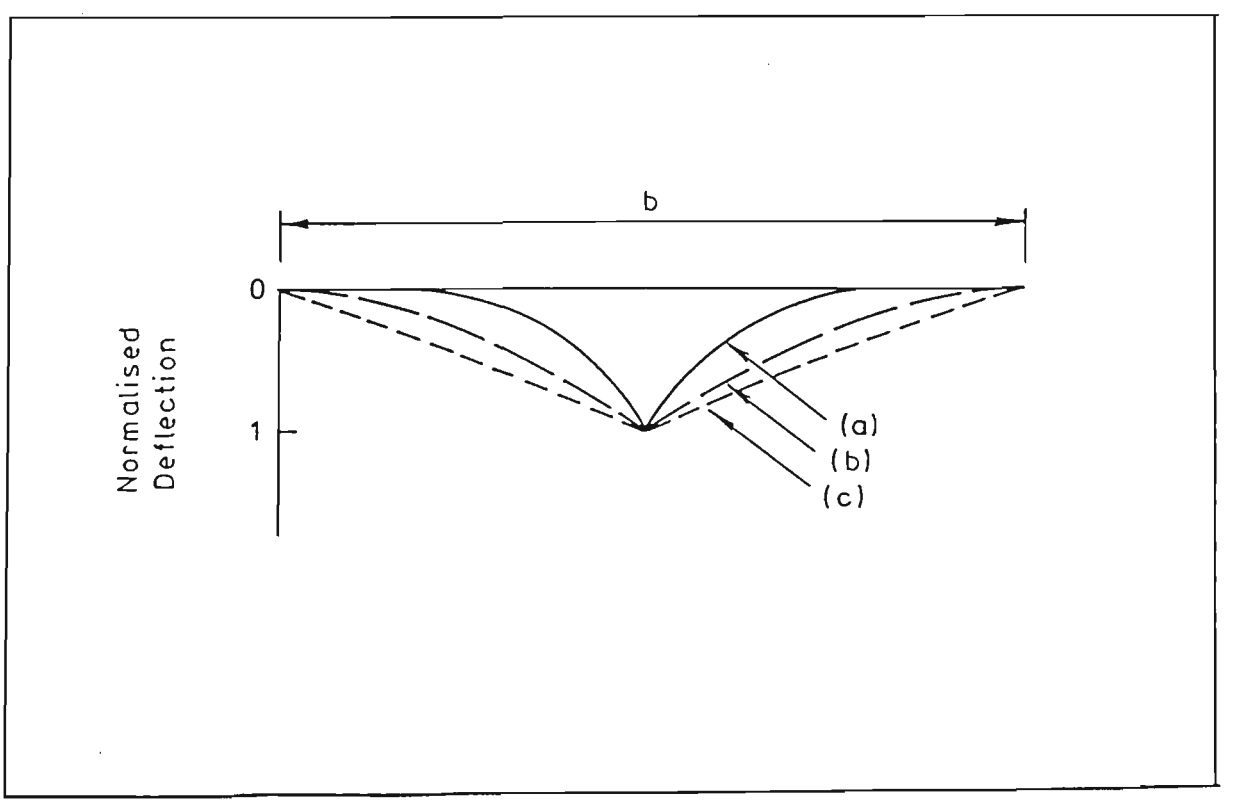

Fig. 7.7-b Normalised deflection for three stages of loading

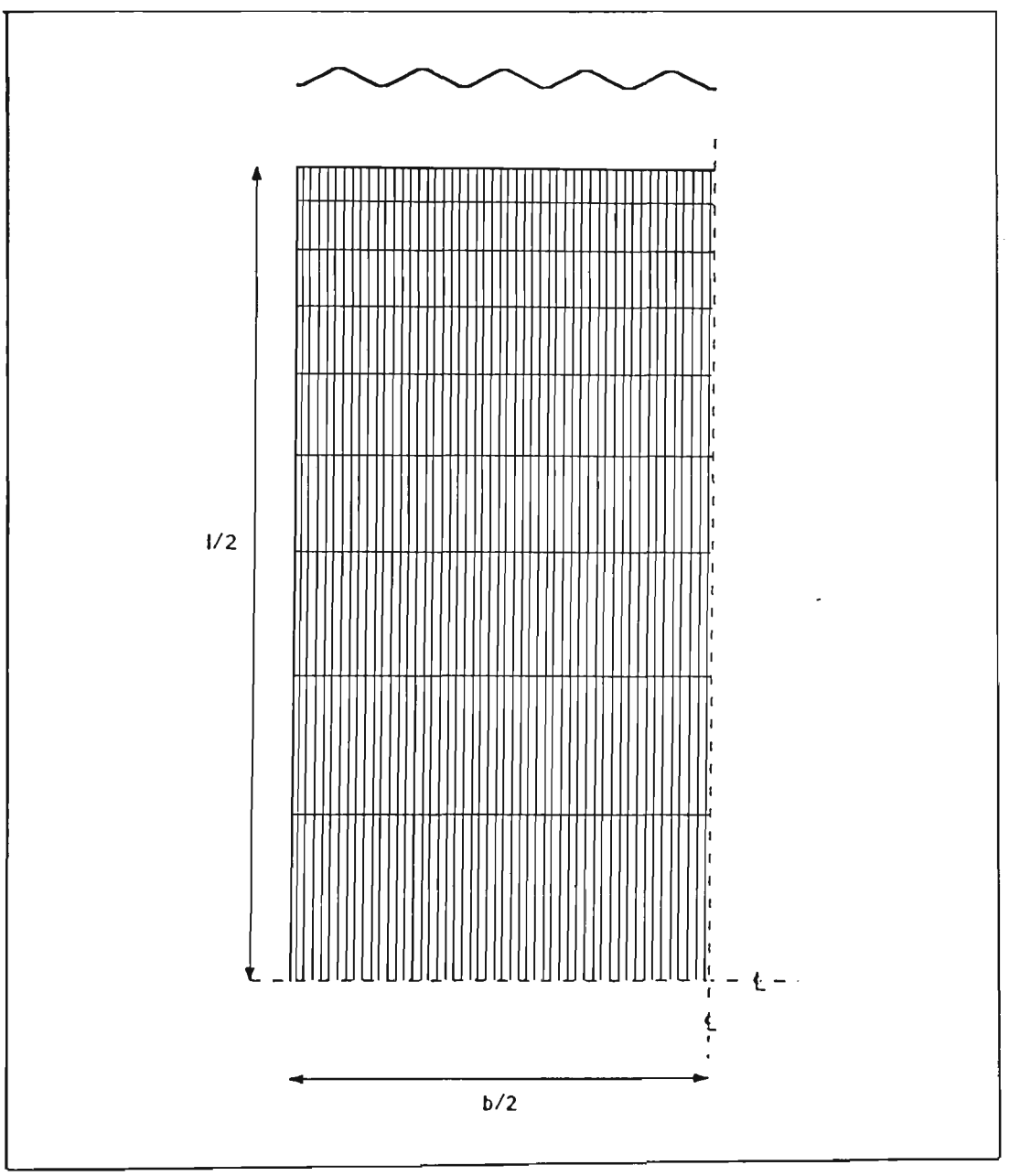

Fig.7.8 Finite element model of corrugated sheet

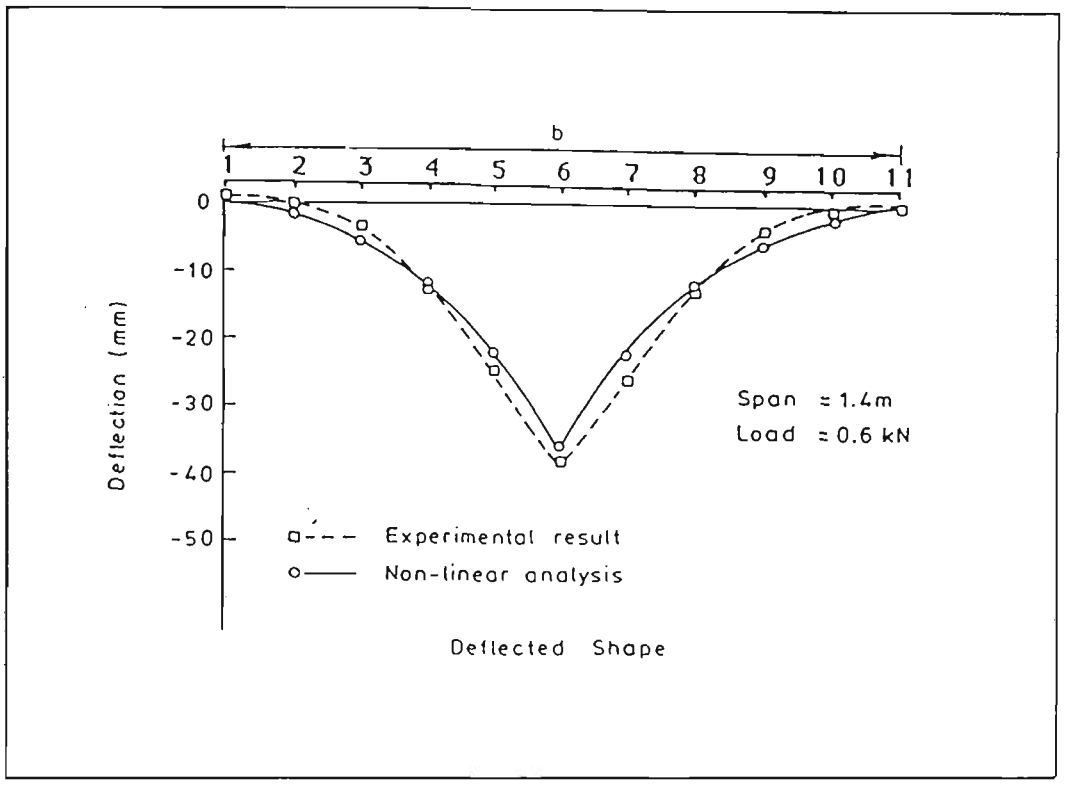

Fig. 7.9 Deflection (ω) : non-linear analysis and experimental test

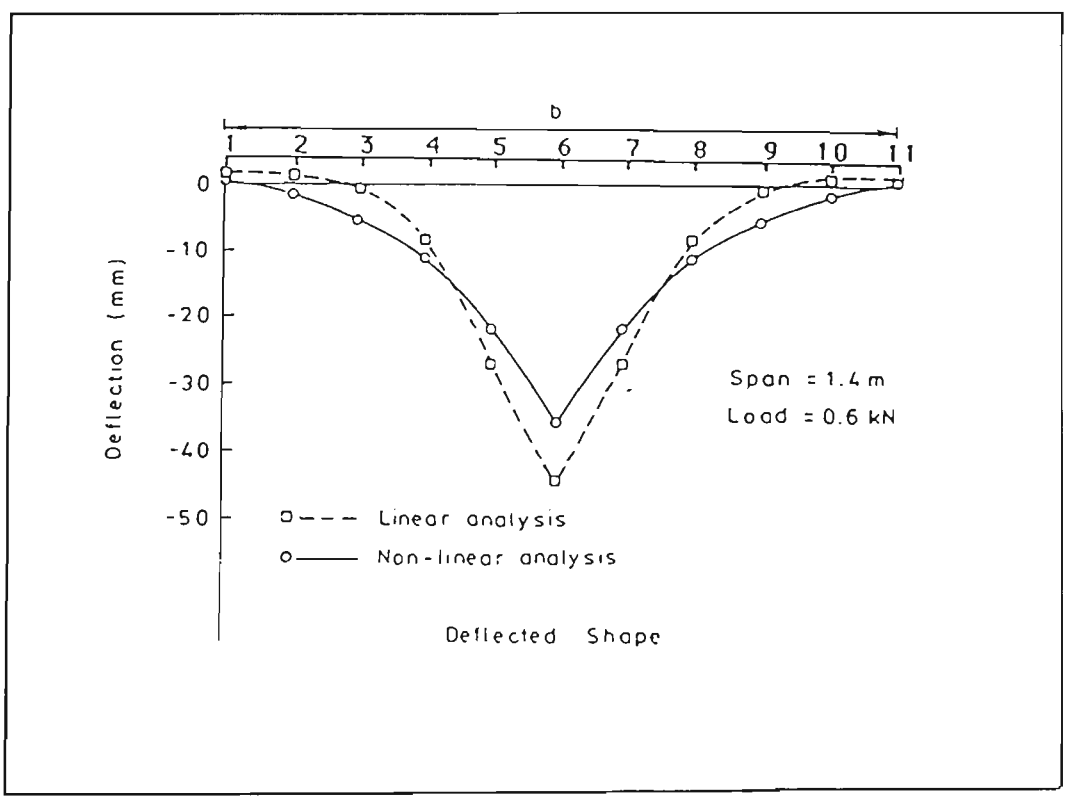

Fig. 7.10 Deflection (ω): linear and non-linear analyses

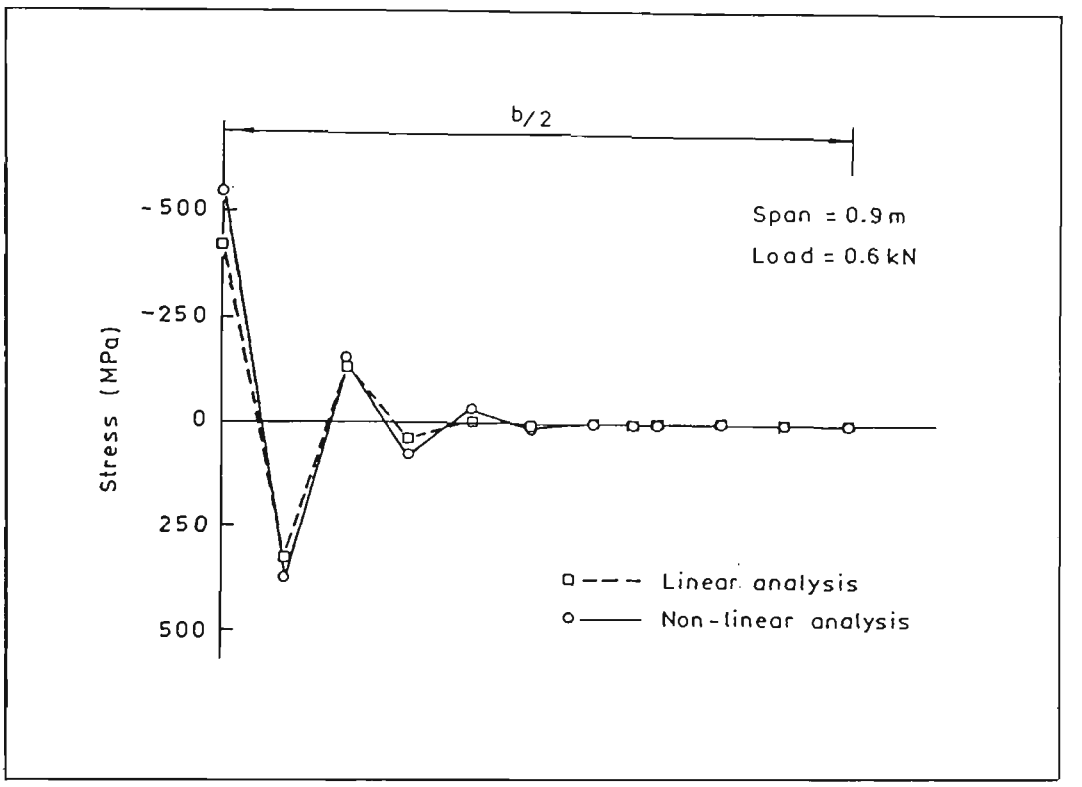

Fig. 7.11 Stress distribution at mid-span for linear and non-linear analyses

(900 mm span)

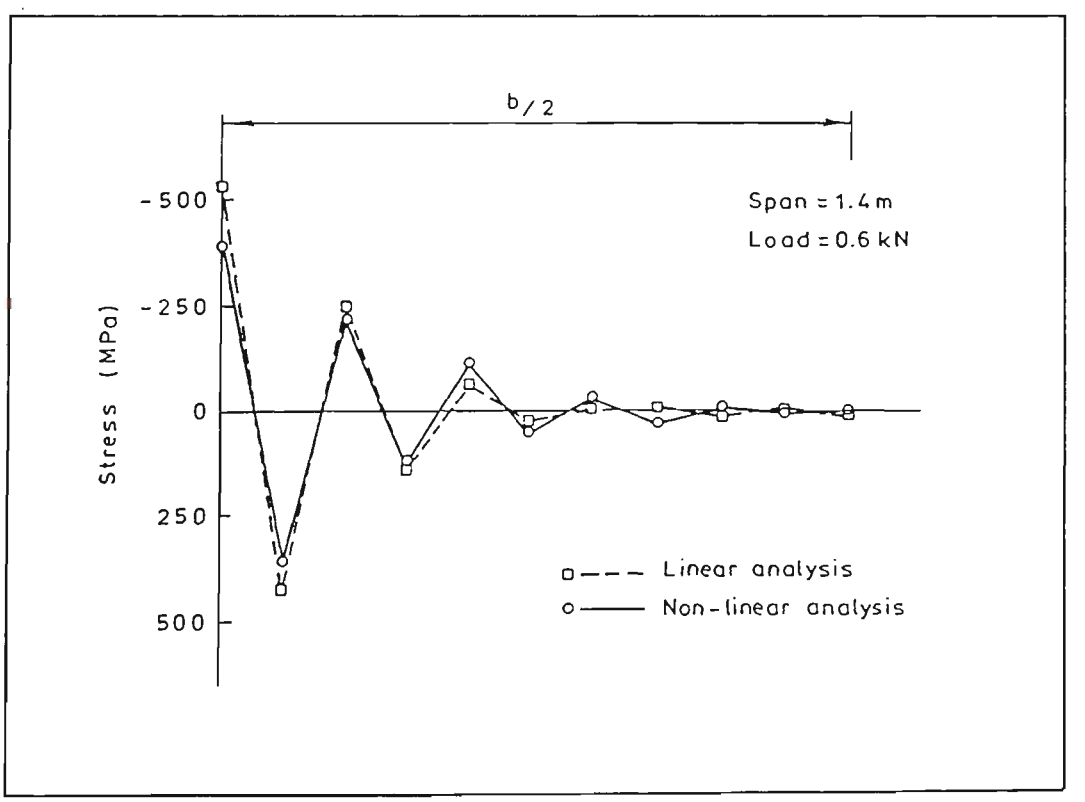

Fig. 7.12 Stress distribution at mid-span for linear and linear analyses

(1400 mm span)

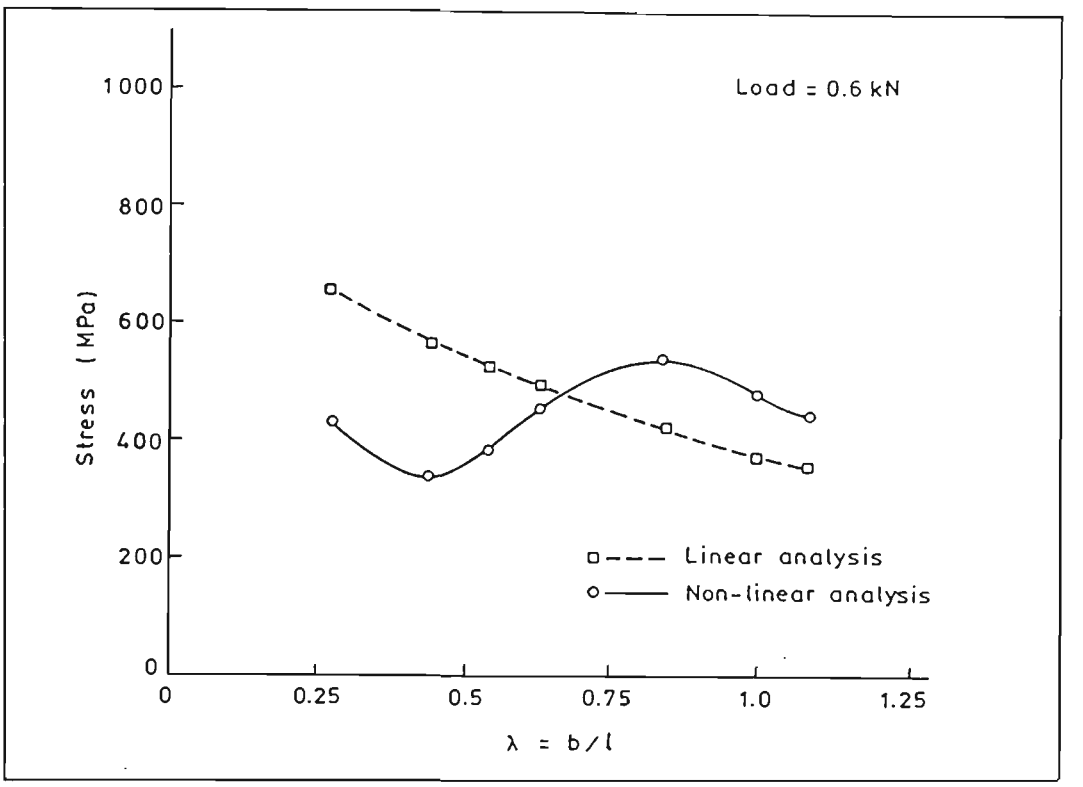

Fig. 7.13 Aspect ratio λ vs. maximum longitudinal stresses (0.6 kN load)

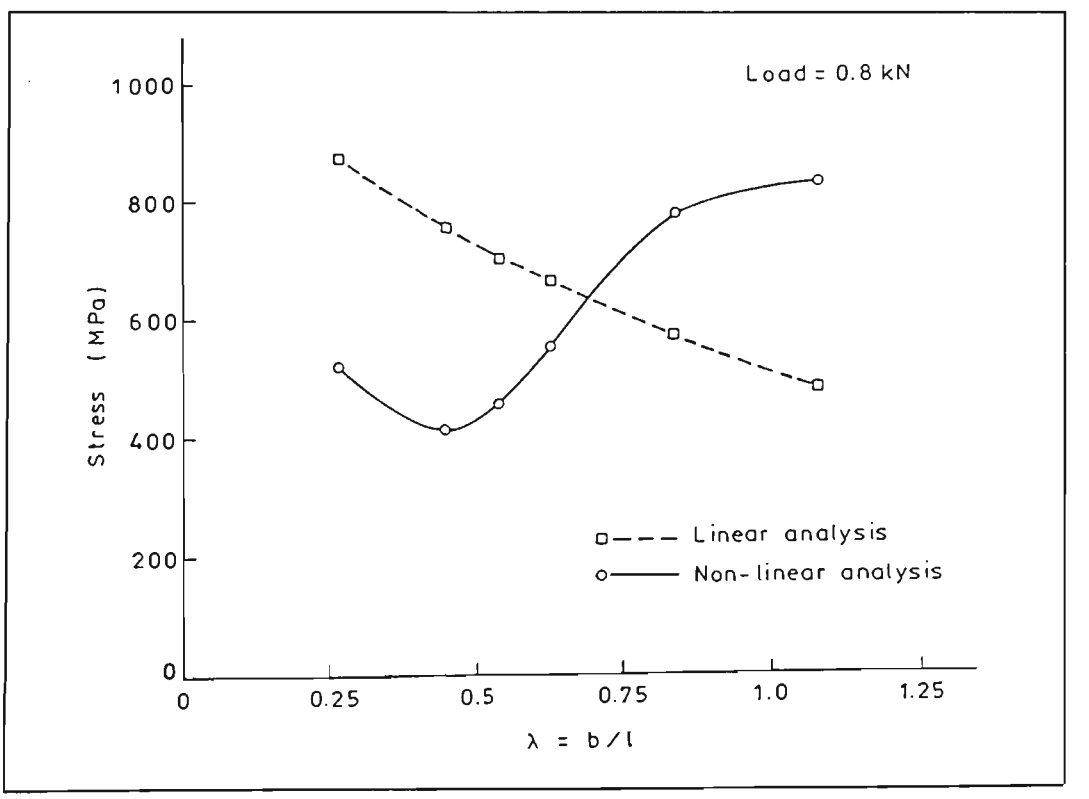

Fig. 7.14 Aspect ratio λ vs. maximum longitudinal stresses (0.8 kN load)

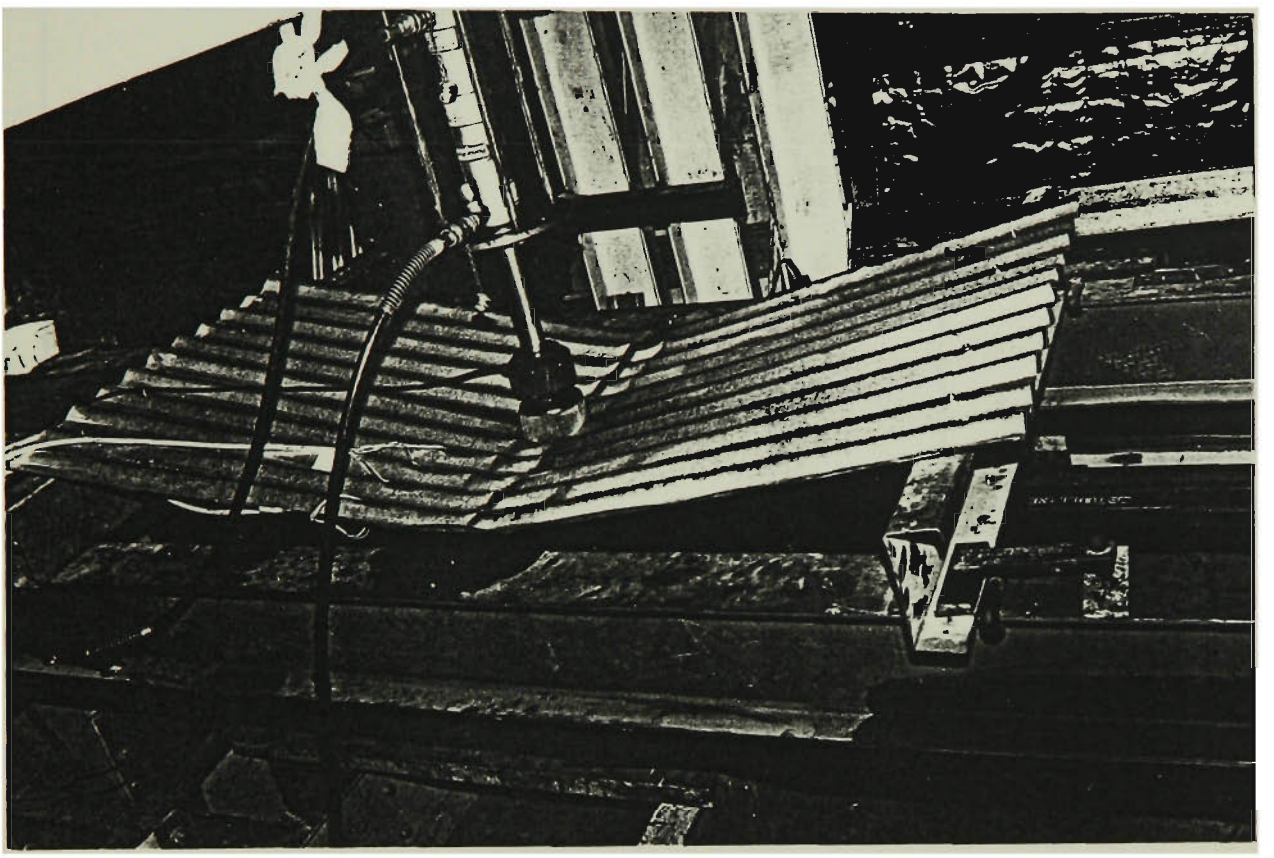

Fig. 7.15 Strain gauges arrangement

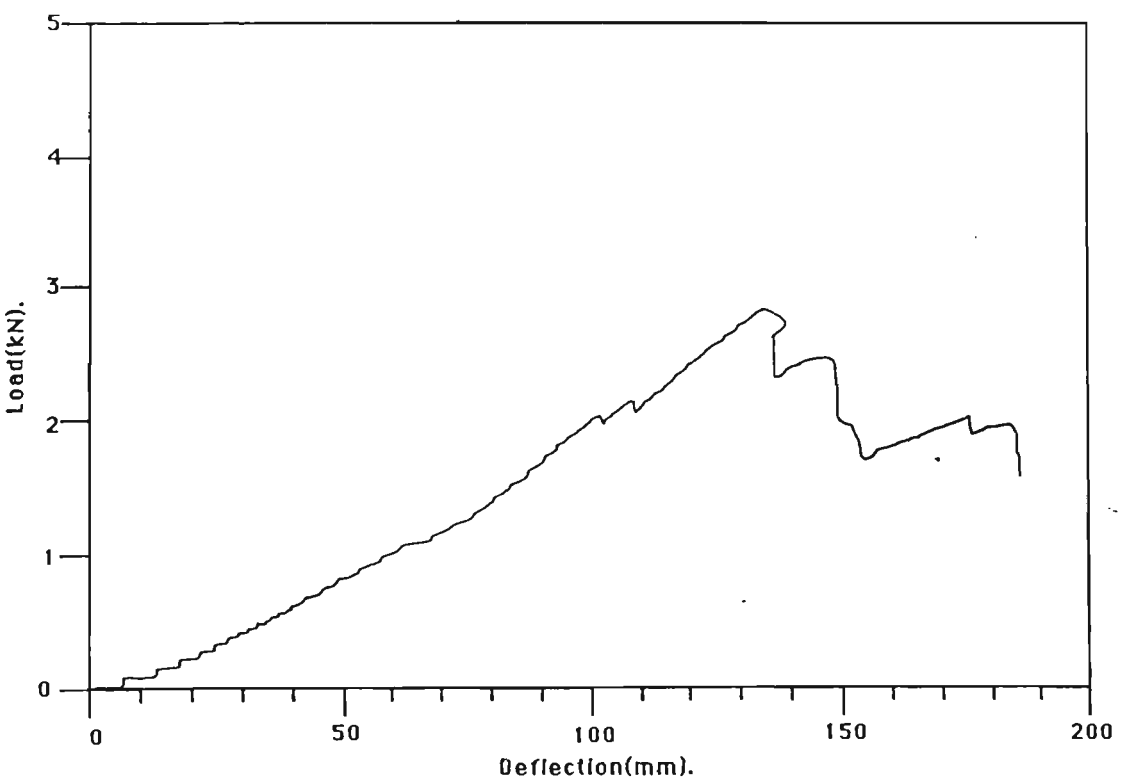

Fig. 7.16 Load-deflection curve for profile sheet type-A (ℓ =1400mm)

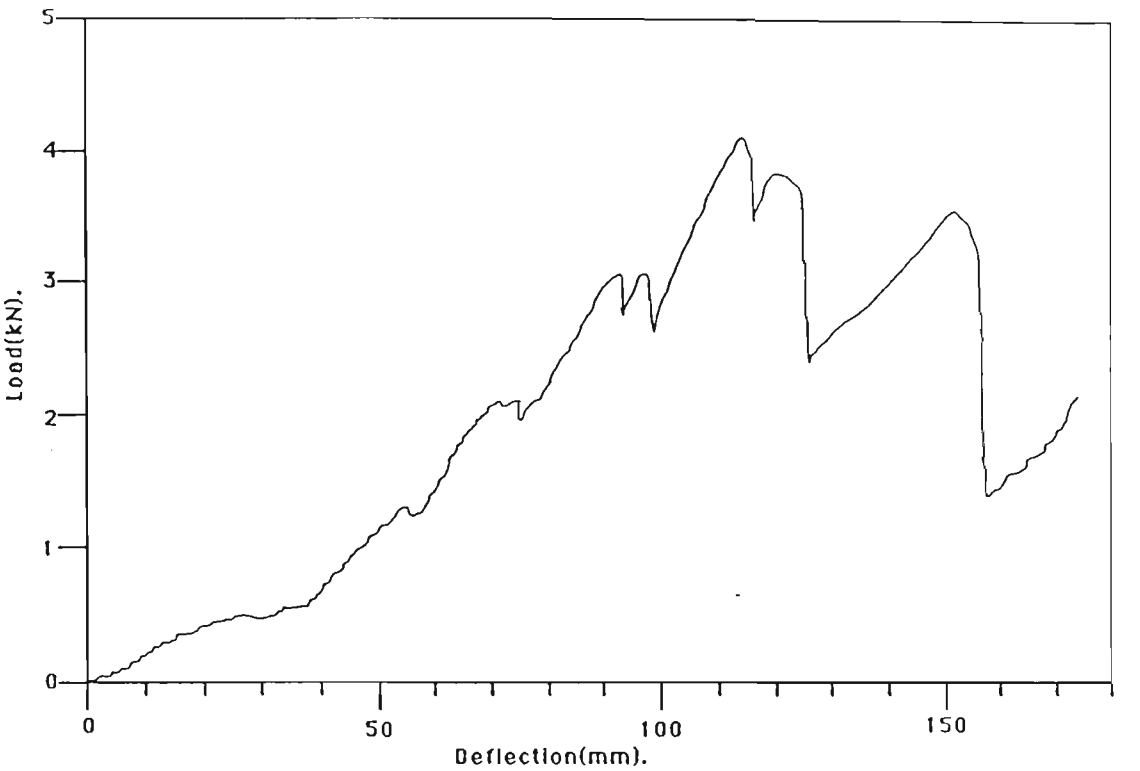

Fig. 7.17 Load deflection curve for profiled sheet type-A (ℓ =900mm)

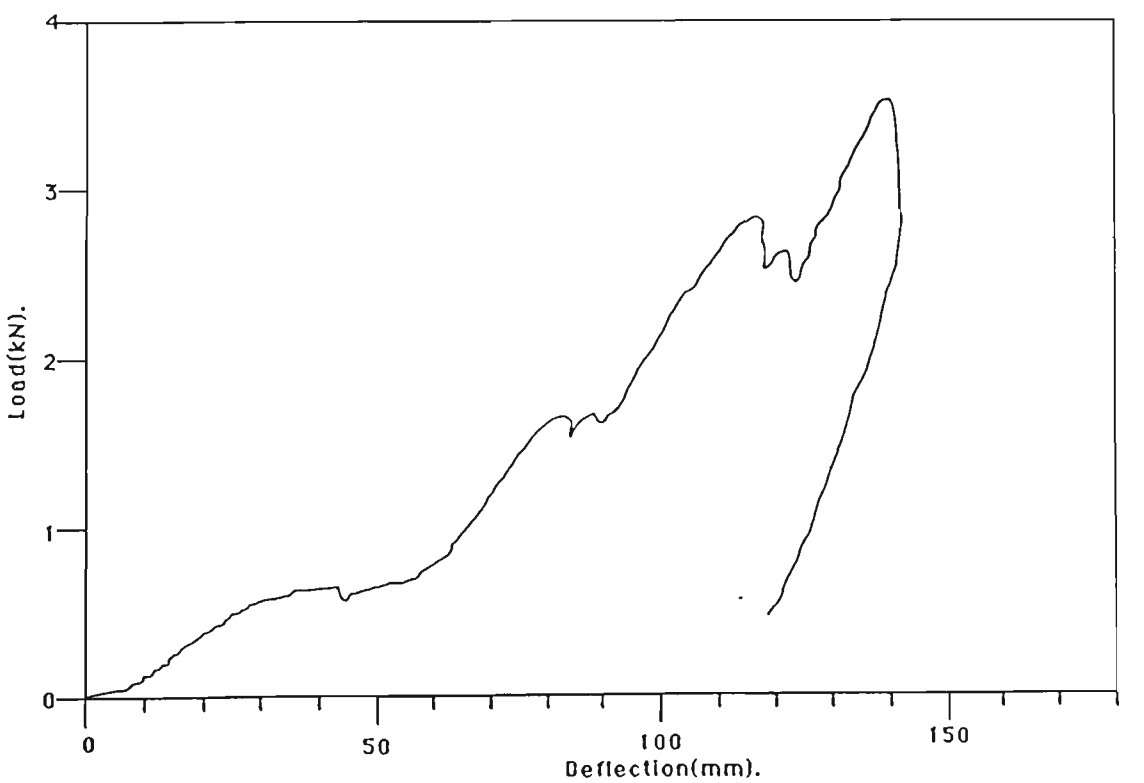

Fig. 7.18 Load deflection curve for profiled sheet type-B (ℓ =1400mm)

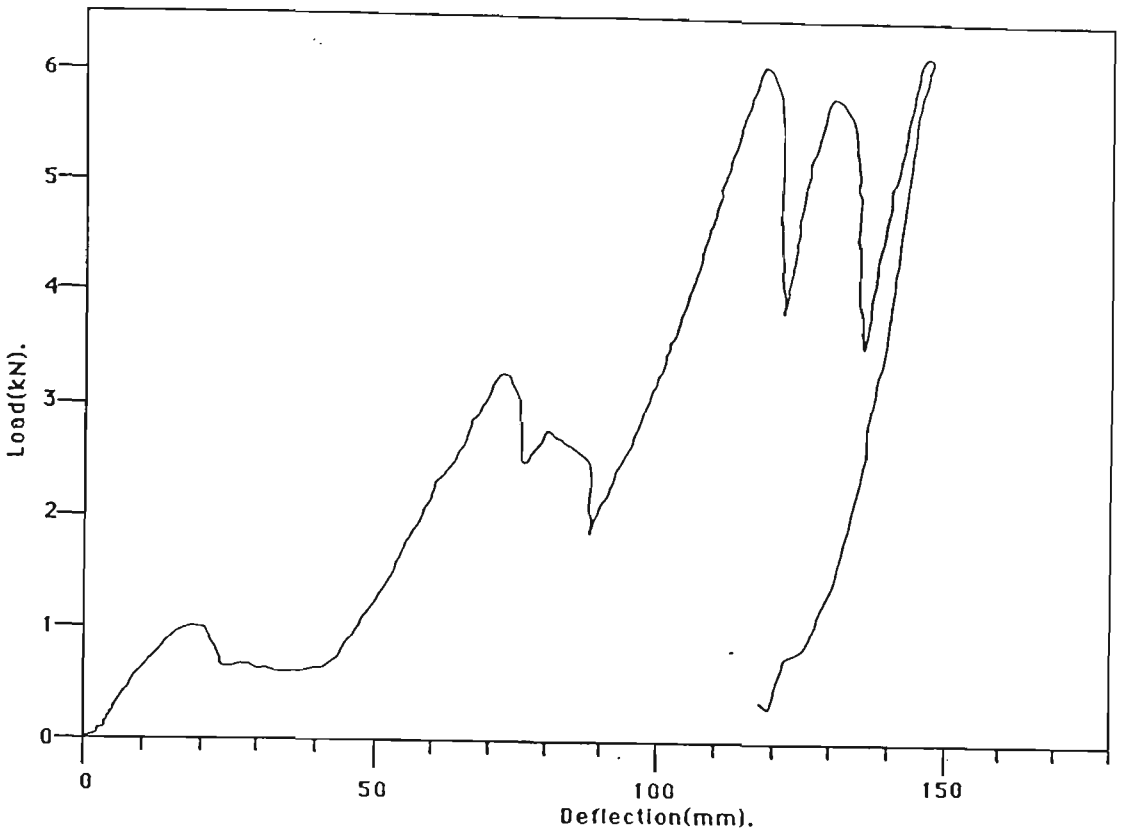

Fig.7.19 Load deflection curve for profiled sheet type-B (ℓ =900mm)

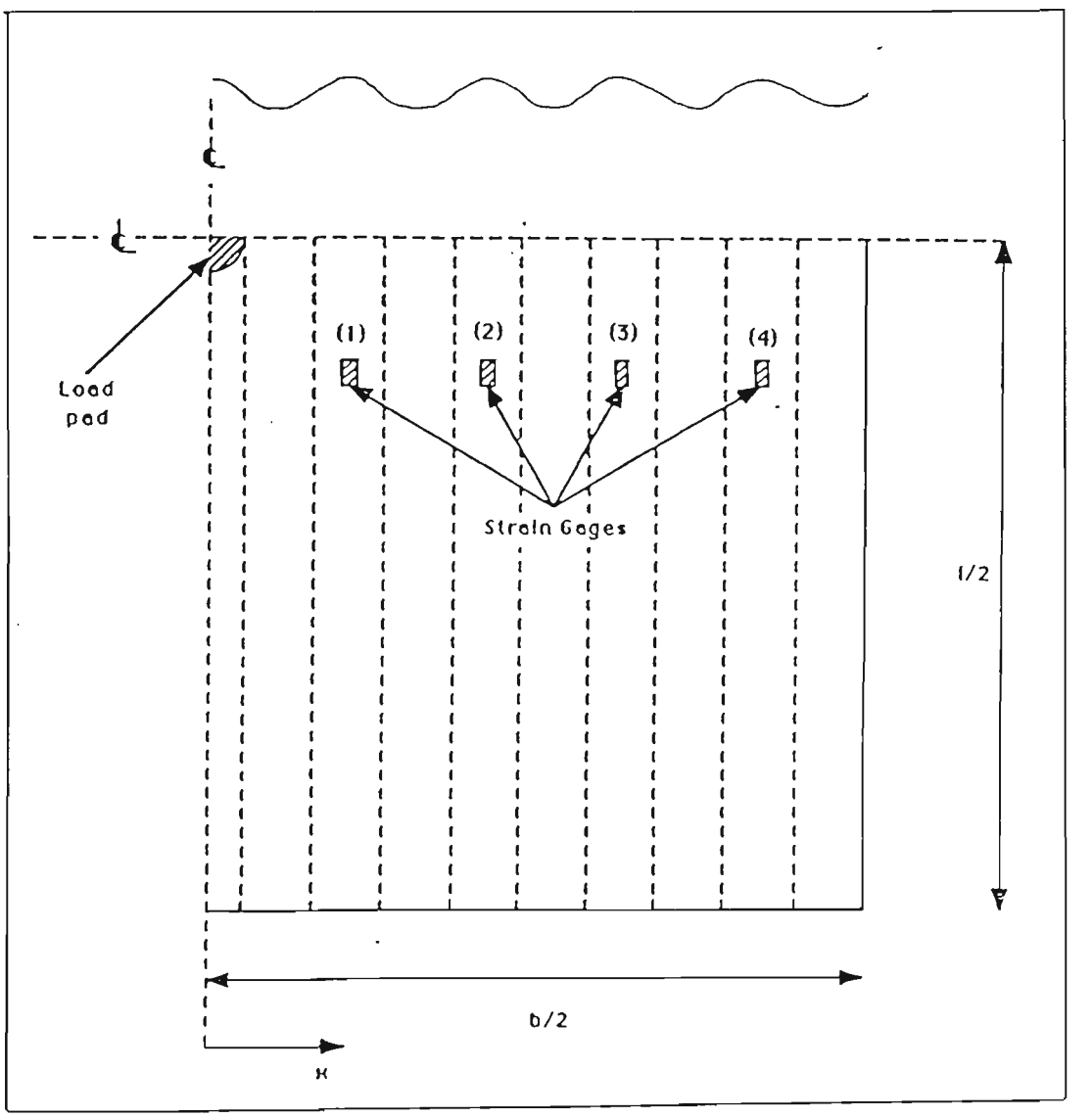

Fig. 7.20 Strain gauge arrangement

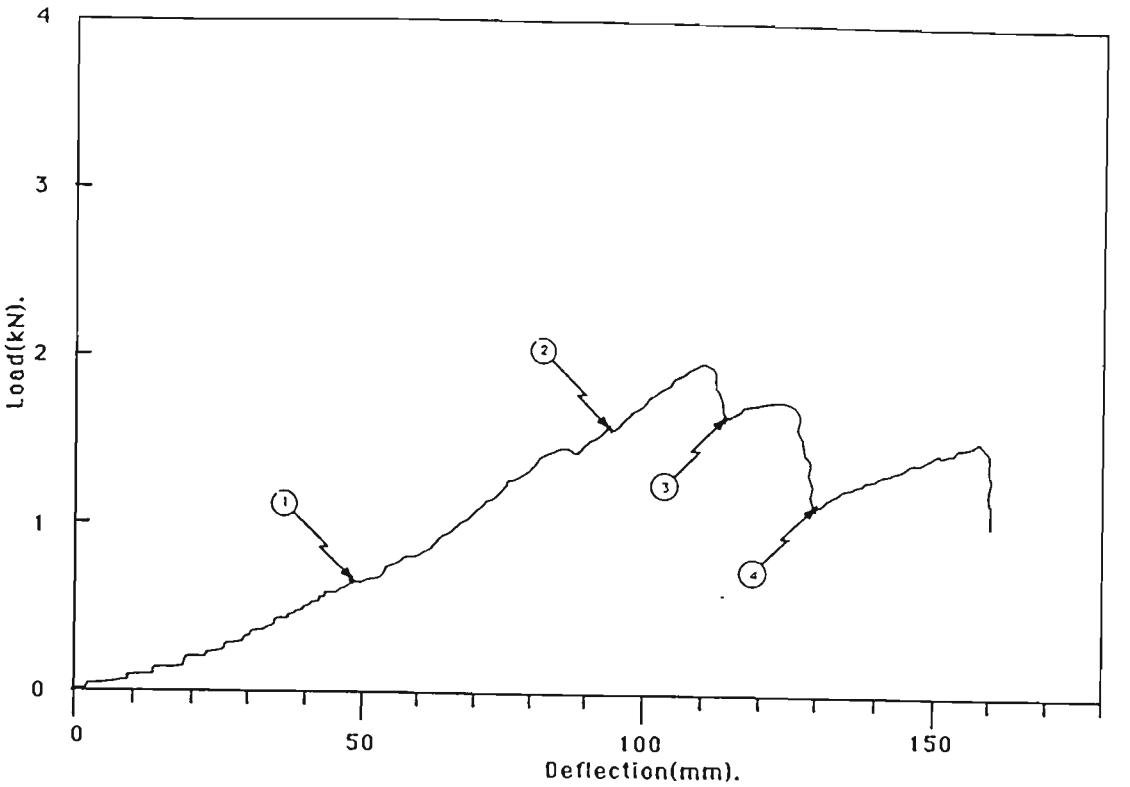

Fig. 7.21 Load-deflection curve for profiled sheet type-A ; ℓ =1500mm
(numbers refer to successive stages of loading at
which the stress distribution was recorded)

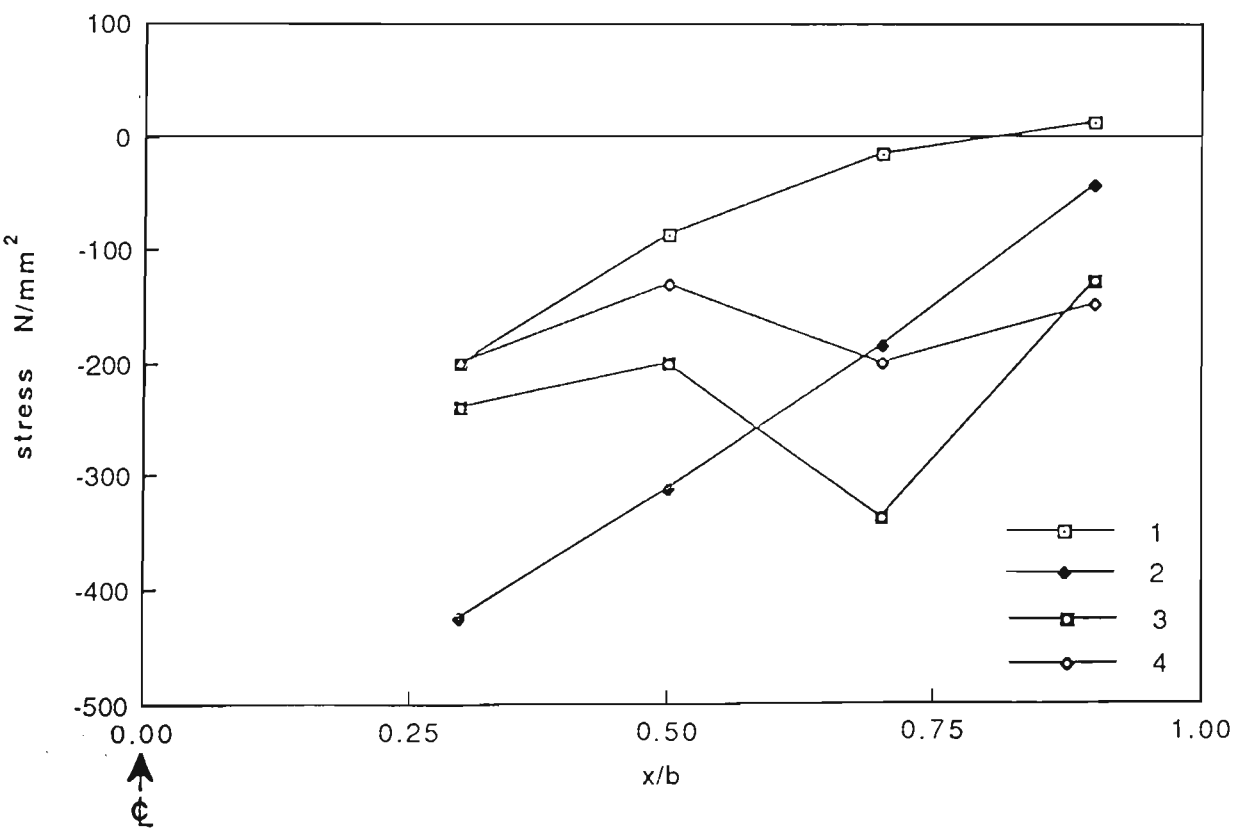

Fig. 7.22 Stress distribution across half the sheet for profiled sheet type-A ; ℓ = 1500mm
(numbers refer to the successive stages of loading at
which stress distribution was recorded)

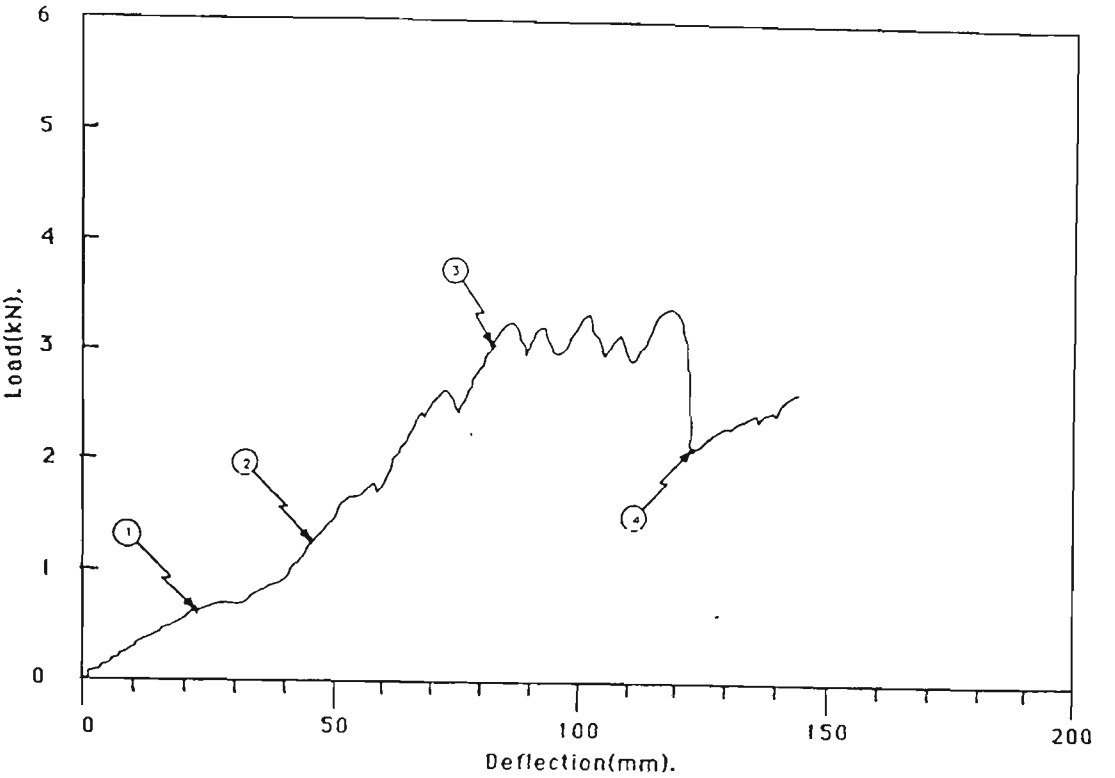

Fig. 7.23 Load-deflection curve for profiled sheet type-A; ℓ = 990mm
(numbers refer to the successive stages of loading
at which the stress distribution was recorded)

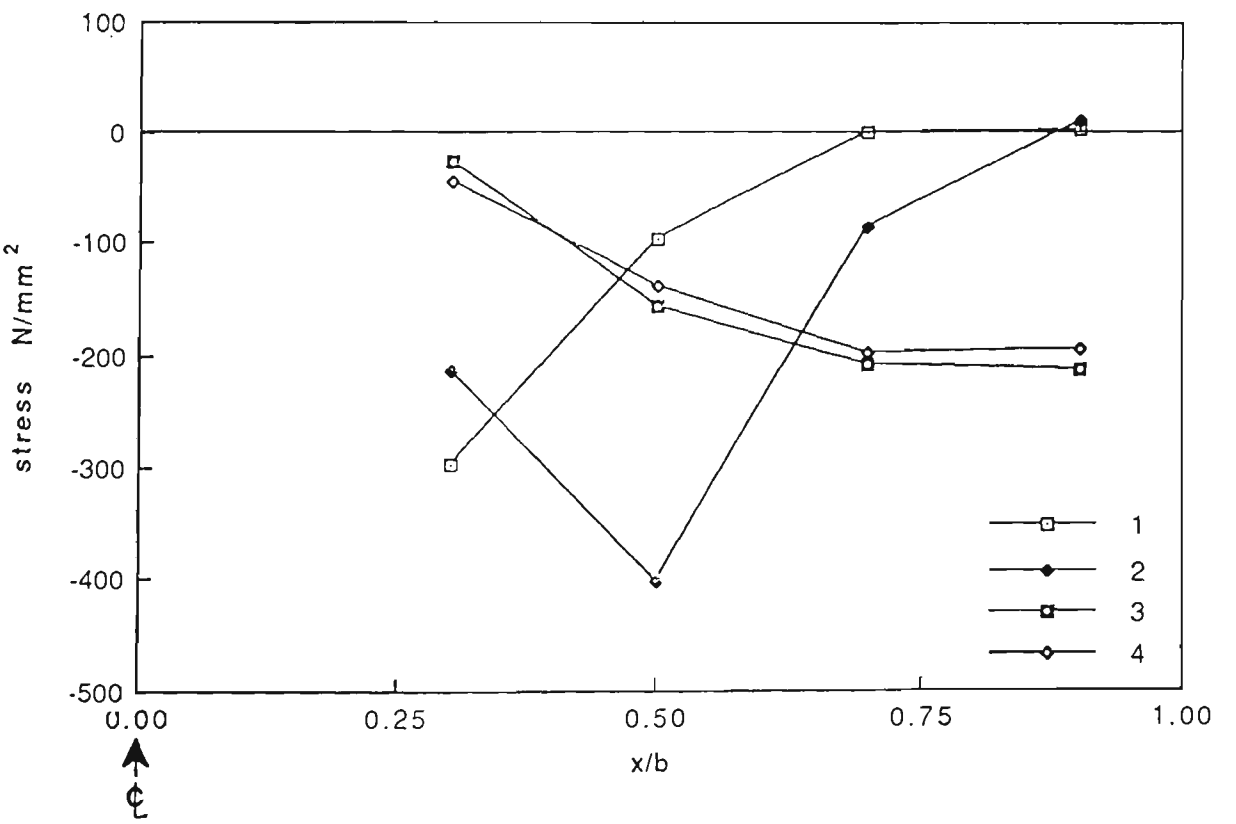

Fig. 7.24 Stress distribution across half the sheet (profiled sheet type-A); ℓ =990mm

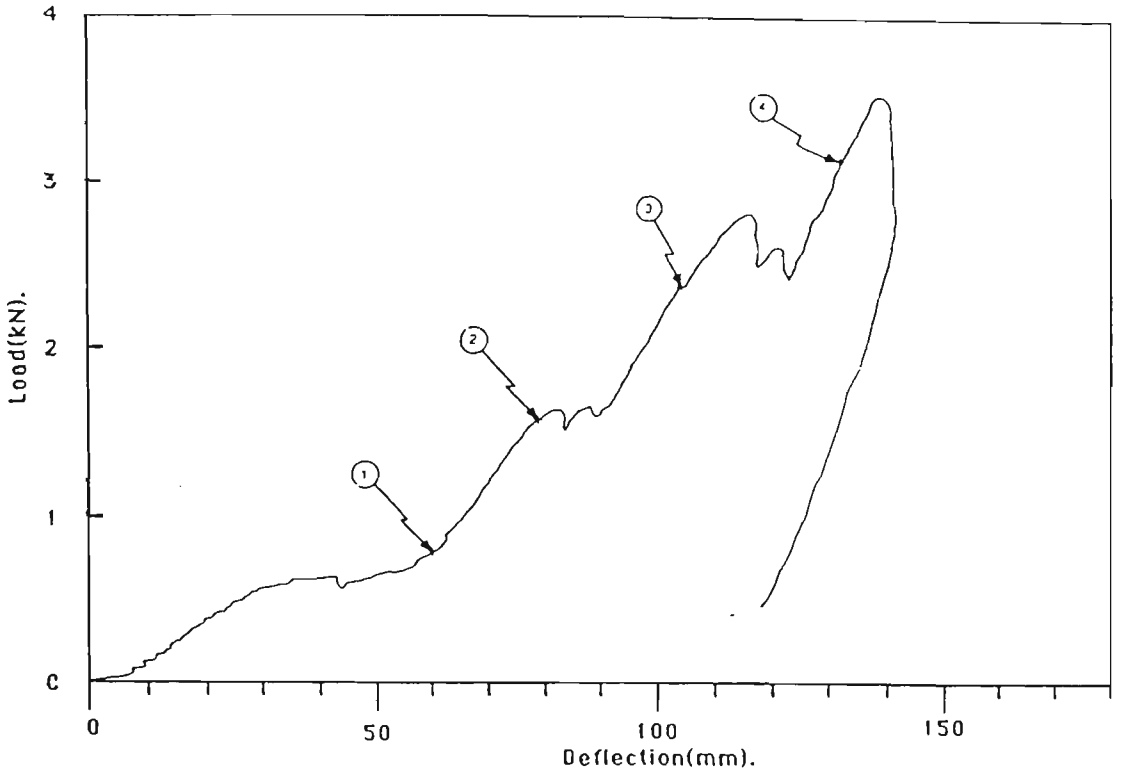

Fig. 7.25 Load-deflection curve for profiled sheet Type-B; ℓ =1400mm
(numbers refer to successive stages of loading
at which the stress distribution was recorded)

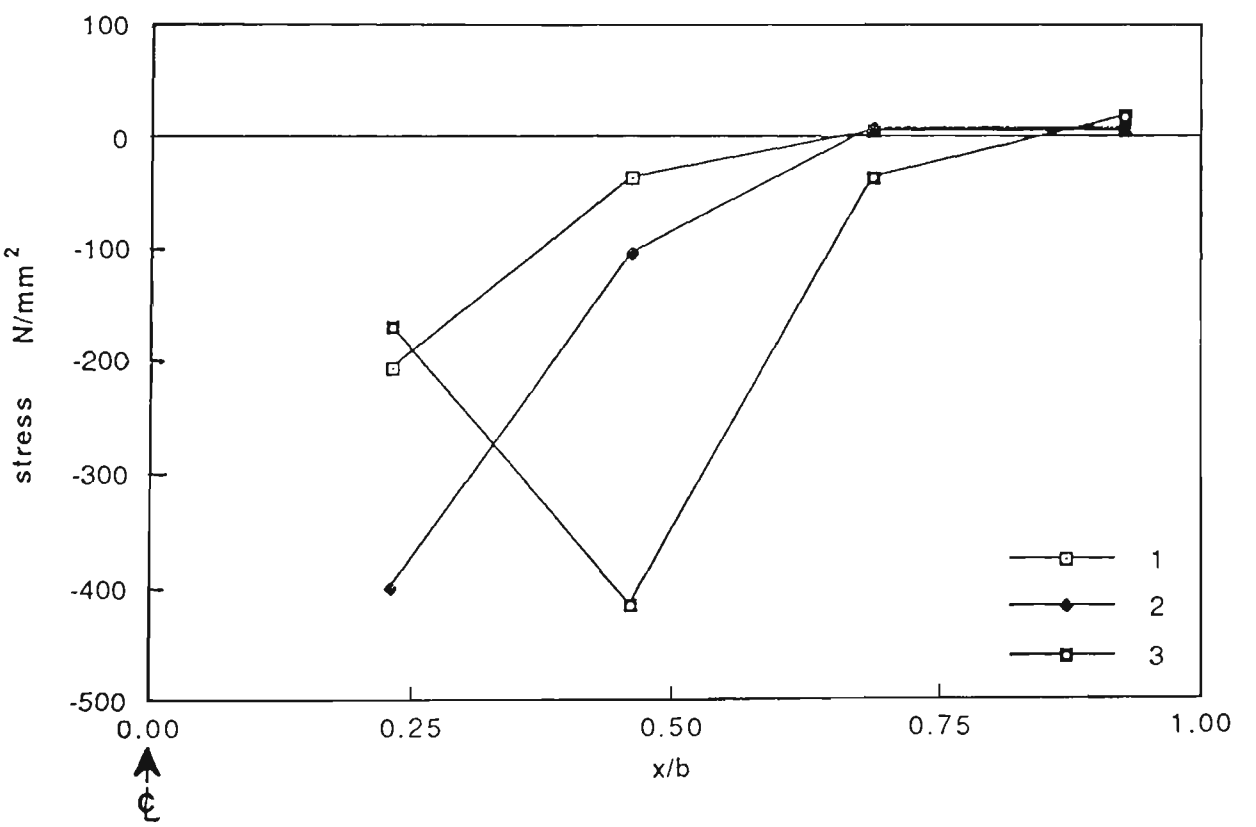

Fig. 7.26 Stress distribution across half the sheet (profiled sheet Type-B); ℓ =1400mm

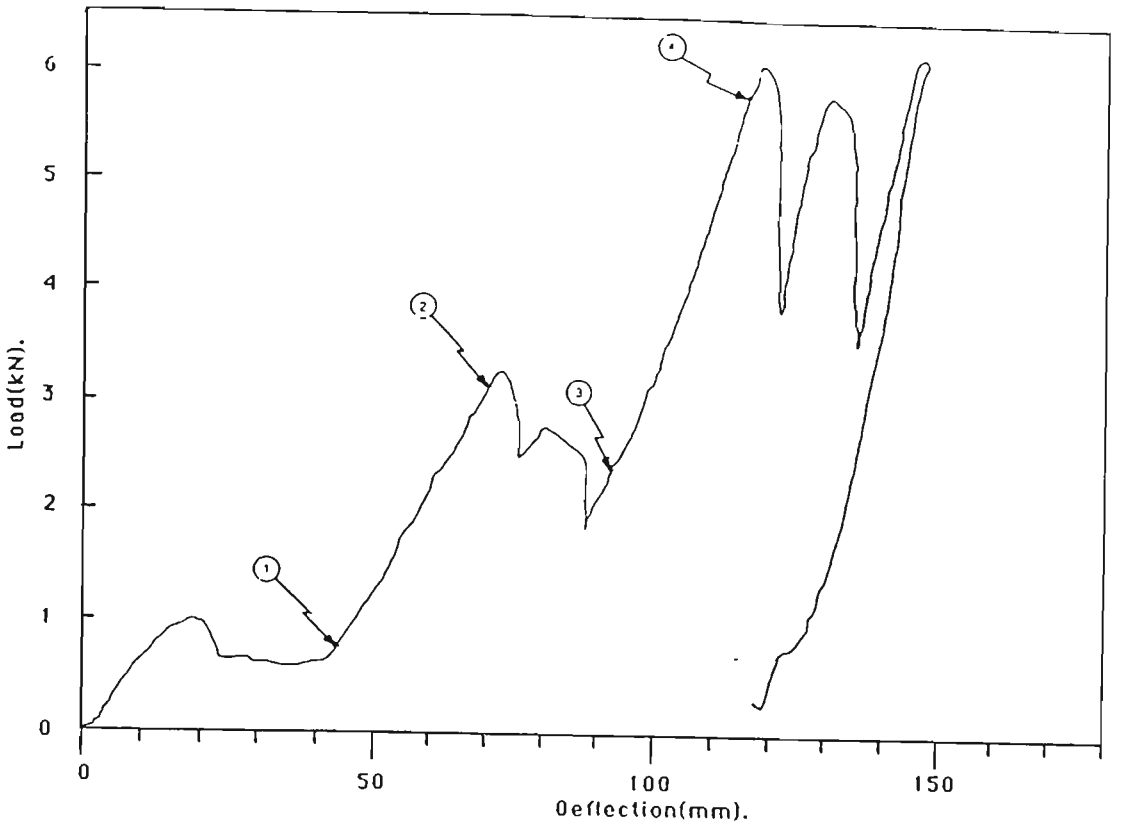

Fig. 7.27 Load-deflection curve for profiled sheet Type-B; ℓ =900mm
(numbers refer to successive stages of loading
at which the stress distribution was recorded)

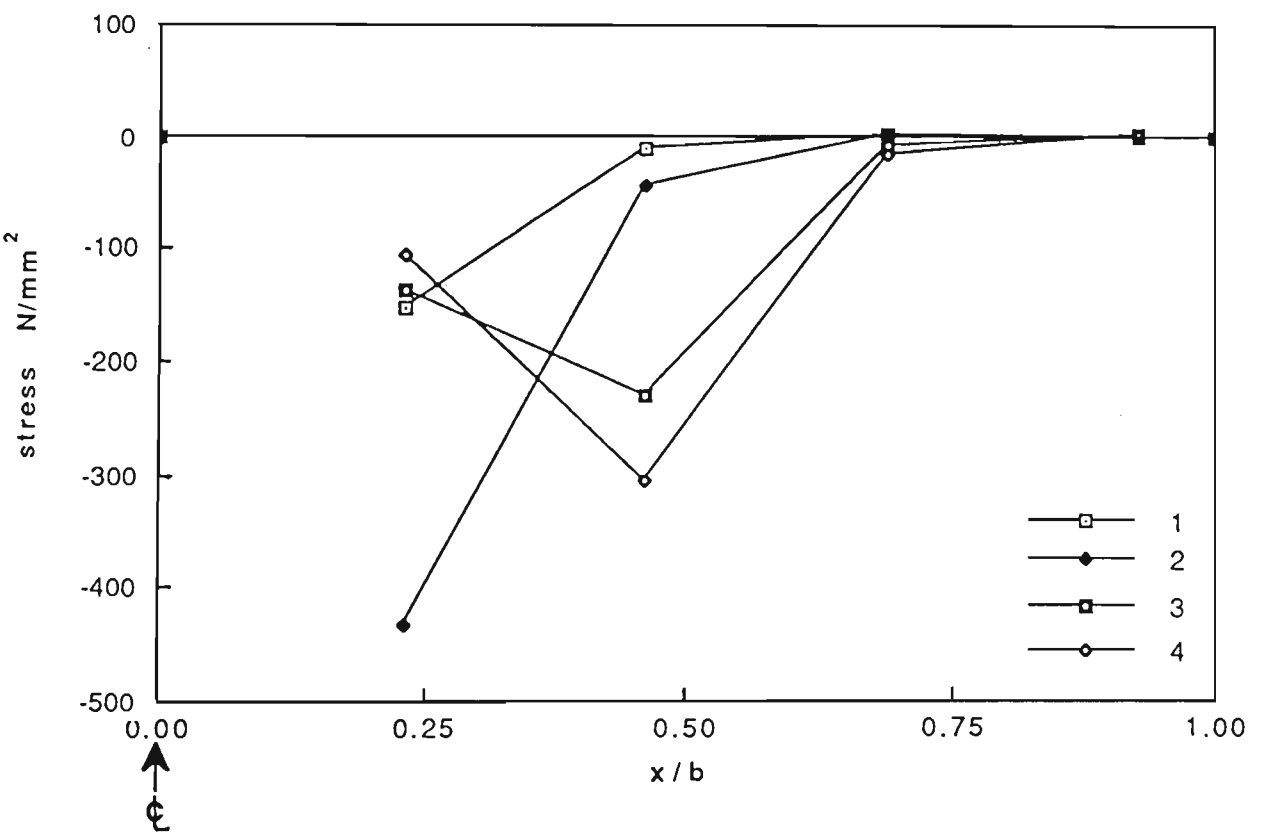

Fig. 7.28 Stress distribution Type-B; ℓ =900mm

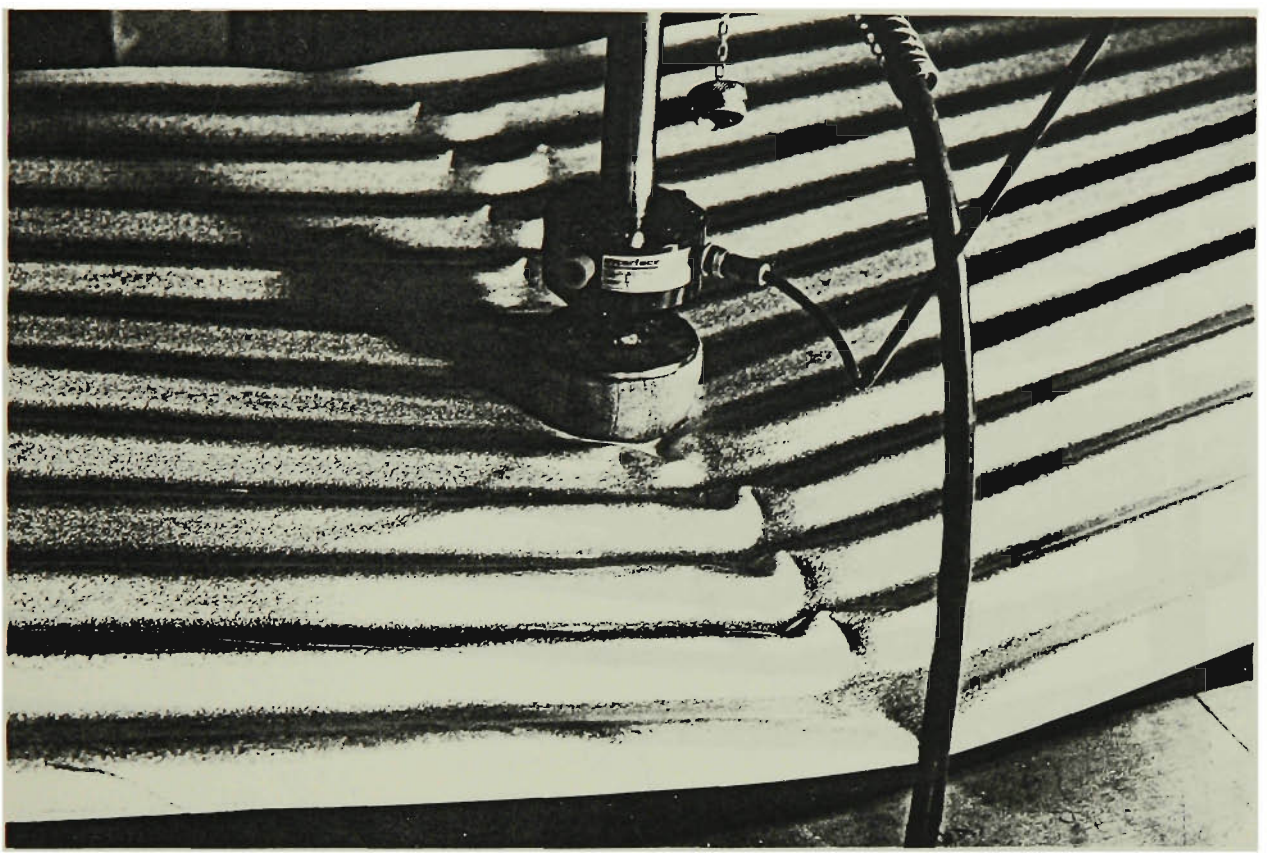

Fig. 7.29-a Pattern of local plastic failure (Type-A)

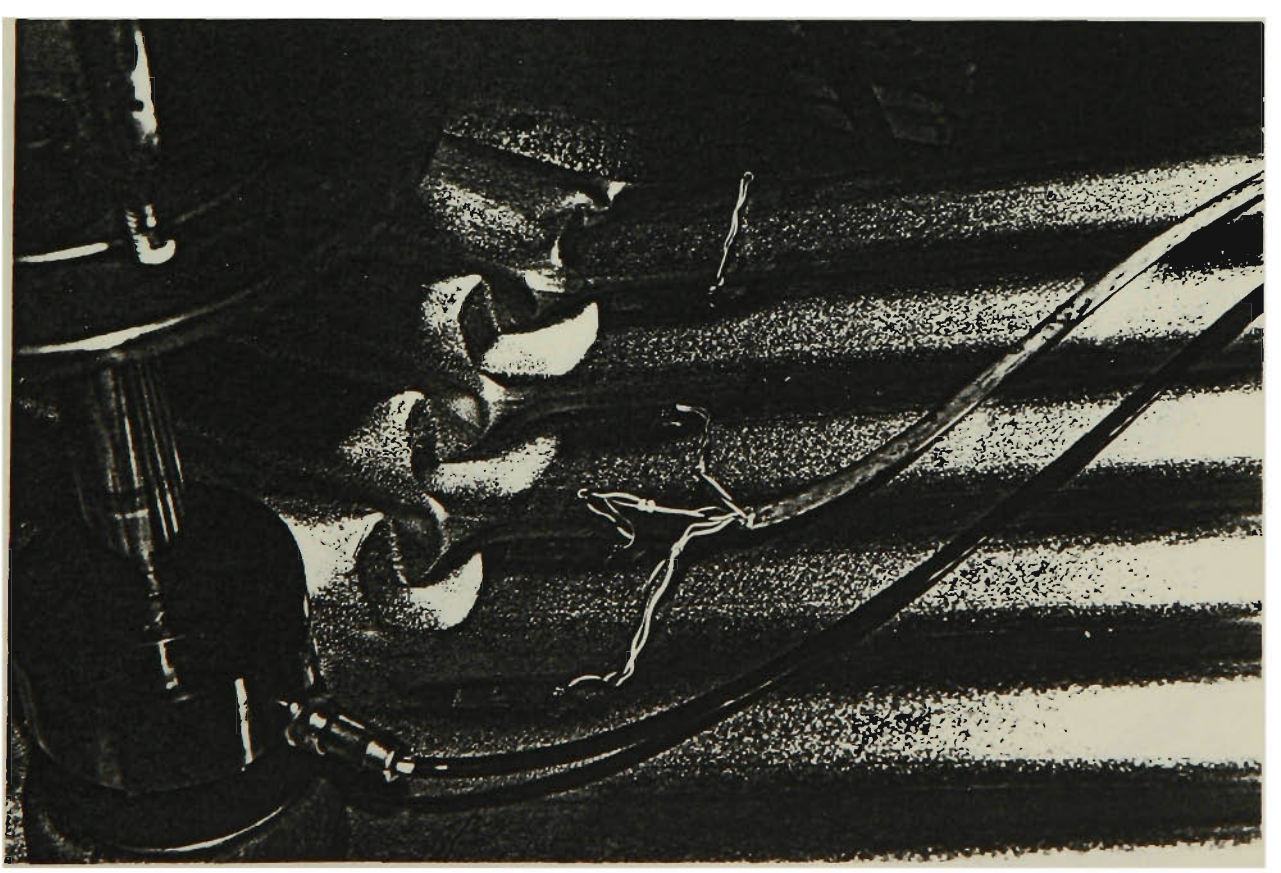

Fig. 7.29-b Collapse mechanism (Type-A)

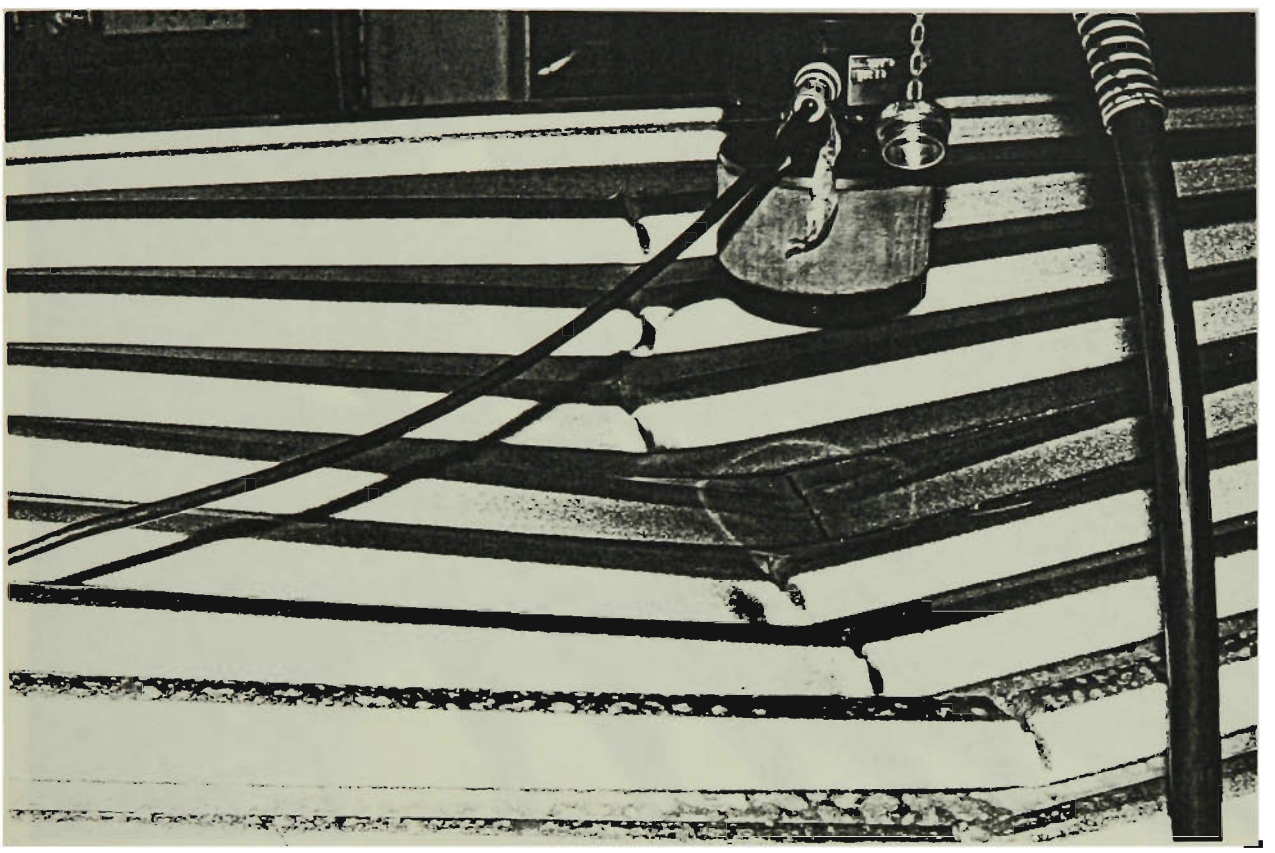

Fig.7.30-a Pattern of local failure (Type-B)

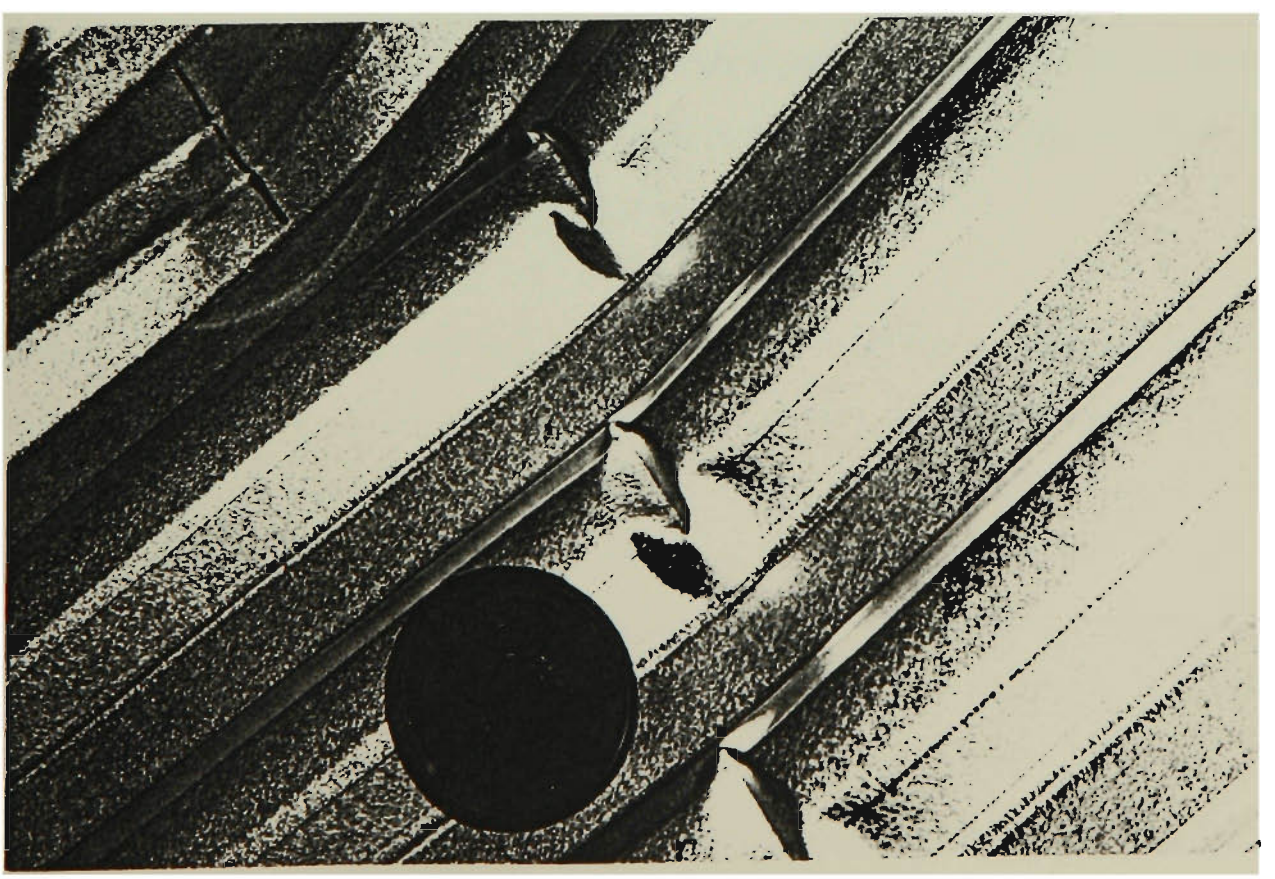

Fig. 7.30-b Local plastic mechanism (Type-B)

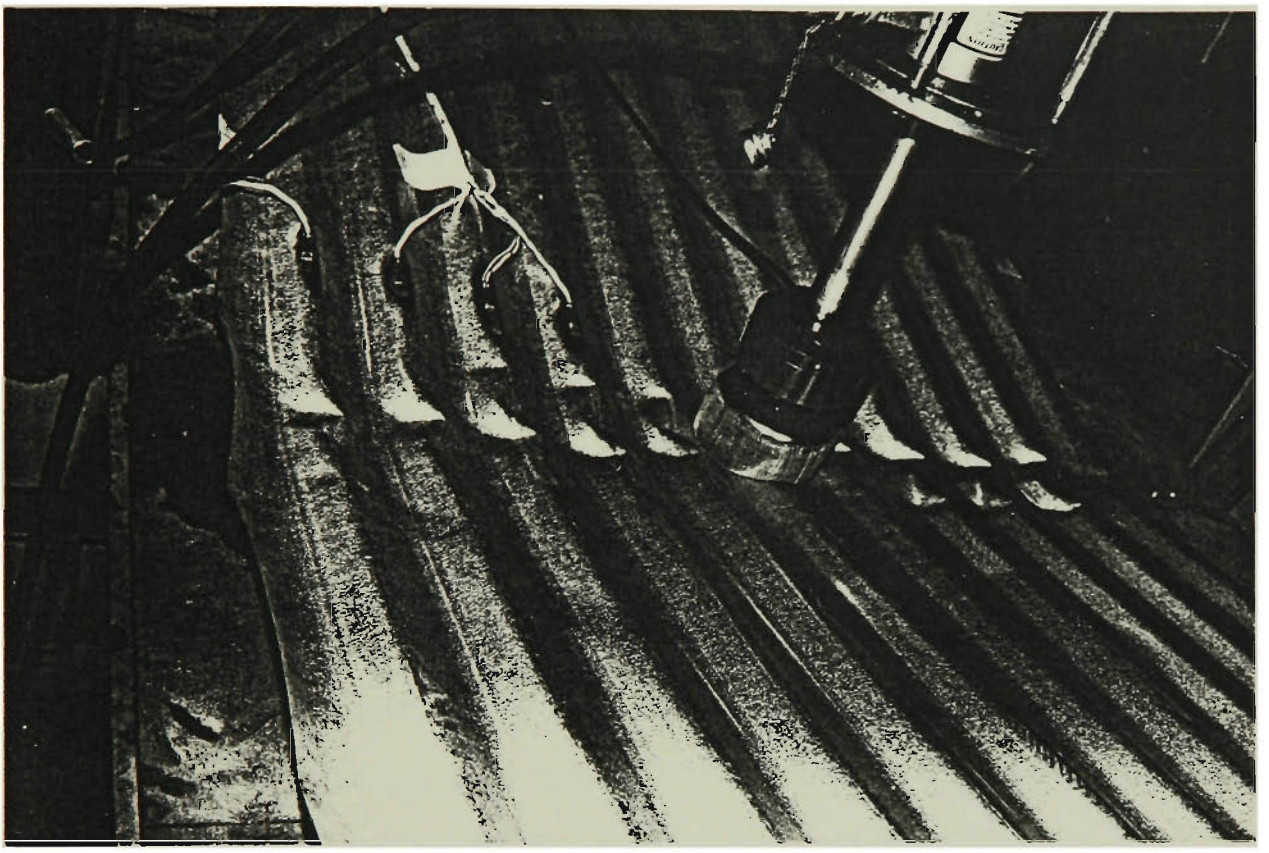

Fig. 7.31 Global collapse of profiled sheeting

Chapter 8

Practical Implications

8.1 Introduction

Substantial improvement in the design of thin-walled structures has been seen in recent years as a result of the progressive increase of the understanding of the behaviour of these types of structures.

The understanding of the relevant physical phenomena associated with certain types of behaviour is indeed the basis of good engineering design. It is important to understand how the load is carried and why there are certain types of stresses associated with this loading condition. It is also equally important to establish the relation between the deflected shape and these stresses.

There are parameters which are critical in determining the behaviour of thin-walled structures; one of these parameters is the aspect ratio. In this study the influence of the aspect ratio on thin-walled structural behaviour is investigated.

The information regarding the stress and deflection of the structure is incorporated with a physical theory of the behaviour. The use of the three elements, the physical hypothesis and the experimental and theoretical analyses, leads to results which have direct practical implications.

The following paragraphs represents an attempt to assimilate the practical implications of this study.

8.2 Transverse Membrane Stresses

In the first part of this study the membrane transverse stresses in a simply supported box girder flange was investigated. Heyman (1982) proposed that a box-section may be regarded as an assembly of two channels put together toe to toe. If a concentrated load is applied at the web/flange junction a twisting movement will be induced as a result of the line of action of the load being offset from the shear centre of each channel. In order to keep the section in a no-twist-position, a lateral flange force is needed. This argument was investigated using a finite element technique, and found to work effectively. The investigation was then extended to cover the effect of the aspect ratio on these lateral stresses. The box girder was assumed to be simply supported at both ends. A rigid diaphragm, which prevented in-plane displacements was also assumed at the end supports.

In a short span (high aspect ratio) the transverse membrane stresses were found to be significant. In fact, they may reach values which are several times the longitudinal membrane stresses in the same region. For large spans (low aspect ratios), the transverse membrane stresses were small in comparison with the longitudinal membrane stresses in the same region. However, they are highly concentrated at the centre, where the concentrated load is applied.

The study leads to the formulation of simple empirical expressions which can be used to predict the magnitude and the distribution of these stresses. The proposed formulae are based on the assumptions that diaphragms with a reasonable practical rigidity are used at the simply supported ends to prevent in-plane lateral displacement.

The concentrated load which is assumed in the analysis could be due to reactions at the supports of the box-girder or the deck anchorage point of a cable stayed bridge. The existence of transverse membrane stresses in a box girder flange may influence the general behaviour of the structure. Consequently, this influence has to be considered especially when the flange has a high aspect ratio. The formulae presented, in the study, give a reasonably accurate and simple way to account for these stresses. The study also provided a physical understanding of the reason why such transverse stresses should exist, and the influence of the aspect ratio on their distribution and magnitude. The study is extended further to investigate the transverse membrane stresses in the flange of an I-beam.

The view was expressed that an I-beam can be composed of two channel put together (back to back). If a concentrated load is applied at the web/flange junction each of the two channels will try to twist as a result of the force applied being offset from the shear centres. Lateral stresses are generated to prevent this twisting and to hold the two channels together to form the I-beam.

The transverse membrane stresses determined by a computer analysis, using the finite element technique, fits the description of the I-beam as an assembly of two channels placed back to back. The assumption provides a clear picture of the deformation which is necessary if the deformations of the two parts

(channels) are to be compatible. Associated with these geometrical conditions are the transverse membrane stresses.

The simple procedure which has been introduced earlier to predict the transverse stresses in a box girder flange, using a dimensionless group of equations and curves, is used again to predict the transverse membrane stresses in the flange of an I-beam. The equations which have been presented enable a reasonable estimate to be made of the transverse stresses in the flange of I-beams of varying aspect ratios. The stresses, in turn, can be used to estimate the forces acting on connectors for I-beams built-up from channels connected back-to-back.

The study, also characterises the influence of the aspect ratio on the transverse membrane stresses in the flange of an I-beam. For short spans (high aspect ratio), the transverse stresses are high when compared with the associated longitudinal stresses. The two stresses, the longitudinal and the transverse, have different signs. Consequently the yield limit of an I-beam can be affected by the existence of the transverse membrane stresses. The analysis assumed diaphragms with a reasonable membrane rigidity at the simply supported ends. However, if an I-beam is used without restricting its in-plane movement at the end support large concentrated transverse membrane stresses will be developed. When considering the case of $b/\ell = 0.5$ these stresses reach a value of 30% of the maximum longitudinal membrane stresses.

8.3 Bending Lag

One other subject that is receiving attention in the literature (for instance, Dowling and Burgan, 1985) is the bending lag of a box girder flange which

arises as a result of the finite torsional stiffness of the flange. The understanding of the phenomenon of bending lag may help explain some modes of failure in shallow box girders with wide stiffened flanges. In such structures, flange failure can be initiated at a point remote from the flange edges due to the interaction of a number of phenomena (Dowling and Burgan, 1985). Bending lag is one of these phenomena.

The study of bending lag (within the linear analysis limit) shows that ignoring the influence of the web/flange interaction will result in an underestimation of the bending lag effect. The study also shows that the bending lag influence can be reduced if the web rigidity of a box girder is increased. When elastic buckling of the box girder flange was assumed (geometrical non-linear analysis) negative bending lag occurred whereby the maximum plate bending moment occurred at the central strip.

8.4 Profiled Sheeting

The study of the profiled sheeting deflection behaviour shows that if the profile depth is relatively shallow, then a sheet with high aspect ratio (short span) would fail under a concentrated load which is lower than that of a sheet with a low aspect ratio (long span). The failure takes the form of a local plastic collapse mechanism, and is principally an aesthetic one. The study indicated that for sheets with a low aspect ratio (long span) the deformation associated with increasing the concentrated load leads to considerable redistribution of stresses across the sheet. For large aspect ratios (short spans), the stresses are concentrated near the centre, where the load is acting. The concentration leads to early development of local collapse mechanisms in the ridges of the sheet.

The study suggests that for relatively shallow profiled sheeting, where the performance of profiled sheeting under concentrated loads is sensitive to the change in the aspect ratio, this effect should be reflected in the design table proposed by the manufacturer.

Another aspect which merits consideration is the extent to which the increase in the profile depth can influence its behaviour. The study shows that increasing the profile depth reduces the capability of the sheet to redistribute the longitudinal membrane stresses across its width. In this case each ridge acts in a manner similar to a "beam" rather that a "plate". Therefore the influence of the aspect on the behaviour of sheets with deep profile height is expected to be limited.

Chapter 9

Conclusion

9.1 Introduction

Different aspects of thin-walled structural behaviour have been presented. In each case the marked effect of the aspect ratio on the behaviour of these types of structures has been recognised and quantified.

9.2 Transverse Stresses in Thin-Walled Structures

In the first part (Chapters 2 to 5) the deformation behaviour of thin-walled beams and transverse stresses associated with this deformation is presented. The following points have been made.

Heyman (1982) proposed, based on simple structural mechanics analysis, that a box cross-section, under a concentrated load, is subjected to concentrated lateral membrane forces in the upper and lower flanges at the centre due to its loading condition.

Schmidt and Salaheldin (1990) investigated this assumption through a numerical analysis of the stress in the flange of a straight simply-supported box girder. The analysis indicated the existence of relatively high values of the transverse stresses in the box girder flange. The analysis also indicated that there is a strong possible correlation between these stresses and the fictitious lateral force calculated using simple structural mechanics analysis.

The investigation was carried further and a comprehensive parametric study, using finite element analyses, of box girders under a central concentrated load was conducted. Attention was focused on the magnitude and the distribution of the transverse membrane stresses. The relation between these stresses and the fictitious lateral force, calculated using simple structural mechanics analysis, was defined. Based on the correlation between the two types of analyses, simple formulae were introduced, by which the magnitude and the distribution of transverse membrane stresses can be predicted.

The study was then extended to cover the behaviour of I-beam girder flanges under the same loading condition. The study shows that the simple procedure, which was applied to determine the transverse membrane stresses in box girder flanges, can also be used to predict these stresses in the flange of an I-beam girder (Salaheldin and Schmidt, submitted for publication).

The study highlighted the following points.

(i) The stresses acting laterally on the flange are highly affected by the change in the aspect ratio. In larger spans, these stresses are almost concentrated at the centre. However, in shorter spans the stresses are spread along the centre-line of the flange.

(ii) The formulae, which predict the magnitude and the distribution of transverse membrane stresses, are principally a function of the aspect ratio.

(iii) In boxer girder flanges, the transverse membrane stresses can reach a value which is several times the value of the associated longitudinal stresses for large aspect ratios (b/ℓ ratios).

(iv) In the flange of an I-beam girder, the transverse membrane stresses have a different sign to that of the associated longitudinal membrane stresses. The existence of these two stresses, with different signs, could influence the yield limit of the flange.

Overall the study contributes to the understanding of the effect of the aspect ratio on the behaviour of box and I-beam girders. The study has also introduced simple means by which this effect was quantified.

9.3 Bending Lag

Bending lag is defined as the tendency of the longitudinal curvature of a flange plate to diminish with increasing distance from the web (Dowling and Burgan, 1985). Alternatively, bending lag can be defined as the non-uniform distribution of plate bending across the flange, with a maximum value at the web flange junction, which effect is attributed to the finite torsional stiffness of the flange.

In Chapter 6 the bending lag phenomenon is presented through a finite element analysis of a box girder. The study investigated the bending lag effect in the linear and the non-linear elastic range (Salaheldin and Schmidt, 1989).

The study showed that the complete interaction of the web and flange at the web flange junction-line can have a significant influence on the bending lag effect. If this interaction is ignored the bending lag effect will be underestimated. For a box girder with b/ℓ ratio of 0.4, the effective width ratio (for bending lag) was reduced from 0.63 (Dowling and Burgan, 1985) to a much lower value of 0.34.

The analysis also shows that the effect of bending lag can be reduced if the rigidity of webs is increased while the flange rigidity remains the same.

The non-linear elastic analysis of a simple box girder shows the development of a negative bending lag when elastic buckling occurs. In this case the maximum plate bending moment occurs at the middle strip of the flange.

The analysis demonstrated the significant influence of the aspect ratio on the bending lag phenomenon. The increase of the aspect ratio is associated with an increase of the bending lag effect.

9.4 Profiled Sheeting

In Chapter 7 the effect of a concentrated load on the behaviour of simply supported spans of corrugated steel sheets are discussed. Attention is directed to the observation that, in shallow profiled sheets, initial local buckling occurs at earlier loads in sheets with smaller rather than larger spans, which reflects the effect of the aspect ratio on this type of structural behaviour. These phenomena have been investigated both experimentally and through computer modelling (Salaheldin et al., 1987).

The study shows that, in shallow sheets, the aspect ratio has a significant influence on the performance of this type of sheeting. For a high value of this

aspect ratio, λ, a local plastic failure mechanism is formed at an early stage of loading. However, tests indicate that, despite the local failure, a considerable post buckling strength is available. This finding raises the question of the effect of local buckling on the total stability and load carrying capacity of the sheet.

The study indicates that the deformability of the sheet plays an important part in the redistribution of stresses; for low aspect ratios the sheeting is capable of achieving a considerable re-distribution of stresses, which is reflected in high critical loads.

In the case of a shallow profiled sheeting, when the behaviour under a concentrated load is suspected to be influenced by the aspect ratio, it is recommended that the manufacturer should incorporate this effect as a limit.

The Australian Code AS 1562 - 1980 has been evaluated, and the point is made that the local plastic deformation, which is considered by this code as a failure, is mainly an aesthetic failure rather than a strength failure.

When a deeper profile was tested the results showed that the effect of the aspect ratio on the formation of local plastic collapse mechanisms was almost eliminated. The increase in depth changes the behaviour of the sheets from plate-like behaviour, where deformation is associated with redistribution of stresses, to beam-like behaviour, where almost no strength is to be gained in the process of deformation. The study is a step along the way of achieving a better structural quality control (testing and failure criteria) of profiled metal sheeting than is currently outlined in the Australian Standard.

Appendix 1. — NOTATION

a	wavelength of corrugation
b	flange width
b_e	effective width of corrugated sheet (Chapter 7); effective width of box girder flange (Chapter 6)
d	depth of girder
e	distance between the shear centre of a channel and the web centre
f	height of corrugation
k	buckling coefficient of stiffened plates
ℓ	girder span
s	distance between the shear centre of a channel and the applied load
t_d, t_f	diaphragm and flange thicknesses, respectively
x	distance across the girder measured from the web/flange junction
y	distance along the girder measured from the support
D_x	bending stiffness in x direction
D_y	bending stiffness in y direction
D_{xy}	torsional stiffness
E	Young's modulus
E_f	modulus of elasticity of flange
E_w	modulus of elasticity of web

F_i	lateral (transverse) force obtained by integrating the transverse stresses determined by finite element analysis
F_s	lateral force obtained using simple structural mechanics analysis
I	cross-section second moment of area
K_1, K_2	non-dimensional coefficient
P	single central static point load applied at the web/flange junction
P_c	the load at which first local plastic collapse mechanism occurs (profiled sheet - Chapter 7)
P_{ce}	critical elastic load for rectangular plates
R	developed length of corrugated sheet
η	the ratio of σ_{TC} determined using finite element technique to predicted σ_{TC}
$\lambda = \frac{b}{\ell}$	aspect ratio
μ	Poisson's ratio
σ_B	bending longitudinal stresses calculated on the basis of simple theory of bending
σ_N	longitudinal membrane stress
σ_{NC}	longitudinal membrane stress at the centre of the box girder flange
σ_T	transverse membrane stress along centre-line of the box girder flange
σ_{TC}	transverse membrane stress at the centre of the box girder flange
τ	shear stress
σ_{Tmax}	transverse membrane stress at the centre of the element near the flange centre at girder centre line

τ_e shear stresses along the web/flange junction

τ_{max} maximum shear stress

τ_s shear stresses across the flange at the simply supported end

ω vertical deflection (Chapter 7)

$\Phi = \frac{Pe}{\ell t_f d}$ dimensional parameter

$\Omega = \frac{\sigma_{TC}}{\sigma_{NC}}$ the ratio of transverse membrane stress to the associated longitudinal membrane stress at the centre

Appendix 2. — REFERENCES

Abdel-Samad, S.R., Wright, R.N. and Robinson, A.R., (1968), "Analysis of Box Girders with Diaphragms", Journal of the Structural Division,ASCE,Vol. 94, No. ST10, October.

Abdel-Sayed, G., (1969) "Effective Width of Steel Deck-Plate in Bridges", Journal of the Structural Division, ASCE, Vol. 95, ST7, July.

Abdel-Sayed, G., (1970) "Critical Shear Loading of Curved Panels of Corrugated Sheets", J. Eng. Mech. Divn., ASCE, Vol.96, EM6, Dec.

Baehre, R., (1983) "Cold-Formed Steel Structural Elements. Development in Design and Application". In Instability and Plastic Collapse of Steel Structures, Ed. L. J. Morris, Granada.

Blodgett, H.B., (1934) "Moment of Inertia of Corrugated Sheets", Civil Engineering, Vol.4, September.

Briassoulis, D., (1986) "Equivalent Orthotropic Properties of Corrugated Sheets", Comps. Structs., Vol.23, 2.

British Standards Institution, (1976) "Code of Practice for Performance and Loading Criteria for Profile Sheeting in Building", BS 5427.

British Standards Institution, (1982) "Steel, Concrete and Composite Bridges Part 3: Code of Practice for Design of Steel Bridges", BS 5400.

Bryan, E. R. and Davies, J. M., (1984) "Design of Profiled Steel Sheeting and Decking", in Behaviour of Thin-Walled Structures, Eds. J. Rhodes and J. Spence, Elsevier.

Bulson, P. S., (1984) "Bulbs, Lips and Beads", in Behaviour of Thin-Walled Structures, Eds. by Rhodes, J. and Spence, J.,Elselvier Applied Science, Essex, England.

Chapman, J.C., Dowling, P.J., Lim, P.T.K., and Billington, C.J., (1971) "The Structural Behaviour of Steel and Concrete Box Girder Bridges", The Structural Engineer, Vol.49, March.

Chih-Hung, L., (1981) "Study of Corrugated Plates", PhD Thesis, University of South Carolina, College of Engineering.

Davies, J.M., and Lawson, R.M., (1978) "The Shear Deformation of Profiled Metal Sheeting", Int. J. Num. Meth. Engg, Vol.12.

Davies, J.M., (1979) "Tests on Light Guage Steel Cylindrical Shells", Proc. Instn. Civ. Engrs, Vol.67, June.

Dowling, P.J., and Burgan, B.A., (1985) "Torsional Lag in Wide Flanged Girders", IABSE Periodica, Vol. 4.

European Convention for Constructional Steel Work, (1977) "European recommendations for the testing of profiled metal sheets" ECCS-XVII-77-2E, April.

Heyman, J., (1982) "Elements of stress analysis", Cambridge University Press, Cambridge.

Huber, M.T., (1914) "Die Grundlagen einer rationellen Berechnung der Kreuzweise bewehrten Eisenbetonplatten", Zeitschrift des Osterreichischen Ingenieur und Architekten-Vereines, No. 30.

Huber, M.T., (1923) "Die Theorie der Kreuzweise bewehrten Eisenbetonplatten Nebst Anwendungen auf Mehere Bautechnish Wichtge Aufgaben uber Rechteckige Platten", Der Bauingenieur, Vol. 4.

Koo, K. K. and Cheung, Y. K., (1989) "Mixed Variational Formulation for Thin-Walled Beams with Shear Lag", Journal of Engineering Mechanics, ASCE, Vol. 115, No. 10, October.

Lamas, A.R.G., and Dowling, P.J., (1979) "Effect of Shear Lag on the Inelastic Buckling Behaviour of Thin-Walled Structures", Proceeding of the International Conference on Thin Walled Strucutres, University of Strathcylde, Glasgow, April.

Lamas, A.R.G., Frieze, P.A., and Dowling, P.J. (1983) "Interaction Between Shear Lag and Stiffener-Induced Buckling in Steel Box Girders", In Instability and Elastic Collapse of Steel Structures, Ed. Morris, L.J., Granada, U.K.

MacNeal, R.H., (1978) "A simple quadrilateral shell element", Computers and Structures, Vol.8.

Mang, A.H., Girya-Vallabhan, V.C., and Smith, H.J. (1976) "Finite Element Analysis of Doubly Corrugated Shells", Journal of the Structural Division, ASCE, Vol. 102, No. ST10, October.

Moffat, K. R. and Dowling, P. J., (1975) "Shear Lag in Steel Box Girder Bridges", The Structural Engineer, Vol. 53, October.

Murray, N. W., (1984) "Introduction to the Theory of Thin-Walled Structures", Oxford University Press, London.

Murray, N. W. and Khoo, P. S., (1981) "Some Basic Plastic Mechanisms in Thin-Walled Steel Structures", Int. J. Mech. Sci., Vol. 23.

Salaheldin. M.M., and Schmidt, L.C., (1989) "Linear and Non-linear Response of a Simple Box Girder", J. Construct. Steel Research, Vol. 13.

Salaheldin, M.M., and Schmidt, L.C., "Transverse Flange Stress Prediction in a Box Girder", (submitted for publication).

Salaheldin, M.M., Schmidt, L.C., and Upfold, R.W., (1987) "Deflection Behavior of Statically Loaded Corrugated Sheet", First National Structural Engineering Conference, I.E. Aust., Melbourne, August.

Salaheldin, M.M. and Schmidt, L.C., "Transverse Stresses in I-beam Flanges", (submitted for publication).

Schmidt, L.C. and Salaheldin, M., (1990) "Transverse Flange Stresses in a Simple Box Girder", Thin Walled Structures, (1-4).

Seydel, E. B., (1931) "Schebknickversuche mit Wellblechtafein", Jahrbuch d. Deutch., Versuchsanstalt fur Luftfahrt, E. V. Munchen Und Berlin.

Standards Association of Australia, (1980) "Determination of Resistance of Metal Roofing to Concentrated Forces and Wind Forces by Test", AS 1562-1980.

Standards Association of Australia, (1988) "Cold-Formed Steel Structural Code", AS 1538-1988.

Szilard, R., (1974) "Theory and Analysis of Plates; Classical and Numerical Methods", Prentice-Hall, Inc., Englewood Cliffs, New Jersey.

Timoshenko, S., and Goodier, J.N., (1951), "Theory of Elasticity", New York, McGraw Hill.

Timoshenko, S., and Woinowsky-Krieger, S., (1959) "Theory of Plates and Shells", 2nd Ed., McGraw-Hill, New York.

Trahair, N.S., Abel, A., Ansourian, P., Irvine, H.M., and Rotter, J.M., (1983) "Structural Design of Steel Bins for Bulk Solids", Australian Institute of Steel Construction, Sydney.

Troitsky, M.S., (1976) "Stiffened Plates; Bending Stability and Vibrations", Elsevier.

Wolford, D.S., (1954) "Sectional Properties of Corrugated Sheets Determined by Formula", Civil Engineering, Vol.103, February.

Wright, R.N., Abdel-Samad, S.R., and Robinson, A.R., (1968), "BEF Analogy for Analysis of Box Girders", Journal of the Structural Division, ASCE, Vol. 94, No. ST7, July.

Appendix 3. — KOO AND CHEUNG METHOD OF SHEAR LAG EVALUATION

The method of Koo and Cheung (1989) for shear lag evaluation is based on a mixed variational principle. In the analysis, the cross section of a thin-walled prismatic structure is assumed to be rigid in its own plane, but flexible out of its plane. The proposed method involves the choice of displacement and stress functions and the formulation of governing equations. A numerical example was given to demonstrate the accuracy of this method when compared with both the finite strip method and the classical theory of bending.

A thin-walled tube subjected to a concentrated load at the free end (Fig.A3.1-a) was considered. The dimensions of the cross section are shown in Fig.A3.1-b. As a result of the symmetrical condition only half the cross section was considered for analysis (Fig.A3.1-c). Fig.A3.2 shows the distribution of the longitudinal stresses in one quarter of the cross section of the location where Z = 0.0 from the geometrical dimensions given in Fig.A3.1-a and A3.1-b. The flange aspect ratio, which is defined as the width to length ratio of the flange, is 0.8.

The distribution of longitudinal membrane stresses across the flange (Fig.A3.2) does not reflect the severe shear lag effect which is expected at such a high aspect ratio.

In order to check the results of Koo and Cheung, a finite element analysis model was used to examine the distribution of longitudinal membrane stresses across the flange. The model simulates the geometrical configuration and the loading condition presented in Fig.A3.1 (Koo and Cheung, 1989).

The finite element technique employs a four-noded quadrilateral shell element (McNeal, 1978). Due to the symmetrical condition only half the box is modelled. The concentrated load was applied along the line of the web (the boundary conditions are shown in Fig.A3.1-c). A finite element mesh with 10 nodes along the span, 15 nodes across half the flange width, and 9 nodes down the web was used.

Young's Modulus, E, was assumed to be 200 GPa, and Poisson's ratio, μ, was assumed to be 0.3 for the material. Fig.A3.3 displays the distribution of longitudinal membrane stresses across the box, as calculated by the finite element analysis. The stress distribution (Fig.A3.3) reflects a severe effect of shear lag. As the stress are calculated at the centre of each element, the value of the maximum stress at the web/flange junction had to be extrapolated using a curve fitting procedure for the finite element stresses. Fig.A3.3 also shows the distribution of the longitudinal stresses according to simple theory where the effect of shear lag is neglected, and therefore a constant distribution of stresses is assumed across the flange. The same figure also shows the longitudinal stresses as predicted by Koo and Cheung (three term solution). All the stresses are normalised with respect to the maximum longitudinal membrane stress given by the finite element analysis (σ_{NC}). At the web/flange junction the difference between maximum

longitudinal stress predicted using finite element analysis and that which is predicted using Koo and Cheung method, is 53%.

According to the finite element analysis results the effective width ratio, which is defined as the effective width to the actual width of the flange, is estimated to be 0.28. According to the published results (Koo and Cheung, 1989), the effective width ratio is 0.56. For an aspect ratio of 0.8, the British Code (1982) gives an effective width ratio of about 0.3.

The above investigation leads to the belief that the published results (Koo and Cheung, 1989) are in error.

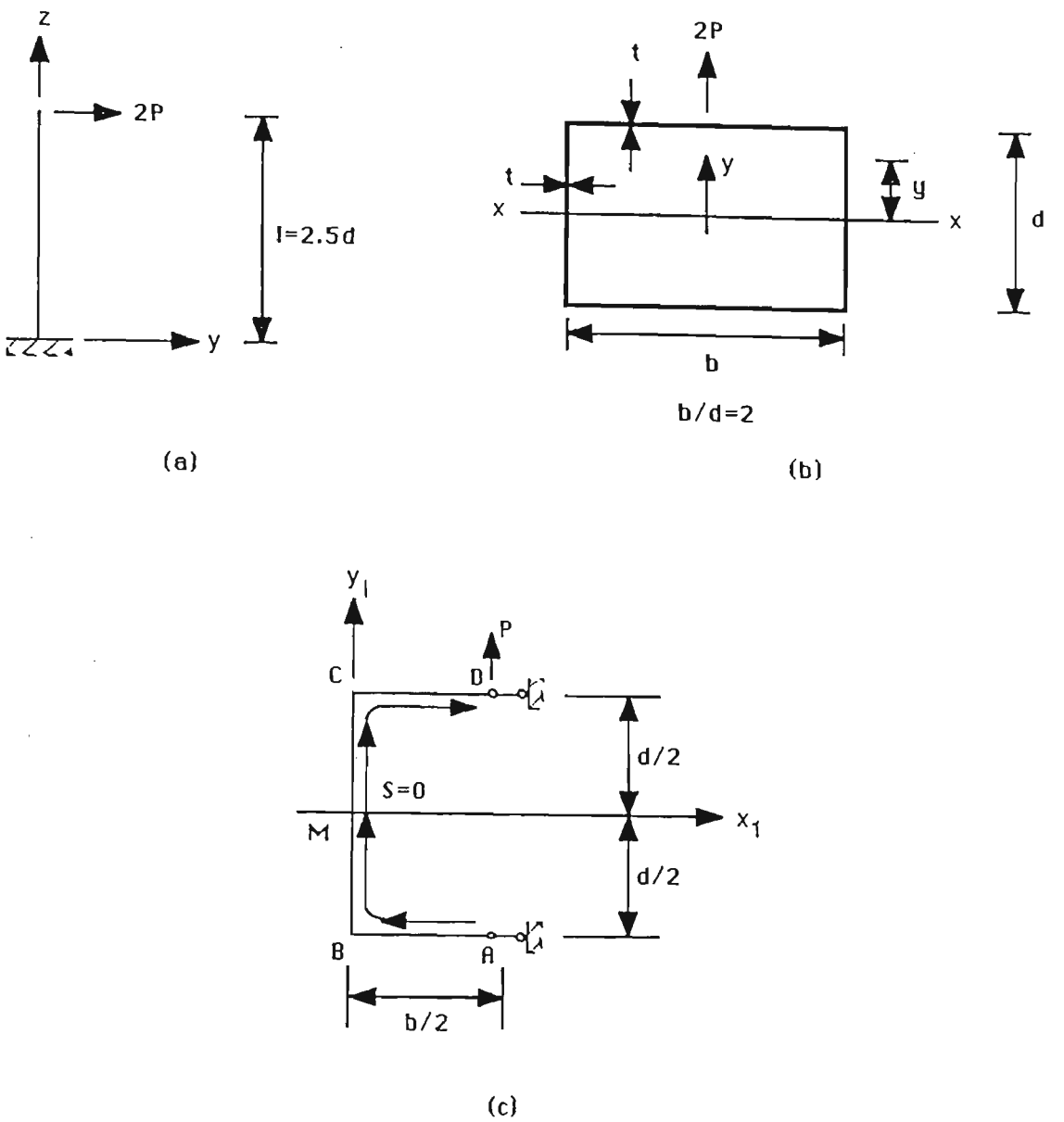

Fig.A3.1 Cantilever beam subject to point load: (a) Cantilever beam; (b) Cross section; (c) Equivalent cross section (Koo and Cheung, 1989)

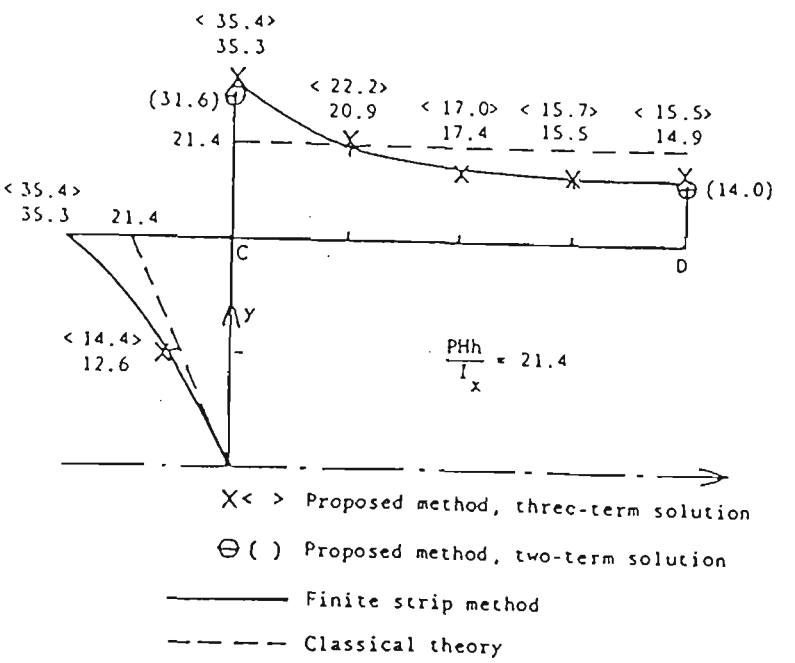

Fig.A3.2 Normal stress at lower end (Koo and Cheung, 1989)

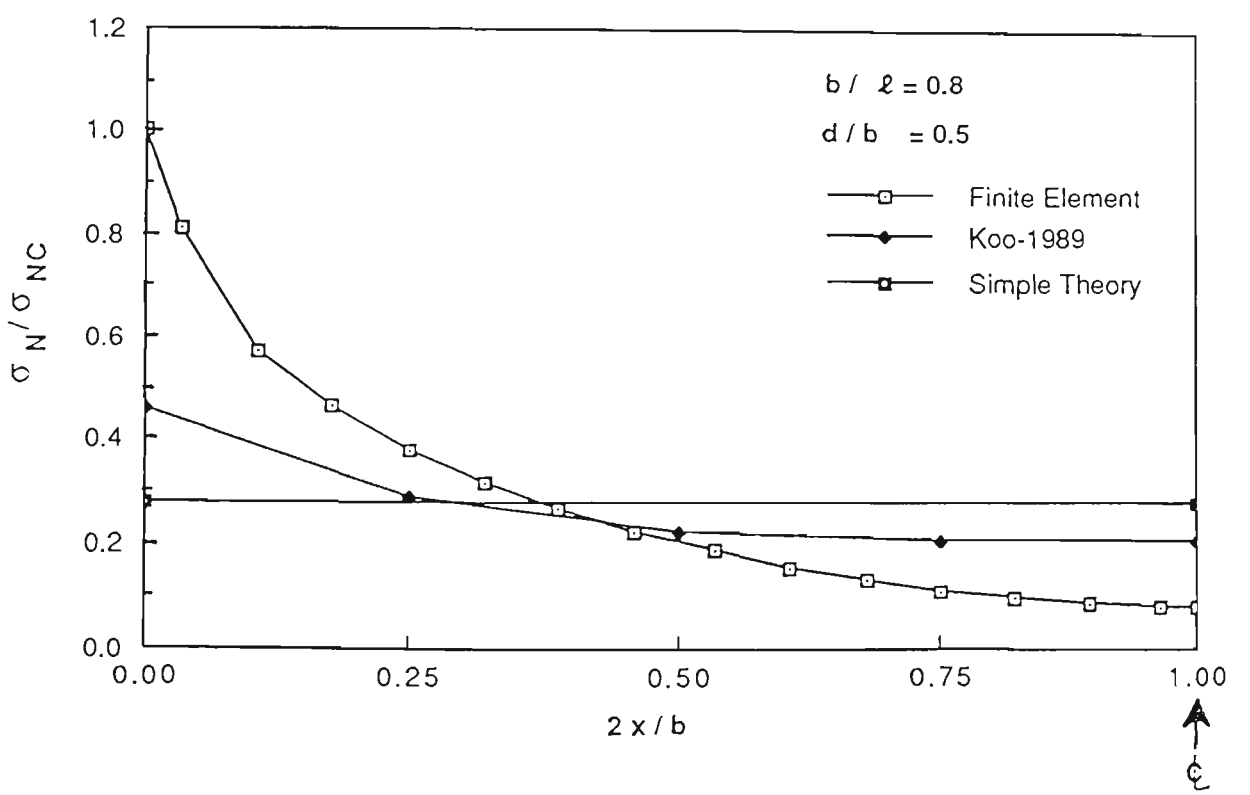

Fig.A3.3 Distribution of longitudinal stresses across the flange of the cantilever box - comparison